

**Investigating behaviour and failure modes of  
FRP and hybrid steel/FRP shear walls**

By Natalja Petkune

A thesis submitted in partial fulfilment of the requirements of the Faculty of Science,  
Engineering and Computing at Kingston University for the Degree of Doctor of Philosophy.

2016

## **Abstract**

The behaviour of steel shear walls has been investigated for several decades. They have been used in a number of high rise buildings as a primary lateral loading system. Steel shear walls have significant advantages in terms of their light weight, high stiffness and energy absorption in comparison with other structural systems. Hybrid structural elements are becoming popular in thin walled structures, sandwich panels and shear walls. Hybrid shear walls (HSW) are an innovative structural lateral load resisting system. In this thesis HSW are defined as consisting of steel framed elements and steel infill plates laminated with fibre reinforced polymers (FRP) material. By reducing out-of-plane deformations of the infill plate and increasing energy absorption capacity, such systems have the potential to provide highly effective structural solution.

The aim of this PhD project was to conduct experimental studies and investigate the behaviour of steel framed shear walls with steel, hybrid (steel/CFRP and steel/GFRP) and pure FRP (glass FRP and carbon FRP) infill plates. Medium scale specimens with dimensions of approximately 1 m width and 1 m height were tested under displacement controlled cyclic sinusoidal loading with amplitudes increasing from 0.2 mm to 35 mm in accordance to the ATC-24 protocol. Analysis of the behaviour of specimens was done predominantly via comparing load values and energy absorption.

Analysis of the results has shown that hybrid steel and FRP specimens have higher stiffness in comparison to the control steel specimen and a higher energy absorption capacity. Additional analysis performed was that of specific energy absorption to weight, the importance of the surface of connections between primary fish plates elements and infill plates and the strengthening of damaged specimens.

## **Acknowledgements**

Firstly, I would like to express my sincere thanks to my family and friends who supported me throughout my PhD journey, gave me continuous encouragement and motivation to carry on and complete PhD degree. Secondly, I would like to express my gratitude to my director of studies Dr Ted Donchev with his professional experience, valuable guidance, understanding and patience. Also I would like to thank other supervisors Dr Homa Hadavinia, Prof David Wertheim, Prof Mukesh Limbachiya for their assistance.

Special thank you to technicians: Sean Downey, Dean, Alex Vine, Peter, Mario, Peter, Howard for providing technical support and assistance at Penhryn Road and Roevale laboratories.

I would like to thank my PhD colleagues and all students I co-supervised during my PhD project for exchange of knowledge, skills and spending long hours with me in the labs.

Also I would like to acknowledge support from Kingston University SEC Doctoral School, especially from Prof Andy Augousti, Jackie Deacon and Rosalind Percival. I recognize that this research would not have been possible without all the necessary facilities for research and the financial assistance provided by Kingston University, and would like to express my gratitude for the financial funding received from KU SEC Doctoral School and University's Graduate School towards attending SMAR2015, CICE2014 and CECOM2012 conferences.

## **List of publications connected with thesis (included in Appendix A)**

### **Journal paper:**

Petkune, N., Donchev, T., Hadavinia, H., Wertheim, D., Limbachiya, M., (2016) Performance of pristine and retrofitted hybrid steel / fibre reinforced polymer composite shear walls. *Journal of Construction & Building Materials*, 117, pp. 198-208.

### **Conference papers:**

Petkune, N., Donchev, T., Hadavinia, H., Wertheim, D., Limbachiya, M. (2016) *Behaviour of steel framed shear walls with FRP infill plates*. CICE2016. December 2016. Hong Kong, China.

Petkune, N., Donchev, T., Hadavinia, H., Wertheim, D., Limbachiya, M. (2015) *Strengthening of steel and hybrid shear walls*. The 12<sup>th</sup> International Symposium on Fibre-Reinforced Polymers for Reinforced Concrete Structures & The 5<sup>th</sup> Asia-Pacific Conference on Fibre-Reinforced Polymers in Structures. FRPRCS-12/APFIS-2015. December 2015. Nanjing, China.

Petkune, N., Donchev, T., Wertheim, D., Hadavinia, H., Limbachiya, M. (2015) *The use of the IRT to assess Steel and FRP hybrid elements*. SMAR 2015: Third Conference on Smart Monitoring Assessment and Rehabilitation of Civil Structures. September 2015. Antalya, Turkey.

Petkune, N., Donchev, T., Hadavinia, H., Limbachiya, M., Wertheim, D. (2014) *Investigation of the behaviour of hybrid steel and FRP shear walls*. The 7th international Conference on Fibre Reinforced Polymer (FRP) Composites in Civil Engineering (CICE 2014), August 2014. Vancouver, British Columbia, Canada.

Petkune, N., Donchev, T., Hadavinia, H., Limbachiya, M., (2014) *Investigation in connections between steel, composite and hybrid structural elements*. MCM-2014: Mechanics of composite materials. June 2014. Riga, Latvia.

Petkune, N., Donchev, T., Wertheim, D., Limbachiya, M., Hadavinia, H. (2013) *Application of infrared thermography for assessment of condition of structural element*. SMAR 2013: Second Conference on Smart Monitoring Assessment and Rehabilitation of Civil Structures. September 2013. Istanbul, Turkey.

Petkune, N. (2013) *Assessment of modes of failure in hybrid steel and FRP shear walls*. Proceedings of the 15<sup>th</sup> Young Researchers' Conference. 14 March 2013. London, UK.

Petkune, N., Donchev, T., Petkova, D., Hadavinia, H., Limbachiya, M., Hussein, Y. (2012) *Opportunities for strengthening of damaged steel shear walls*. CECOM: Conference on Civil Engineering Infrastructure Cased on Polymer Composites. November 2012. Krakow, Poland.

## **Contents**

<b>Abstract.....</b>	<b>2</b>
<b>Acknowledgements .....</b>	<b>3</b>
<b>List of publications connected with thesis (included in Appendix A) .....</b>	<b>4</b>
List of figures.....	11
List of tables .....	17
Acronyms .....	18
<b>1. Chapter 1: Introduction.....</b>	<b>20</b>
1.1 Introduction to the studies .....	21
1.2 Aims and objectives .....	22
1.3 Scope of the work .....	23
1.4 Outline of the thesis.....	24
<b>2. Chapter 2: Literature Review .....</b>	<b>25</b>
2.1 Background to study .....	26
2.2 Seismic loading and seismic codes.....	26
2.3 Fibre reinforced polymers.....	27
2.4 Shear walls .....	29
2.4.1 Concrete shear walls .....	29
2.4.2 Steel Shear Walls.....	30
2.4.2.1 SSW system in buildings.....	31
2.4.2.2 Experimental and numerical studies of SSW system.....	33
2.5 Hybrid shear walls.....	35

2.6	Strengthening of shear walls .....	38
2.7	Infrared thermography .....	41
2.7.1	IRT use in composite materials .....	42
2.8	Conclusions to Chapter 2 .....	43
<b>3</b>	<b>Chapter 3: Small scale testing: connections .....</b>	<b>44</b>
3.1	Introduction to connection tests .....	45
3.2	Methodology to connection tests.....	45
3.2.1	Specimen description.....	45
3.2.2	Type of connections.....	47
3.2.3	Testing procedure .....	48
3.3	Behaviour of small scale connection specimens.....	50
3.4	Small connections experimental results.....	53
3.5	Analysis of experimental results .....	55
3.6	Conclusions to Chapter 3 .....	57
<b>4</b>	<b>Chapter 4: Experimental test setup for shear wall specimens .....</b>	<b>58</b>
4.1	Experimental set-up for shear walls .....	59
4.2	Description of the equipment.....	59
4.2.1	Testing Rig.....	60
4.2.2	Loading Equipment .....	62
4.2.3	Logging equipment .....	64
4.2.4	Measuring instruments.....	65
4.2.4.1	Loadcell .....	65

4.2.4.2	Linear Displacement Sensors .....	67
4.2.4.3	Cable- Extension Displacement Sensor.....	69
4.2.4.4	Strain gauges.....	70
4.3	Shear wall specimen specification .....	72
4.3.1	Steel frames specification and preparation for testing .....	73
4.3.2	Infill plates.....	75
4.3.2.1	Steel infill plates.....	75
4.3.2.2	Hybrid infill plates: steel/GFRP and steel/CFRP.....	75
4.3.2.3	Pure FRP plates: GFRP and CFRP.....	79
4.3.3	Assembling specimens .....	79
4.3.3.1	Connection between steel frame and infill plates.....	79
4.3.3.2	Fixing frame in the position .....	82
4.4	Specification of the newly developed shear walls specimens.....	83
4.5	Testing protocol .....	84
<b>5</b>	<b>Chapter 5: Experimental results of newly developed shear walls .....</b>	<b>86</b>
5.1	Testing of the SSW* and SSW specimens.....	87
5.2	Testing of the HCSW* and HCSW specimens.....	91
5.3	Testing of the HGSW.....	96
5.6	Testing of the CSW.....	98
5.7	Testing of the GSW .....	100
5.8	Modes of the destruction for all specimens .....	102
5.8.1	Damages identified by IR thermography .....	102
5.8.2	IRT passive data.....	103
5.8.3	IRT active data.....	105
5.8.4	Summary of the damages for all specimens .....	109

<b>6</b>	<b>Chapter 6: Analysis of experimental results of newly developed shear walls</b>	<b>113</b>
6.1	Introduction to the analysis of the results.....	114
6.2	Parameters for the analysis and failure modes of the specimens.....	114
6.3	Comparison of average load values, $F_{avg}$ , for all specimens .....	116
6.3.1	Comparison of HCSW* and HCSW behaviour.....	117
6.3.2	Comparison of HCSW and HGSW behaviour .....	118
6.3.3	Comparison of CSW and GSW behaviour .....	120
6.3.4	Comparison of hybrid group and pure FRP group behaviour.....	121
6.3.5	Comparison of initial stiffness ( $K_0$ ), changes in stiffness for whole testing range ( $K$ ) and dynamic stiffness ( $K_D$ ).....	122
6.4	Deformability .....	124
6.5	Ultimate load capacity .....	126
6.6	Analysis of energy absorption.....	127
6.6.1	Energy absorption per individual cycle- EIC.....	128
6.6.2	Energy absorption at any specific level of displacement, ESD.....	129
6.6.3	Cumulative energy absorption (CEA).....	132
6.7	Summary of the experimental results .....	134
6.8	Comparison between experimental and normalised results.....	136
6.9	Conclusions .....	137
<b>7</b>	<b>Chapter 7: Strengthening of shear walls .....</b>	<b>140</b>
7.1	Introduction to the strengthening of shear walls.....	141

7.2	Temporary strengthening to steel plate shear wall specimen (SPSW).....	141
7.2.1	Scheme for strengthening of steel plate shear wall specimen SPSW.....	141
7.2.2	Discussion of results for temporary strengthening .....	143
7.3	Permanent strengthening of shear walls.....	147
7.3.1	Scheme for permanent strengthening.....	147
7.3.2	Permanent strengthening of SSW.....	150
7.3.3	Permanent strengthening of HCSW .....	151
7.3.4	Permanent strengthening of HGSW .....	152
7.3.5	Analysis of the results on the basis of load-displacement curves .....	153
7.3.6	Energy absorption in different types of shear wall specimens.....	156
7.4	Conclusions to Chapter 7 .....	158
<b>8</b>	<b>Chapter 8: Conclusions and recommendation for future work .....</b>	<b>160</b>
8.1	Conclusions to the thesis .....	161
8.2	Recommendations for future studies .....	163
	<b>References .....</b>	<b>165</b>
	<b>Appendices.....</b>	<b>172</b>

## List of figures

Figure 1.1. Scheme for the PhD project.....	23
Figure 2.1. a) 35-storey Kobe building in 1995 after earthquake (in the background) b) Kobe building in 1996 .....	33
Figure 2.2 Types of steel shear walls (Astaneh-Asl and Council, 2001).....	34
Figure 2.3. a) One story b) 4-story specimens tested by Rezaii <i>et al.</i> , 2000 .....	35
Figure 2.4. Testing of the Hybrid GFRP Shear Wall specimen with opening .....	36
Figure 2.5. Tearing and joint failure in the infill plate .....	37
Figure 2.6. Tensile fiber damage (left) and principal stress distribution (right) in 35 <sup>o</sup> FRP layer with $t=1$ mm at 2.5% drift .....	37
Figure 3.1. a) type 1 bolted connection b) type 2 bolted and adhesive connection. ....	48
Figure 3.2. Dimensions for specimens. ....	48
Figure 3.3. Displacement vs time.....	49
Figure 3.4. Test set up a) universal tensile machine b) test specimen. ....	49
Figure 3.5. a) S1 b) S2 specimens after testing. ....	50
Figure 3.6. a) CH1 b) CH2 c) CHa1 d) CHa2 specimens after testing.....	51
Figure 3.7. a) GH1 b) GH2 c) GHa1 d) GHa2 specimens after testing. ....	51
Figure 3.8 a) CF1 b) CF2 c) GF1 d) GF2 specimens after testing. ....	52
Figure 3.9. Load vs Displacement graphs each type of the specimens .....	54
Figure 3.10. Ultimate load for small scale specimens.....	56
Figure 4.1. Diagram of testing equipment. ....	60
Figure 4.2. Testing rig.....	61
Figure 4.3. Lateral support system. ....	62
Figure 4.4. Loading system. ....	62
Figure 4.5. Screw jack support.....	63
Figure 4.6. Datalogger DT85G and three multiplexers CEM20.....	64

Figure 4.7. Loadcell configuration a) location for loadcell b) levelling of loadcell.....	66
Figure 4.8. Calibration of loadcell a)&c) tension b)&d) compression.....	67
Figure 4.9. Displacement measurement.....	68
Figure 4.10. Positioning of the CDS. a) test set-up b) CDS Positioning. ....	69
Figure 4.11. Strain position on the infill plate.....	71
Figure 4.12. Scheme for strain gauge attachment on the frame.....	71
Figure 4.13. Scheme for strain gauge attachment on the frame (top and side section).....	72
Figure 4.14. Dimensions of single-storey shear wall specimen.....	73
Figure 4.15. Dimensions of sample.....	74
Figure 4.16. Steel infill plate. ....	75
Figure 4.17. FRP Specimen for tensile testing. ....	77
Figure 4.18. Design specification for hybrid specimens. ....	78
Figure 4.19. a) Oven/vacuum curing b) curing cycle.....	79
Figure 4.20. Connection between infill plate and fish plates- top view of the I-beam of the frame and infill plate.....	80
Figure 4.21. Plan view of the frame showing connection between infill plate and fish plates. .....	80
Figure 4.22. Illustration of the frame being subjected to push and pull loading. ....	84
Figure 4.23. Cycling loading in accordance to ATC- 24 protocol. ....	85
Figure 5.1. Load vs displacement graph for SSW*.....	87
Figure 5.2. SSW* specimen at 25 mm displacement.....	88
Figure 5.3. SSW specimen a) Hysteresis curve b) Load vs Displacement. ....	89
Figure 5.4. SSW specimen after 35 mm displacement a) diagonal tension field development b) plastic hinges c) twist holes along diagonal lines d) summary of damages to the SSW at 35 mm displacement. ....	91
Figure 5.5. HCSW* specimen a) Hysteresis curve b) Load vs Displacement.....	92

Figure 5.6. Damages to HCSW* specimen after 35 mm displacement a) delamination level b) failure in connection c) plastic hinges d) tearing in FRP layers e) crack in the beam-column connection. ....	93
Figure 5.7. HCSW specimen a) Hysteresis curve b) Load vs Displacement.....	94
Figure 5.8. Damages to HCSW specimen after tested to 30 mm displacement a) delamination and cracking of fibres b) buckling of the fish plate c) sliding of the plate d) development of hole in the corners. ....	96
Figure 5.9. HGSW specimen a) Hysteresis curve b) Load vs Displacement. ....	96
Figure 5.10. HGSW specimen tested to 30 mm displacement a) front b) back side of plate c and d) failure in connection.....	98
Figure 5.11. CSW specimen a) Hysteresis curve b) Load vs Displacement. ....	99
Figure 5.12. CSW specimen with a) opening of the crack during 1 <sup>st</sup> cycle of 25 mm displacement testing b) ruptures in the specimen tested to 25 mm displacement c) delamination of thin strips of CFRP. ....	99
Figure 5.13. GSW specimen a) Hysteresis curve b) Load vs Displacement.....	100
Figure 5.14. GSW specimens tested to 30 mm displacement a) delamination b) damages to connection c) buckling to fish plates. GSW tested to 35 mm displacement d) delamination e) damages to connection f) plastic hinges. ....	102
Figure 5.15. IRT camera set-up during testing.....	103
Figure 5.16. IR images demonstrating temperature distribution for SSW specimen.....	104
Figure 5.17. Heat releases at maximum 30 mm displacement in horizontal direction for HCSW* specimen a) shear wall photo b) IR image. ....	104
Figure 5.18. IR images of HCSW* specimen at 30 mm displacement after MATLAB processing a) demonstrating temperature distribution and tensile field profile b) temperature distribution along A'-A' line.....	105

Figure 5.19. IRT active data analysis for HCSW* a) 20 mm image b) 20 mm visual delamination c) 20 mm IRT delamination d) 30 mm image e) 30 mm visual delamination f) 30 mm IRT delamination.....	106
Figure 5.20. Delamination of the HCSW specimen. a) 20 mm image b) 20 mm visual delamination c) 20 mm IRT delamination d) 30 mm image e) 30 mm visual delamination f) 30 mm IRT delamination.....	107
Figure 5.21. Delamination of the HGSW specimen a) 30 mm image b) 30 mm visual delamination c) 30 mm IRT delamination.....	108
Figure 5.22. Delamination area for HCSW*, HCSW and HGSW specimens.....	108
Figure 6.1. Cyclic load - displacement for a) SSW b) HCSW* c) HCSW d) HGSW e) CSW f) GSW during cyclic loading.....	115
Figure 6.2. Variation of average load- displacement for five newly developed and SSW (control) shear wall specimens. ....	116
Figure 6.3. Comparison of load – displacement curves for HCSW*, HCSW and SSW (control) specimens. ....	118
Figure 6.4. Comparison of load – displacement curves for HCSW, HGSW and SSW (control) specimens. ....	119
Figure 6.5. Load vs displacement results for CSW, GSW and SSW (control) specimens. ....	120
Figure 6.6. Comparison of load - displacement results for HCSW, HGSW, CWS, GSW and SSW (control) specimens. ....	121
Figure 6.7. Lines showing history of variations of stiffness for SSW specimen. ....	122
Figure 6.8. Stiffness values for all specimens. ....	123
Figure 6.9. Lines showing history of dynamic stiffness for SSW specimen.....	124
Figure 6.10. Evolution of dynamic stiffness during cyclic loading for all specimens.....	124
Figure 6.11. Comparison of the deformability at the same level of loading. ....	125

Figure 6.12. Comparison of ultimate load capacities for shear wall specimens and corresponding displacement. ....	126
Figure 6.13. Energy absorption for individual cycles. ....	128
Figure 6.14. Differences for energy absorption between cycles at the same level of loading for all specimens. ....	129
Figure 6.15. Variation of energy absorption at each level of loading for all specimens. ....	130
Figure 6.16. Differences in ESD at different intervals. ....	131
Figure 6.17. Comparison of cumulative energy absorption. ....	133
Figure 6.18. Share of the energy absorption at various stage of loading for all shear wall systems. ....	134
Figure 6.19. Steel frame contribution. ....	135
Figure 6.20. Normalised results for a) average load b) ultimate load c) ESD and d) CEA. ....	137
Figure 7.1. Scheme for 1st layer of GFRP wrapping around SRSW-str1 and 2nd layer of GFRP wrapping around SRSW-str2. ....	142
Figure 7.2. Steel shear wall specimen SPSP at different stages of loading. ....	144
Figure 7.3. a) SRSW-D b) Strengthened shear wall specimen with 2 layers of GFRP wrapping after loading to 15 mm. ....	145
Figure 7.4. Average load for strengthened specimen at small displacements. ....	145
Figure 7.5. Average load comparison for SPSW, SPSW-str1, SPSW-str2 specimens at 10 and 15 mm displacement. ....	146
Figure 7.6. Retrofitting scheme: position of CFRP laminates on shear wall columns (A-A and B-B sections). ....	149
Figure 7.7. Positioning of CFRP laminates and GFRP fabric on the plan view of the frame. ....	150
Figure 7.8 a) Pristine SSW and b) retrofitted SSW-R specimens after loaded to 35 mm displacement. ....	151
Figure 7.9. HCSW-R specimen tested to 35 mm. ....	152

Figure 7.10. HGSW-R specimen tested to 35 mm.....	153
Figure 7.11. Load-displacement results for pristine SSW and retrofitted SSW-R specimens. .....	153
Figure 7.12. Load-displacement results for pristine HCSW and retrofitted HCSW-R specimens. ....	154
Figure 7.13. Load-displacement results for pristine HGSW and retrofitted HGSW-R specimens. ....	155
Figure 7.14. Comparison of the load-displacement results of different shear wall systems. .....	156
Figure 7.15. Hysteresis loops for hybrid specimens at 1 <sup>st</sup> cycle of 25 mm displacement loading.....	156
Figure 7.16. Energy absorption in hybrid specimens between 5 mm and 30 mm. ....	157
Figure 7.17. Comparison of energy absorption in different types of shear wall specimens. .....	157

## List of tables

Table 2.1. Typical properties of the Fibre and steel properties.....	28
Table 3.1. Specimen description.....	46
Table 3.2. Comparison of $F/\Delta l$ values for specimens.....	55
Table 4.1. Properties of UB 127 x 76 x 13 mm.....	73
Table 4.2. MTM-28-1 prepreg $0^\circ$ configuration (cured 1 hour at $120^\circ\text{C}$ and tested at room temperature).....	76
Table 4.3. Properties of the FRP materials used.....	78
Table 4.4. Connection between fish plates and infill plates.....	81
Table 4.5. Specimen description and characteristics.....	83
Table 5.1. Description of different damages.....	109
Table 5.2. Damages for all specimens at 10 mm displacement.....	110
Table 5.3. Damages for all specimens at 20 mm displacement.....	111
Table 5.4. Damages for all specimens at 30 mm displacement.....	112
Table 6.1. Summary of the key important results for various shear wall systems.....	135
Table 6.2. Weight of the specimen and their factors.....	136
Table 7.1. Scheme for testing of temporary strengthened specimens.....	142
Table 7.2. Description of SSW and HSW specimens.....	147
Table 7.3. Properties of the FRP materials used for retrofitting of shear walls.....	148

## Acronyms

$\Delta$ [mm]	Displacement
$\Delta_{NL}$ [mm]	Displacement at the start of nonlinear behaviour
ACI	American Concrete Institute
AISC	American Institute of Steel Construction
AFRP	Aramid Fibre Reinforced Polymer
ATC	Applied Technology Council
BFRP	Basalt Fibre Reinforced Polymer
BS EN	British Standard European Norm
BSI	British Standards Institution
CDS	Cable – Extension Displacement Sensor
CEA	Cumulative energy absorption
CEM	Channel Expansion Module
CFRP	Carbon Fibre Reinforced Polymer
CSW	Carbon Shear Wall
EA	Energy absorption
EC	Eurocodes
EIC	Energy absorption per individual cycle of loading
ESD	Energy absorption at any specified level of displacement
$F_{avg}$	Average load at each displacement level
FEMA	Federal Emergency Management Agency
$F_{max}$	Ultimate load values
FRP	Fibre Reinforced Polymer
GFRP	Glass Fibre Reinforced Polymer
GSW	Glass Shear Wall
HSW	Hybrid Shear Wall

HCSW	Hybrid Carbon FRP and Steel Shear Wall
HCSW*	Hybrid Carbon FRP and Steel Shear Wall without adhesive at fish plate and infill plate connections
HGSW	Hybrid Glass Fibre Reinforced polymers and Steel Shear Wall
IRT	Infrared Thermography
$K_0$	Initial stiffness
$K_D$	Dynamic stiffness
LVDT	Linear Variable Differential Transducer
NDT	Non-Destructive Testing
RC	Reinforced Concrete
SEA	Specific Energy Absorption
SW	Shear Wall
SSW	Steel Shear Wall

## **Chapter 1: Introduction**

This Chapter is aimed at providing an introduction to the thesis. It describes the background to the project and the importance of the conducted PhD project. It also includes the scope of the PhD project and the layout of the dissertation.

## 1.1 Introduction to the studies

Many countries experience severe damage from earthquakes. Seismic design includes the provision of new structures with lateral load resisting systems and the strengthening of existing building structures. These systems are moment resisting frames, braced frames, shear walls, trusses and coupled shear walls cores etc. The choice of lateral load resisting system depends on a number of factors, such as the architectural and structural design configuration of the building, geometry of the building and orientation. The scope of this project is to investigate shear walls (SWs), which can be used for medium- and high- rise buildings. SWs provide good properties in terms of stiffness and energy absorption. They can be categorised based on the material they are made from: concrete, masonry units, steel or timber. For the purpose of this research, hybrid shear walls are made from combination of materials such as steel and FRP.

Steel shear walls (SSW) were defined as a system to resist lateral load in regions with high levels of seismic activity and horizontal story shear (Astaneh-Asl, 2000). Since the 1970s SSWs have been popular in USA and Japan for construction of high-rise buildings providing significant reduction in wall thickness, weight of the building and as a result, reduction of foundation loads (Roberts, 1995). In designing high-rise buildings, it is important to have a good weight/strength ratio, as weight of the structural elements increases mass at high levels and as a result heavy vertical loadings. The main advantage of steel shear walls is that they are much lighter than reinforced concrete (RC) shear walls. In addition, they have excellent stiffness, strength and ductility (Seilie & Hooper, 2005). A properly designed SSW has enhanced ductility and large energy absorption capacity. High initial stiffness is an important characteristic for shear walls, which means they are effective in aspect of lateral resisting design.

The aim of this research is to improve the behaviour of SSWs by adding an additional layer of FRP on the steel infill plate - defined as hybrid shear walls (HSWs) and to introduce further progress in this direction via inclusion of pure FRP infill plate as one of the main structural components for shear walls. Limited studies have been conducted on analysis of HSWs by researchers. As further steps for developing such innovative structural elements with enhanced initial stiffness, three types of infill plates were investigated in this project: steel only (control), pure FRP and hybrid steel/FRP. Two types of FRP were used to produce hybrid and pure FRP specimens: glass FRP (GFRP) and carbon FRP (CFRP).

Hybrid shear walls were designed by attaching a FRP layer to the steel infill panel and placing the infill plate into steel framed elements. Pure FRP shear walls were also placed into steel framed elements. The second phase of the project was testing strengthened specimens using temporary and permanent retrofitting techniques. Shear wall samples were tested under quasi-static loading.

## 1.2 Aims and objectives

The main aim of the thesis is to investigate the behaviour of steel framed shear wall with different types of infill plates indicated below. The objectives of the study are:

- To conduct experimental testing and investigate the behaviour of hybrid steel/FRP infill plates and pure FRP only infill plate within steel frame boundary elements.
- To compare the behaviour of hybrid and pure FRP specimens with control steel shear wall specimen.
- To investigate connections between steel boundary and infill plate elements of the shear wall.
- To study the behaviour of shear wall specimens using infrared thermography (IRT) and its application as a non-destructive testing (NDT) method for hybrid elements.

- To analyse the process of delamination for hybrid shear wall specimens via processing data from infrared thermography.
- To develop a methodology for strengthening damaged shear wall specimens with FRP material and analyse behaviour of pristine and retrofitted specimens.

### 1.3 Scope of the work

Scope of the research can be divided in four main parts, as shown in Figure 1.1.

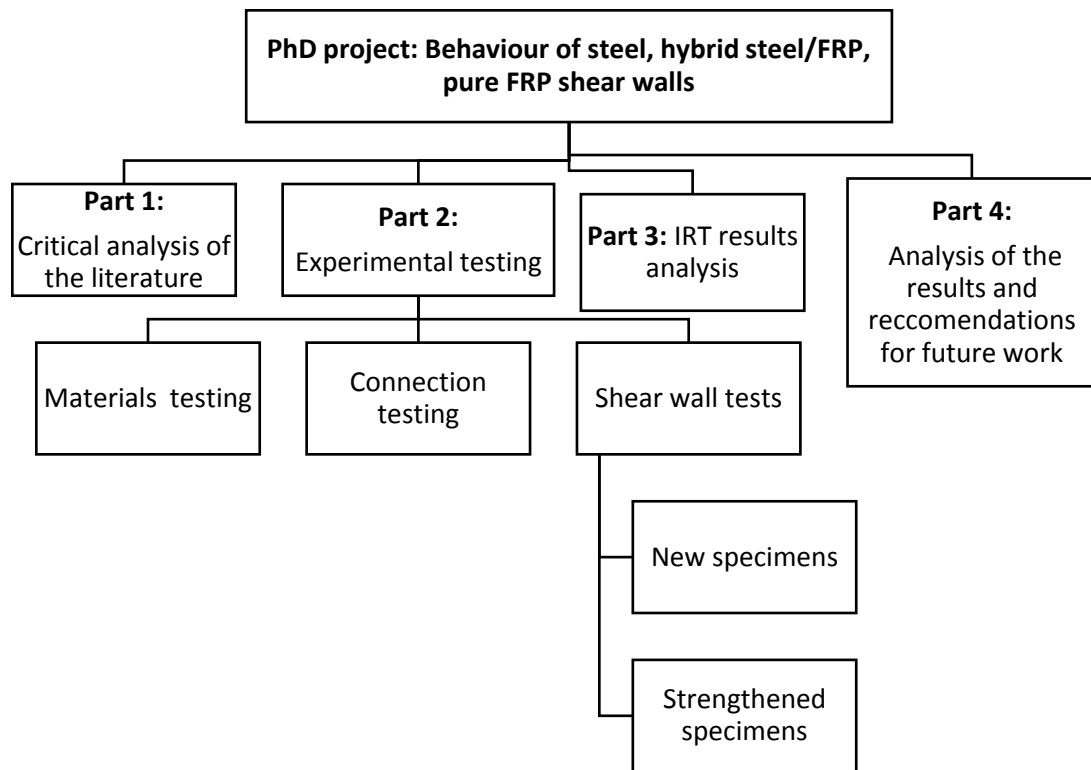


Figure 1.1. Scheme for the PhD project.

Part 1 includes critical analysis of the existing sources (journal papers, conference papers, reports) which contained information about earthquake loading, seismic codes, FRP information and strengthening techniques. The study was limited to two types of FRP: CFRP and GFRP materials.

Part 2 includes experimental testing of the specimens: FRP material tests (tensile test), small scale connection tests between steel boundary elements and infill plates and testing of the shear walls specimens. Testing of newly prepared shear wall specimens and retrofitted samples was conducted.

In Part 3 active and passive infrared thermography data was obtained and further discussed and analysed in Chapter 5.

Part 4 of the project includes analysis of the obtained results, conclusions and recommendations for future development.

#### **1.4 Outline of the thesis**

The thesis is organised in eight chapters, listed as below:

CHAPTER 1: Introduction

CHAPTER 2: Literature review

CHAPTER 3: Small scale testing: connections

CHAPTER 4: Experimental test setup for shear wall specimens

CHAPTER 5: Experimental results of newly developed specimens shear walls

CHAPTER 6: Analysis of the experimental results of newly developed specimens shear walls

CHAPTER 7: Strengthening of shear walls

CHAPTER 8: Conclusions and recommendations for future work

References

Appendices.

## Chapter 2: Literature Review

This Chapter contains a critical analysis of the literature to date. Recent studies conducted on the investigation of different types of shear walls and the use of FRP materials for seismic design have been reviewed and compared. It also reflects on important issues connected with shear wall design. The following topics have been looked at:

- Earthquake loading and design
- Existing seismic codes in different countries
- Different types of shear walls depending on material constructed from and their functionality
- Use of FRP material in civil engineering
- Strengthening of shear walls
- Use of IRT.

## 2.1 Background to study

Described below are details of seismic loading and earthquake design; the application of SSW under seismic loading; features and comparisons of steel and concrete steel walls; investigations of HSW; use of IRT and the use of FRP materials for strengthening and retrofitting steel shear walls.

## 2.2 Seismic loading and seismic codes

Seismic codes provide guidance to design structures under earthquake conditions. Design codes and procedures have been developed in different countries according to the necessary specifications. For this project seismic codes from United Kingdom and USA were reviewed.

Eurocodes (EC) have been developed to substitute British Standards in United Kingdom. Besides United Kingdom, EC have been adopted in many European countries like France, Germany, and Belgium. Eurocode 8 (EC8) describes the design of structures for earthquake resistance. Different parts of EC8 specify design requirements for specific structures. The most important parts of EC8 in connection with this study are:

- EC 8: Part 1- General rules seismic actions and rules for buildings (British Standards Institution, 2004)
- EC 8: Part 3- Assessment and retrofitting of buildings (British Standards Institution, 2005a)

Different seismic codes have been adopted in United States; the use of the codes depends on regions. Seismic design provisions are based on the National Earthquake Hazards Reduction Program (NEHRP) Recommended Provisions for Seismic Regulations for New Buildings and Other Structures.

Institutes involved in the provision and modification of specific codes are:

- Applied Technology Council (ATC)

- Federal Emergency Management Agency (FEMA)
- American Concrete Institute (ACI)
- American National Standards Institute (ANSI)
- American Institute of Steel Construction (AISC)
- American Society for Testing and Materials (ASTM).

Seismic codes in different countries have been developed to incorporate steel shear wall designs. Steel plate shear wall design was added to the US seismic code in the 2005 edition of the AISC 341-05 Seismic Provisions for Structural Steel Buildings as section “Special Plate Shear Walls” (American Institute of Steel Construction, 2005). These provisions were developed from “Limit States Design of Steel Structures” Canadian Standards Association (CSA, 2001) standard CAN/CSA-S16-01 published as “Limit States Design of Steel Structures”. Originally limited information of seismic design of shear wall systems was incorporated in the Canadian Standard as a non-mandatory appendix in the 1994 (Sabelli *et al.*, 2008).

The ATC-24 protocol produced by the Applied Technology Council in 1992 provided the first guidance for seismic testing of steel structures. It explains how steel structures perform under seismic excitations. The guidance is given to test samples in a slow cyclic load application (ATC-24, 1992). The methodology for experiments (loading histories, interpretation of the laboratory results) for this study was developed in accordance to this protocol, which is further discussed in Chapter 4.

### **2.3 Fibre reinforced polymers**

The use of FRP composite materials in civil engineering has increased in recent years as they have good mechanical properties. They have excellent strength-weight ratio providing weight reduction. Composite materials are lightweight as fibres and polymers, which are used as matrices, have low density (Barbero, 2011).

As composite materials are lightweight, they offer a great reduction of weight when structural elements are designed. However, it is important to note that they experience delamination during their lifetime, as FRP have low intra-laminar strength. When structural elements are subjected to load, the polymeric matrix of FRP is responsible for the absorption of impact energy and distribution of it to material (Meola & Carlomagno, 2010).

In addition, composites have resistance to corrosion and easy installation in comparison to traditional methods. FRP has been a popular choice for strengthening, repair and retrofitting structural elements. It can be used as external reinforcement for masonry walls and internal reinforcement for RC structures. There are different types of FRP materials depending on the material used in manufacturing. Most popular types of FRP materials are: carbon FRP (CFRP), glass FRP (GFRP), aramid FRP (AFRP), basalt FRP (BFRP).

Typical properties for different types of fibres in comparison to steel can be found in Table 2.1. Material properties of composite materials vary depending on fibre orientation and content (Barbero, 2011).

**Table 2.1. Typical properties of the Fibre and steel properties (Halliwell & Reynolds, 2004).**

	E- glass	Aramid	High strength carbon	Low modulus carbon	Steel ( S275)
<b>Tensile strength (MPa)</b>	2400	3600	3300-6370	2600-4700	275 Yield 430 Ultimate
<b>Tensile modulus (GPa)</b>	70	130	230-300	345-590	205
<b>Failure strain (%)</b>	3.5	2.5	1.5-2.2	0.6-1.4	20
<b>Density (kg/m<sup>3</sup>)</b>	2500	1440	1800	1900	7900

CFRP and GFRP have a wide spectrum of applications and have been used in many industries including aeronautical and civil engineering. Characteristics of CFRP include: high specific tensile strength, high specific elastic modulus, high strength-weight ratio, low density, low thermal expansion coefficient, good heat resistance, chemical stability, lack of

corrosion and self-lubrication (Kubota *et al.*, 2008). GFRP has lower tensile strength and modulus in comparison to CFRP.

As discussed above, CFRP and GFRP have good mechanical properties and were used as a composite material for hybrid shear wall design in this project. To improve the strength of the structure, prevent corrosion of the steel and also allow construction of lightweight shear panels with a relatively small depth, prepreg CFRP and GFRP materials were attached to steel infill plates. A customised fabrication process of the elements can provide excellent results in terms of the high specific stiffness and high specific strength. For the shear wall design, the number of FRP layers and the direction of the fibres are crucial for their properties as discussed further in Section 2.5.

## **2.4 Shear walls**

In this project, shear walls are investigated and tested under quasi-static loading. Shear walls are used as lateral resisting systems in structural design. They consist of an infill plate, boundary beam and column elements. SWs are mainly used for high-rise buildings, however they can be used for medium high buildings as well. Types of shear walls can be categorised by the materials they are made from: concrete, steel, hybrid steel/FRP etc. In this project steel, hybrid and pure FRP infill plates are investigated within steel framed elements.

### **2.4.1 Concrete shear walls**

Concrete shear walls are used as a traditional lateral load resisting system and are popular in countries with seismic zones. However, many of the existing concrete walls are old and can have insufficient in-plane stiffness and flexural and shear strengths. In order to prevent severe damage or even collapse, these walls require effective strengthening techniques (Lombard *et al.*, 2000).

In addition to the new shear walls and steel bracing elements, old strengthening techniques for concrete shear walls are shotcrete or ferrocement application, filling in openings with RC and masonry infills (FEMA, 2006). Disadvantages of these techniques are that they will add more weight to the structure, change the magnitude and distribution of the seismic loads and that they are labour intensive.

A more recent method of strengthening is to use composite elements to repair existing structures. Lombard *et al.* (2000) investigated the behaviour of the application of carbon fibre tow sheets reinforcing concrete shear walls externally. The dimensions of shear walls used were 2 x 1.5 x 0.1 m. Both analytical and experimental models were developed and analysed. The shear wall system demonstrated that it can recover initial elastic stiffness, increase yield load and ultimate flexural capacity of shear walls damaged under seismic loads. The use of CFRP has also been effective as a strengthening method for undamaged walls. Carbon fibre sheets increase pre-cracked stiffness, secant stiffness at yield and cracking loads.

FRP composites provide effective and lightweight solution. FRP materials have in addition excellent corrosion resistance and are easier to handle as mentioned earlier. FRP material was used for strengthening structural elements in this project as well.

#### **2.4.2 Steel Shear Walls**

Steel shear walls have become a popular lateral resisting system in the last few decades. They are often used in earthquake resistant designs as they resist horizontal story shear. SSWs consist of a steel infill plate, boundary columns and horizontal floor beams. The steel plate wall and boundary columns act as a vertical plate girder, where columns act as flanges of the girder and the steel plate acts as a web (Astaneh-Asl, 2000).

A steel shear wall system has numerous advantages to be considered in seismic design in order to improve the behaviour of structures. These advantages are (Astaneh-Asl, 2001):

- *A large energy absorption capacity and relatively high ultimate strength.* SSWs can absorb a large amount of energy, which is beneficial in earthquake design.
- *Large displacement ductility,* when designed properly and subjected to earthquake loading.
- *High initial stiffness,* which assists in limiting the drift of the system during earthquake loading.
- *Lower weight* in comparison to RC shear wall systems. Thus, the mass of the structure with SSW is reduced and less weight is carried by the columns and foundation.
- *Thickness* of SSWs is considerably less than of RC shear walls. SSWs require less area of the floor plan, which allows better utilisation of the gross area of the building.
- *Ease and fast construction* of SSW also makes them beneficial for the application of seismic retrofitting for existing buildings.
- *Shop- welded and field- welded steel shear walls* are more efficient and economical in terms of *speed of construction, cost of construction and field inspection.* They can be particularly effective in cold regions with low temperatures, when a concrete shear wall construction is not effective.

#### **2.4.2.1 SSW system in buildings**

Steel shear walls have been used in the construction industry since 1970's mainly in high earthquake zones in USA and Japan to provide a seismic retrofitting solution for low

and medium-rise buildings. In Japan predominantly stiffened SSW are used, whereas in North America unstiffened and thin steel plate shear walls are more common (Seilie & Hooper, 2005). The first shear walls were designed with horizontal and vertical stiffeners placed close to each other (Astaneh-Asl, 2000). The first building with a steel shear wall system was Shin Nittetsu Building or Nippon Steel Building in Tokyo, Japan in 1970 (Roberts, 1995).

Some of the examples of using steel shear walls include (Astaneh-Asl, 2000):

- 51-story high rise building in San Francisco (with SSW used as a primary load resisting system).
- United States Federal Courthouse, Seattle, WA (23- story building).
- Sylmar Hospital, Los Angeles, CA (six- story building).
- Canam- Manac Headquarters Expansion, St. George, Quebec (six- story building).
- Hyatt Regency Hotel at Reunion, Dalas, TX (50- story building).
- The Century, San Francisco, CA (46- story building).
- Shinjuku Nomura Building, Tokyo, Japan (51- story building) (Seilie & Hooper, 2005).

There are buildings with a shear wall system which have experienced earthquake loading like Sylmar Hospital in Los Angeles and a Kobe office in Japan. The minor structural damages they experienced confirmed effectiveness of the steel shear walls.

Sylmar Hospital in Los Angeles was built to replace Olive View Hospital, which was demolished after severe damage during the 1971 San Fernando earthquake. This hospital consists of concrete shear walls in the lower two floors and steel plate shear walls implemented in the perimeter of the upper four floors. Sylmar Hospital has experienced the 1987 Whittier earthquake and 1994 Northridge earthquake, which significantly

damaged non-structural elements like the suspended ceiling and sprinkler system, indicating very high stiffness of the whole structure.

One 35-story high-rise office building in Kobe was subjected to a strong earthquake in 1995. The building experienced minor damage only through the local buckling of the stiffened steel plate on the 26<sup>th</sup> floor. It was reported by Fujitani *et al.* (1996) in Astaneh-Asl (2000) publication, that soft stories developed between the 24<sup>th</sup> and 28<sup>th</sup> floors, permanent roof drift was 225 mm in northern and 35 mm in western directions. Figure 1.1a shows the Kobe building in the background experiencing only minor damages, whereas City Office building in front of it lost its top three floors (Figure 2.1a and b).

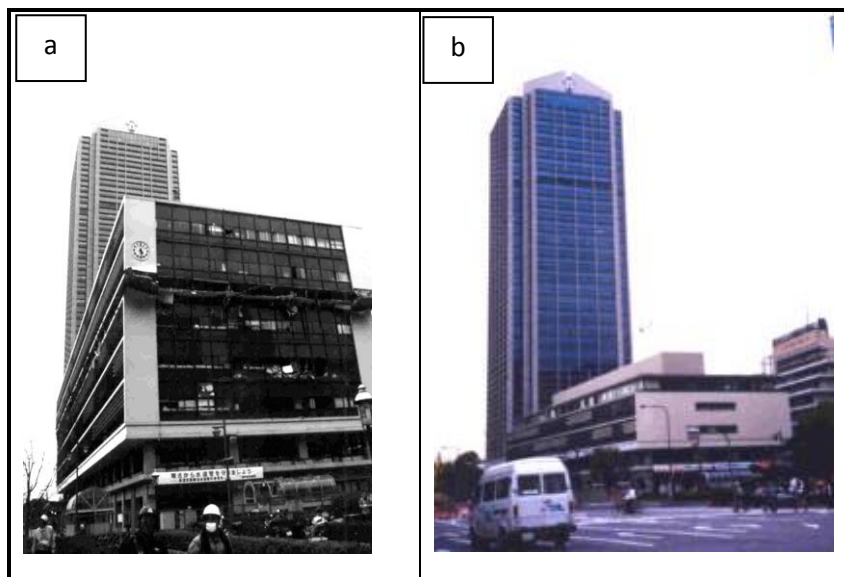


Figure 2.1. a) 35-storey Kobe building in 1995 after earthquake (in the background) b) Kobe building in 1996 (Astaneh-Asl, 2000).

#### 2.4.2.2 Experimental and numerical studies of SSW system

During the last thirty years, many researchers have conducted experimental studies and analytical modelling of steel shear walls. Extensive small- and large- scale experimental studies have been conducted and theoretical models have been developed to investigate the behaviour of stiffened and unstiffened shear walls in USA, Japan, Canada and UK.

Two types of walls: stiffened and unstiffened are demonstrated in Figure 2.2, with and without openings.

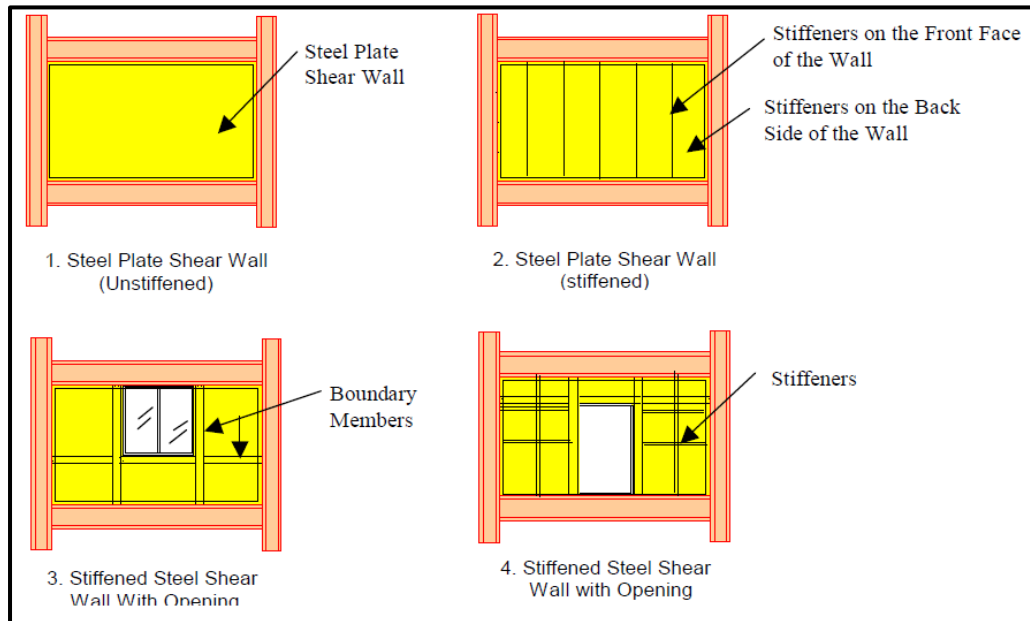


Figure 2.2 Types of steel shear walls (Astaneh-Asl and Council, 2001).

Below is a summary of important developments and findings conducted during this period (Astaneh-Asl, 2000).

The first significant work on steel shear walls was conducted by Thornburn *et al.* (1983) in Canada. Kulak (1985) and his associates Timler and Driver (Timler and Kulak, 1983) conducted cyclic testing of steel shear walls and developed simple truss bar models of shear walls. A non-linear finite element model for steel plate shear walls was developed by Driver *et al.*, (1998). It was tested on a large-scale, four-storey building with single bay unstiffened steel plate shear walls. Rezaii (1999) and Rezaii *et al.* (2000) conducted cyclic and shaking table tests of steel plate shear walls. Two single story and four-story single bay steel plate shear wall specimens were subjected to low, medium and high cyclic loading. Significant inelastic deformations were achieved by single story specimens, infill plate producing redundant diagonal story braces reduced demand on the moment-resisting

connections (Figure 2.3a). Four-story specimen had failed when yielding of the columns developed (Figure 2.3b).

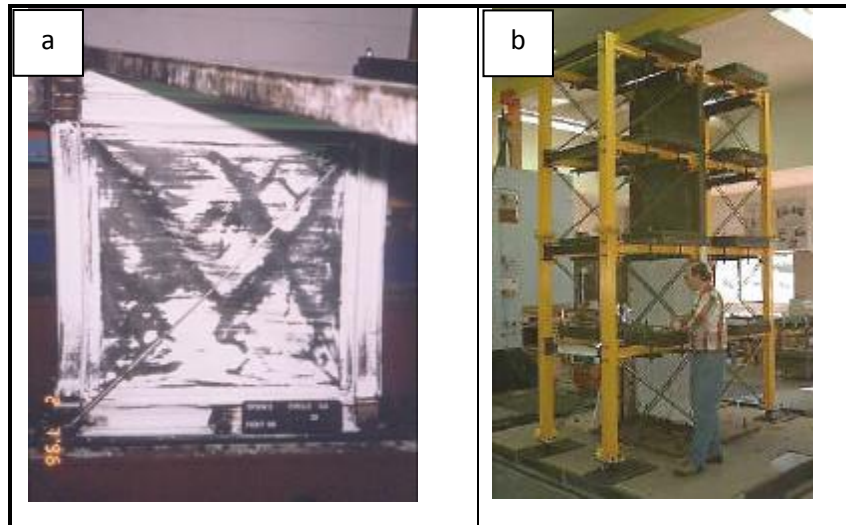


Figure 2.3. a) One story b) 4-story specimens tested by Rezaii *et al.*, 2000 (After Astaneh-Asl, 2000).

Based on the study conducted by Caccese and Elgaaly (1993) on cyclic tests on small scale steel frames infilled with steel plate shear walls and on study conducted by Sabouri-Ghomi and Roberts (1992) analytical model of the hysteresis behaviour of the steel plate shear walls was conducted.

Alinia *et al.* (2007) conducted numerical studies to investigate the effect of stiffeners in shear walls. They concluded that unstiffened SSW have very ductile behaviour and do not have good energy dissipation capacity as they buckle at early stages of loading. In some cases stiffeners are used in to increase the buckling capacity of shear wall, prevent pinching of hysteresis curves and increase energy dissipation capacity.

## 2.5 Hybrid shear walls

Hybrid shear walls are an innovative lateral resisting system and defined for the purpose of this project as consisting of steel frames and steel infill plates laminated with FRPs.

Maleki *et al.* (2011) investigated the application of GFRP in production of hybrid steel/FRP shear wall specimens. Theoretical and experimental studies were carried out in order to determine how GFRP sandwich plates can enhance the behaviour of shear wall under seismic loading. When the hybrid GFRP steel shear wall system was tested, uniform tension fields developed within infill plate during the test and the initial stiffness of the system was preserved. Loading capacity of the hybrid specimens increased in comparison to the steel shear wall specimen with the same thickness of the steel plate used for laminating hybrid specimen. As a result, it was demonstrated that use of GFRP laminates affects in-plane stiffness and out-of-plane deformation of infill plates. It was also found that variation of the fibre orientation influencing flexural demand for steel boundary elements. Higher load capacity results were achieved for symmetrical lay-up of 2 layers of GFRP fabric on both sides at  $45^\circ$  inclination of the fibres. Maleki *et al.* (2012) tested hybrid steel/GFRP shear walls with openings as shown in Figure 2.4. It was found that GFRP improves significantly stiffness of specimens with openings.

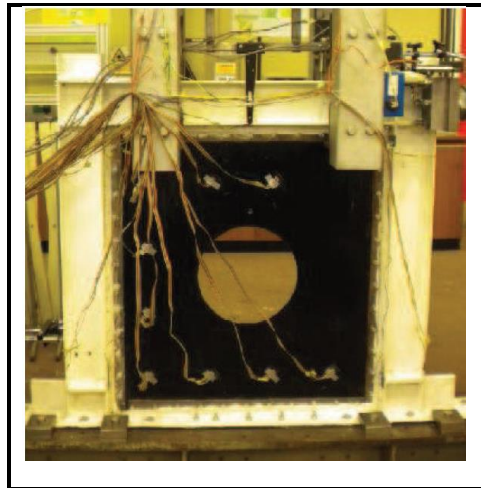


Figure 2.4. Testing of the Hybrid GFRP Shear Wall specimen with opening (Maleki *et al.*, 2012).

Similar to Maleki's studies (2011), Nateghi-Alahi and Khazaei-Poul (2012) tested steel shear walls with infill plates laminated with GFRP at  $0^\circ$  and  $90^\circ$  fibre inclination angle and at  $45^\circ$  fibre inclination angle. Steel plate was laminated with 1 layer and two layers on both sides of the plate. Infill plates laminated with GFRP have significantly increased ultimate

strength and initial stiffness. The cumulative energy dissipation of hybrid steel/GFRP shear walls is larger than steel shear walls. It also has to be noted that the direction of the fibres play a part too, and laminates in the direction of the tension field provide better improvements in terms of the shear strength and initial stiffness. The most common failure modes of the specimens occurred in steel and adhesive interface, GFRP delamination and joint failure as demonstrated in Figure 2.5.

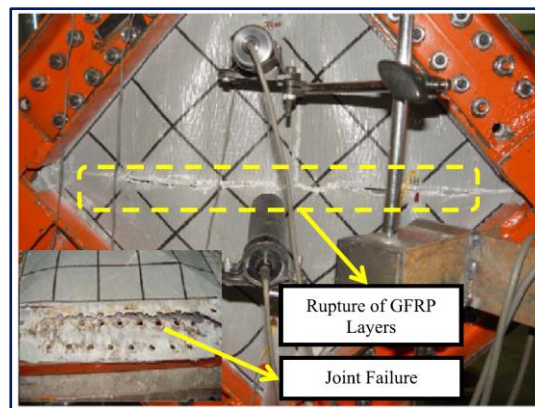


Figure 2.5. Tearing and joint failure in the infill plate (Nateghi-Alahi, Khazaei-Poul, 2012).

An effective angle orientation of carbon fibres at the angle of tension fields can improve the behaviour of shear wall plates. In numerical study conducted by Rahai and Alipour (2011), strength was improved by over 20%, whereas the stiffness of the shear wall increased by 10%. This can be explained by the fact that during loading the FRP layer does not take the load until the steel plate is completely yielded. Fibre damage was expected along the diagonal and corners of the plate as tension stress zones are spread diagonally as well as demonstrated in Figure 2.6.

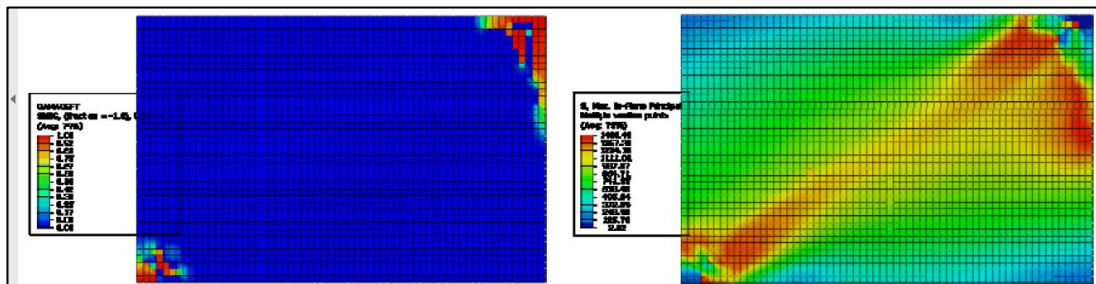


Figure 2.6. Tensile fiber damage (left) and principal stress distribution (right) in 35° FRP layer with  $t=1$  mm at 2.5% drift (Rahai and Alipour, 2011)

Hatami *et al.* (2012) conducted experimental and numerical studies to compare the behaviour of SSW and steel shear walls with carbon fibres. In the experimental study, one layer of CFRP was applied on each side of the 3 mm steel plate. They studied the fibre content/ angle and width of the panel to investigate how it influences the behaviour of the steel shear wall. In order to attach CFRP layer to steel infill plate, epoxy resin and hardener were applied. It was found that when a higher content of fibre is used, energy absorption, stiffness, over- strength and capacity of the steel shear wall is increased and ductility decreased. Fibre polymers were more effective in energy absorption values in thinner SSWs. Experimental studies conducted on hybrid carbon/steel shear walls showed improvements in terms of enhanced stress distribution, which was further improved with deformation progression. It was noticed that damages occurring between connection of columns and beams are much less in comparison to corresponding damage of SSW at the same level of displacement.

Another aspect influencing behaviour of the specimens is the connection between primary fish plates and infill plates of the shear wall affects the behaviour of the whole system. Hybrid steel and carbon FRP shear wall with adhesive between bolted connections significantly improved the stiffness and energy dissipation values of the system in comparison to HCSW with bolted connection only (Petkune *et al.*, 2014).

## 2.6 Strengthening of shear walls

When steel shear walls experience earthquake loading, they can undergo minor or extensive structural damage depending on the extent of the earthquake. Inspection of damage to all structural elements of the shear wall is crucial in order to choose an appropriate strengthening technique. Structural damage can occur at boundary elements i.e. columns and beams; at the connection between boundary elements and the infill plate,

and the infill plate itself. Careful consideration needs to include development of the hinges in beams and columns and buckling of the infill plate.

Strengthening techniques allow partial restoration of the strength capacity; they can be used as a temporary or permanent solution to provide structural stability to a building. The most common ways of retrofitting shear walls are replacement/strengthening of the infill plate, strengthening columns and beams and improvement of the connection between boundary elements and infill plate. Replacement of a damaged steel infill plate for shear walls is one option or otherwise the infill plate can be strengthened using FRP laminates or wrapping.

FRP materials have been used in civil engineering area for more than 20 years. FRP as a strengthening material has been used in improving the capacity of bridges, dams and tubes, to repair reinforced or pressed concrete (Wang & Hsu, 2009) and masonry structures (Marcari *et al.*, 2007), (Grande *et al.*, 2008) which were not designed for earthquake forces or lacked necessary detailing (Binici *et al.*, 2007). The most common fibres used for strengthening purposes are GFRP and CFRP, as they have numerous advantages like high tensile strength, high strength-to-weight ratio, ease of the application and corrosion resistance. They are used to enhance seismic resistance, fatigue loading, enhance the serviceability and ultimate strength of steel flexural members (Rizkalla *et al.*, 2008). FRP can be particularly beneficial in applications when it is important to avoid introducing residual stresses due to welding process.

Many existing concrete structures around the world have been retrofitted using FRP usually as bolted and/or adhesively bonded plates to the tension faces of structures or to the sides of beams as shear strengthening. Another technique to attach FRP is wrapping (longitudinal or full wrapping) (Oehlers & Seracino, 2004).

FRP materials have been used for strengthening steel structural elements as well. Previous studies have shown that strengthening of steel structures with FRP material provides good results. The initial application of FRP laminates produces an effective hybrid shear wall system; therefore the use of FRP could have high potential as a strengthening technique for damaged steel structural elements.

It was found that this way of strengthening allows restoring capacity of the corroded steel structures and improving its fatigue life (Haghani & Al-Emrani, 2008). Teng et al. (2012) discussed a wide range of steel structures strengthened with FRP materials; they highlighted the importance of preparation of the steel surfaces and properties of the adhesive and their influence to the bonding of both materials. Important considerations of designing adhesive joints to bond FRP laminates to steel were described by (Chiew, et al., 2011). Haghani & Al-Emrani (2012) described that the modes of failure between steel and FRP laminates can include debonding along the steel-adhesive or CFRP-adhesive interfaces, delamination of the CFRP laminate and cohesive failure of the adhesive or a combination of several modes. Experimental and numerical studies (Haghani & Al-Emrani, 2012) demonstrated that the failure of the debonding is not governed directly by the ultimate strength of the adhesive and is caused by the concentration of the stresses in the end of the bond line.

Numerous studies have been conducted on the behaviour of steel shear walls; however limited studies are available on the strengthening of the damaged shear walls to recover their initial capacity. When steel shear walls are subjected to earthquake loading, they experience early buckling of the infill plate.

The first stage of strengthening testing was to provide a provisional strengthening solution to damaged steel shear walls. Experimental testing of damaged steel shear walls with the use of GFRP bi-directional fabric around columns and infill plate was proved as an

effective temporary retrofitting solution. Load capacity of the strengthened specimen was increased in comparison to un-strengthened SSW, however significant delamination was noticed as displacement was increased (Petkune *et al.*, 2012). Results of the permanent strengthening showed very good behaviour in terms of the ultimate capacity and energy absorption (Petkune *et al.*, 2015; Petkune *et al.*, 2016), which will be further discussed in Chapter 7.

## 2.7 Infrared thermography

Infrared thermography is a remote mapping system which creates infrared images via absorption and distribution of radiated heat over the investigated element/structure. Objects with a temperature above absolute zero ( $-273.15^{\circ}\text{C}$ ) emit electromagnetic radiation in the infrared region of electromagnetic spectrum, which is detected by infrared (IR) camera. Infrared thermography provides a real-time pseudo colour coded image of the object, allowing the investigation of different types of structures and the monitoring of their condition in a quick and cost-effective way (Bagavathiappan *et al.*, 2013).

The origins of IRT go back to the early 1800s, when Sir William Hershel discovered thermal radiation beyond the deep red in the visible spectrum. In 1880, the first IR photographic image was obtained by William de Wiveleslie and the first IR mono-detector camera was produced. Since then IRT has been used in many disciplines like engineering, medicine and agriculture, however it has been highlighted that IRT is still not adequately known as industrial instrumentation and its application could benefit a lot of potential users (Meola, 2012).

IRT has been used to conduct building diagnostics for many years. Non-destructive and non-contact testing of the building elements is a quick method to check thermal energy of the whole structure. It can detect energy leaking from a building's envelope, missing or damaged thermal insulation in walls and roofs, air leakages around openings and

moisture damages (Balaras & Argiriou, 2002). However, as there is an interaction between indoor and outdoor environment, it is better to perform an energy building audit at night or during a cloudy day in order to minimize heat losses.

Active IRT technologies like impulse thermography and lock-in thermography were developed to investigate inhomogeneities in the structural elements near surface regions. For impulse thermography, the surface of the object is heated by IR radiator and heating and cooling down processes are recorded. Differences between temperature transient curves would allow determining defects like voids in concrete or masonry structures (Maierhofer *et al.*, 2007). Experimental and parametric studies demonstrated that this method is effective for concrete covers up to 10 cm deep (Maierhofer *et al.*, 2005). Hidden defects at various depths in concrete specimens were investigated by Cheng *et al.* (2008). While IRT images clearly identified locations of the defects; their depths were quantified with better precision using elastic wave methods.

### 2.7.1 IRT use in composite materials

FRPs have been popular in the last few decades to repair and strengthen concrete structures. A number of studies were conducted to assess the integrity of the bond between concrete and FRP, delamination of FRP and any defects occurred during laying-up and curing of FRP laminates.

Reinforced concrete beams strengthened with carbon FRP were tested in flexure and shear failure modes by Levar and Hamilton (2003). In comparison to acoustic sounding, IRT detected 25% more of the voids introduced before the test and IRT was proved to be an effective NDT way to evaluate bonding of FRP and concrete during the test as well.

Donchev *et al.* (2013) conducted an experimental study on concrete beams strengthened with carbon FRP and basalt FRP wrapping. Different types of defects were

introduced in the bond layer and IRT detected the size and geometry of the defects in an effective and quick way via external heat introduction.

## 2.8 Conclusions to Chapter 2

To date, steel shear walls with thin infill plates have been investigated by numerous researches and proved to have many advantages in terms of the excellent initial stiffness, high strength and energy absorption capacity. It was identified by Rahai & Alipour (2011) and Nateghi-Alahi and Khazaei-Poul (2012) that the effective angle orientation of carbon fibres at the angle of tension fields can improve the behaviour of shear wall plates. For all hybrid and pure FRP infill plates 45° inclination angle of fibers was used. However, very limited studies have been conducted on the use of hybrid FRP infill plates in shear wall design, which highlighted the importance of the research undertaken here.

It was identified that it is important to compare the behaviour of both Hybrid CFRP and Hybrid GFRP shear walls with respect to the load capacity and energy absorption. Additional study of the strengthening of the hybrid shear walls subjected to earthquake loading has not been conducted previously, and experimental studies in this direction would provide results and possible solutions for practical applications.

A study of the pure FRP elements as part of the hybrid shear walls structure has not been found within the scope of this reviewed literature and will provide important considerations for designing thin-walled FRP structures in structural engineering.

### **Chapter 3: Small scale testing: connections**

A study on the connections between FRP and steel elements was conducted on small scale specimens. It was conducted to find an effective way of connecting fish plate elements of steel frames and infill plates.

### 3.1 Introduction to connection tests

As described in Chapter 2, hybrid structures consisting of steel and fibre reinforced polymers are becoming popular in thin walled structures, sandwich panels and shear walls; therefore it is important to study the behaviour of these structural elements. Connections between steel, hybrid and pure FRP only structural elements are an important aspect of structural design. Different types of specimens have been tested to evaluate bolted and epoxy connection in addition to bolted specimens. The results provided can be used for seismic design considerations when structures are subjected to significant displacements.

One of the important considerations in structural design is the connection between the structural elements. EC3 (British Standards Institution, 2005b) provides a specification for designing steel bolted and welded connections. However, insufficient information is available for designing a connection between steel and hybrid structural elements. Primary connections for a least one type of FRP member with other elements can consist of mechanical joints, bonded joints, interlocking joints or a combination of them. For FRP connections design parameters like fibre orientation, stacking sequence and bolt hole geometry affect joint performance and its failure modes. FRP connections can fail by shear, tension, bearing and cleavage of the laminate or the connector (Duthinh, 2000).

The aim of the small scale connections study was to investigate the behaviour of bolted connections with and without adhesive and to investigate the effect of adding an adhesive film between steel plate and FRP layers.

### 3.2 Methodology to connection tests

#### 3.2.1 Specimen description

Each of the small specimens consists of inner and cover plates, both types of plates have dimensions of 125x70 mm. In total 42 specimens were assembled by placing the inner

plate between two 2.4 mm thick cover plates. There were seven types of inner plates: steel only, two types of hybrid plates made from CFRP and steel, two types of hybrid plates made from GFRP and steel, pure CFRP and GFRP composite plates. Three specimens of each type were tested using type 1- simple bolted connection (S1, CH1, CHa1, GH1, GHa1, CF1 and GF1) and three specimens using type 2 connection- bolted with adhesive (S2, CH2, CHa2, GH2, GHa2, CF1 and GF2). Specification of all specimens is shown in Table 3.1.

Table 3.1. Specimen description.

Type of the specimen	Connection type		Infill plate specification	Average thickness, mm
	Type 1: bolted	Type 2: bolted and adhesive		
Steel [S]	S1	S2	sp	0.68
Hybrid CFRP [CH]	CH1	CH2	[-45/+45/sp/+45/-45]	1.37
Hybrid CFRP with adhesive [CHa]	CHa1	CHa2	[-45/+45/A/sp/A/+45/-45]	1.52
Hybrid GFRP [GH]	GH1	GH2	[-45/+45/sp/+45/-45]	2.37
Hybrid GFRP with adhesive [GHa]	GHa1	GHa2	[-45/+45/A/sp/A/+45/-45]	2.16
Pure CFRP [CF]	CF1	CF2	[-45/+45/-45/+45/+45/-45/+45/-45]	1.25
Pure GFRP [GF]	GF1	GF2	[-45/+45/-45/+45/+45/-45/+45/-45]	2.30

NOTE: S- steel; A- adhesive film (EF72), -45/+45- angle of the fibres inclination

Steel specimens (S1 & S2) were made from steel plates (sp) with a thickness of 0.68 mm. Hybrid infill plates (CH1, CH2) were prepared with steel plates and two layers of prepreg CFRP at 45° inclination of the fibres on both sides. For hybrid plates (GH1, GH2) two layers of prepreg GFRP were applied. Specifications of the FRP materials with manufacturer details and properties are provided in Chapter 4.

In order to reduce early delamination between the steel plate and prepreg FRP layers, for hybrid specimens (CHa1, CHa2, GHa1 and GHa2) the additional layer of film adhesive type EF72 indicated as (A) was placed between the steel plate and CFRP or GFRP plies. Pure CFRP specimens with infill plates (CF1 and CF2) consisted of 8 layers of CFRP with 45° inclination of the fibres. Pure GFRP infill plates (GF1 and GF2) consisted of 8 layers of GFRP with the same angle configuration.

Prepreg technology was used for laminating CFRP/GFRP layers on steel shear plates. They were applied on a clean surface of steel plates, and then a roller was used to remove air entrapments between the steel surface and CFRP/GFRP. Prepared specimens were placed between two aluminium plates covered with polytetrafluoroethylene (PTFE). A polyester sheet and breather cloth covered the mould. After that, specimens were placed in vacuum bag with vacuum pump head attached. When the bag was sealed, oven/vacuum curing was conducted for 2 hours at 120°C. Pure FRP (CF1, CF2, GF1 and GF2) specimens were prepared with the same technology.

### 3.2.2 Type of connections

Each type of the inner plates was tested with two types of connections: type 1 (Figure 3.1 a) and type 2 (Figure 3.1b). In Type 1 (bolted only) connections failed at relatively low levels of loading due to reduced friction between FRP layer and steel surfaces. To improve capacity of the connection, as a second type of connection, epoxy plus™ adhesive (manufactured by Devcon ITW Polymers Adhesive) with a shear strength of 20MPa was applied between the plates in addition to the bolted connection. Before adhesive application, steel and FRP surfaces were prepared by the freeing of grease, dust and moisture. The FRP surface was abraded until it lost its gloss. When adhesive was applied plates were bolted together. Specimens were cured at room temperature for 24 hours.

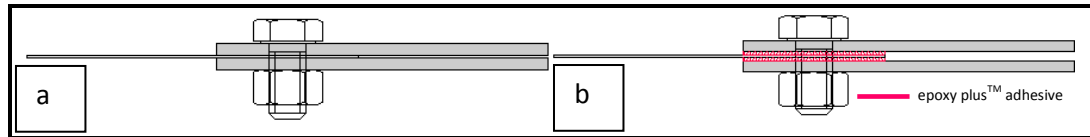


Figure 3.1. a) type 1 bolted connection b) type 2 bolted and adhesive connection.

Assembly of inner and cover elements and specification for the bolted connection is shown in Figure 3.2. Bolt holes of 10 mm were drilled through inner and cover plates and connected with M8 bolts. Hexagon M8 bolts have a minimum breaking torque of 32 N-m for A4-70 steel grade class. A4-70 grade stainless steel corresponds to a grade of 316 or 18/8/3, where “A” means cold worked austenitic stainless steel and “70” represents a minimum tensile strength of 700 N/mm<sup>2</sup> (British Standards Institution, 2009). Spacing between bolts is 40 mm, which corresponds to BS EN1993-1-8 (British Standards Institution, 2005b) provisions to be minimum 2.2 times the bolt hole diameter and edge distance is 15 mm, being minimum of 1.2 do (hole diameter).

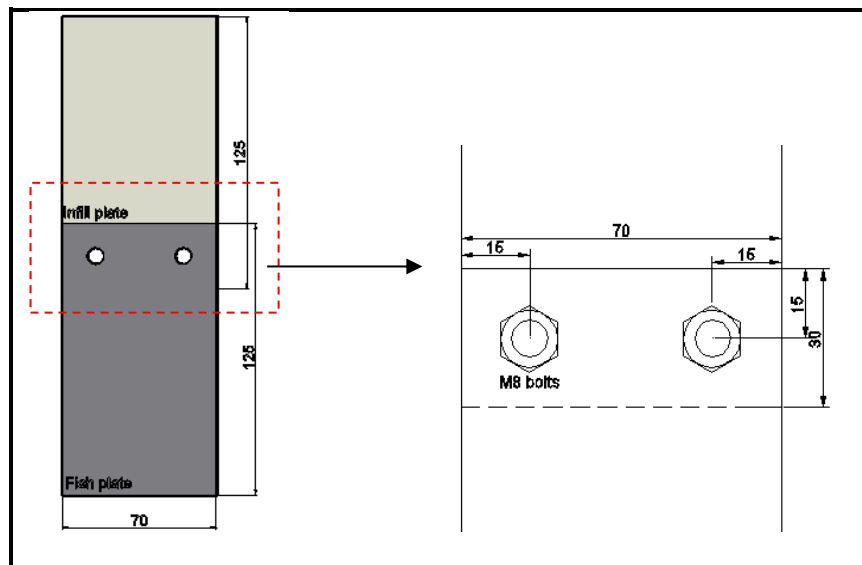


Figure 3.2. Dimensions for specimens.

### 3.2.3 Testing procedure

All specimens were tested in 100 kN Mayes tension loading machine (Figure 3.4). Displacement controlled programme allowed gradual application of displacement in a prescribed manner (Figure 3.3) until failure occurred. 0.02 mm steps with an interval of 10 seconds were applied until 0.2 mm displacement; then displacement has increased by 0.2

mm steps before reaching 1 mm, when displacement increases followed by 1 mm steps. Load corresponding to the displacement was recorded.

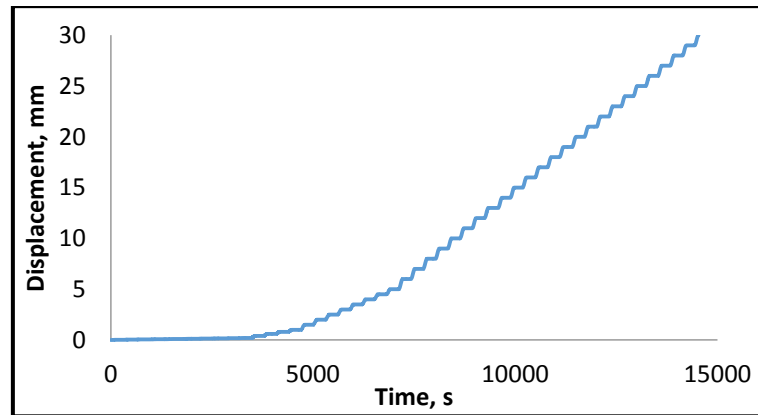


Figure 3.3. Displacement vs time.

To ensure that there is no slippage of the specimen at early stages of loading, load vs slip relationship has been recorded by attaching cermet trimmer on the cover plate with an arm attached to inner plate. When inner plate was moving with arm attached, the change in resistance showed the magnitude of slippage between connections on both sides of the specimen in the direction of the applied load.

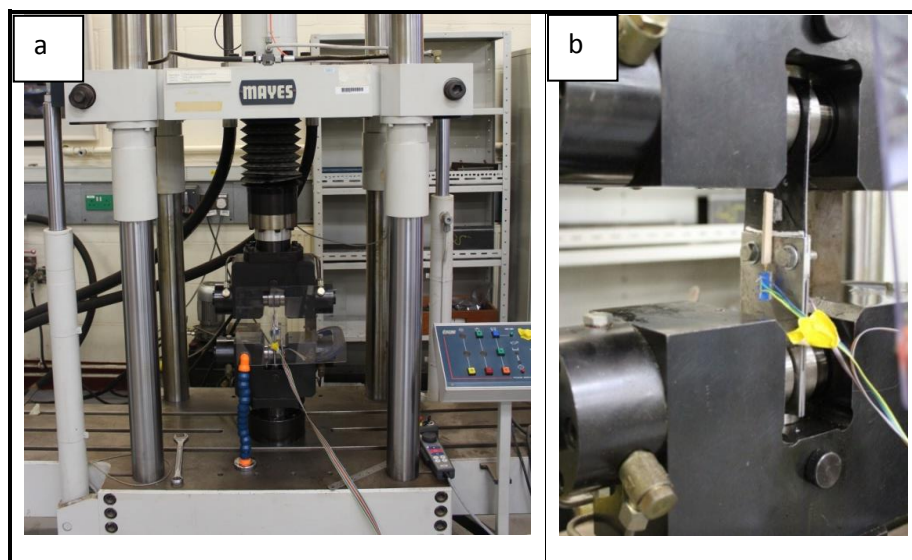


Figure 3.4. Test set up a) universal tensile machine b) test specimen.

### 3.3 Behaviour of small scale connection specimens

Tested specimens experienced fractures of the thin inner plate at the zones of connection and at zone of the plate itself, but no bolt shear failure was recorded. Each type of the plate had experienced different failure modes depending on the plate fracture, widening around bolt hole and fracture from bolt hole to specimen edge.

Steel specimens (S1) experienced destruction (Figure 3.5a) by initial longitudinal tears around holes for bolts in the direction of the load. Tearing extended to the end of the specimens and lead to separation of the small steel edges around the bolt holes. S2 samples with a layer of the adhesive at the connections (Figure 3.5b) destructed through a combination of yielding of the inner plate and yielding and tearing of the bolt connection. One specimen experienced necking failure with small displacements noticed around adhesive connection.

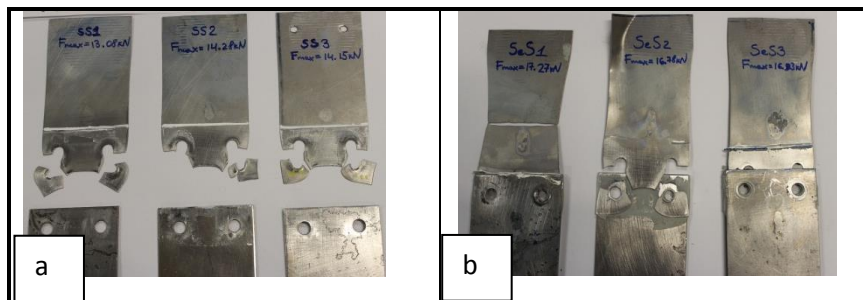


Figure 3.5. a) S1 b) S2 specimens after testing.

For hybrid specimens (CH1 and CHa1) with bolted connection failure only occurred via tear and fracture from bolt hole to specimen edge (Figure 3.6a and Figure 3.6c). Delamination between CFRP layers and steel inner plate progressed during the test. CHa1 specimens experienced less delamination during the test as an additional layer of the epoxy resin was applied between steel inner plate and CRFP.

For CH2 and CHa2 specimens with adhesive and bolted connection, initial failure occurred in the inner plate and at the beginning of the loading very small displacements were recorded at the connections. Yielding of the steel inner plate resulted in the

development of the delamination between CFRP layers and steel. For CH2 specimens (Figure 3.6b), fracture of fibres followed 45° inclination failure, with the same pattern one specimen experienced neck fracture. For CHa2 specimens (Figure 3.6b), with CFRP layers delaminated from steel plate fracture around bolt hole occurred.

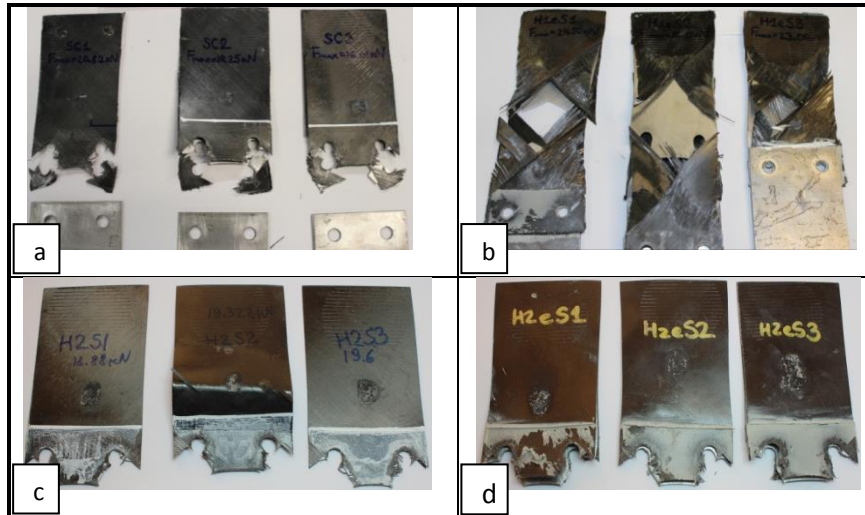


Figure 3.6. a) CH1 b) CH2 c) CHa1 d) CHa2 specimens after testing.

For hybrid specimens with GFRP material (GH1 and GHa1) with bolted connections, there was similar damage as the CH1 and CHa1 specimens. Failure of specimens occurred at the connection via tearing around bolt holes (Figure 3.7a and Figure 3.7c). For GH1 specimens, delamination between GFRP and steel plate occurred at the connection.

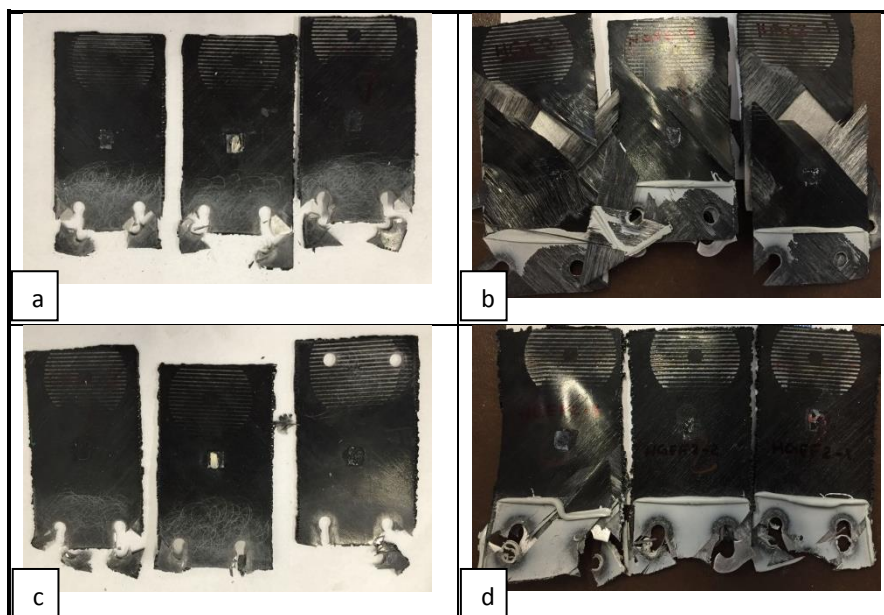


Figure 3.7. a) GH1 b) GH2 c) GHa1 d) GHa2 specimens after testing.

The GH2 specimen (Figure 3.7b) had a similar failure mode to CH2 specimen, GFRP fractured in a 45-degree angle inclination. In GHa2 (Figure 3.7d) initial displacement occurred due to the yielding of the plate, however adhesive film between steel plate and FRP layers prevented delamination. Failure of the specimen occurred at the connection.

For CF1 specimens (Figure 3.8a) failure occurred via both delamination between CFRP layers noticed around the connection and tearing around bolt holes. One of CF1 specimens failed by extension and fracture in the inner plate. For CF2 specimens (Figure 3.8b) failure delamination between CFRP layers was mainly experienced in the middle of the inner plate, small displacements were recorded at the connections at the initial stages of loading.

The GF1 specimen (Figure 3.8c) had similar damage to CF1 specimen, the specimen fractured at the connection. The GF2 specimen (Figure 3.8d) failed in the inner plate in the direction of the GFRP fibres, no tearing occurred around the bolt hole

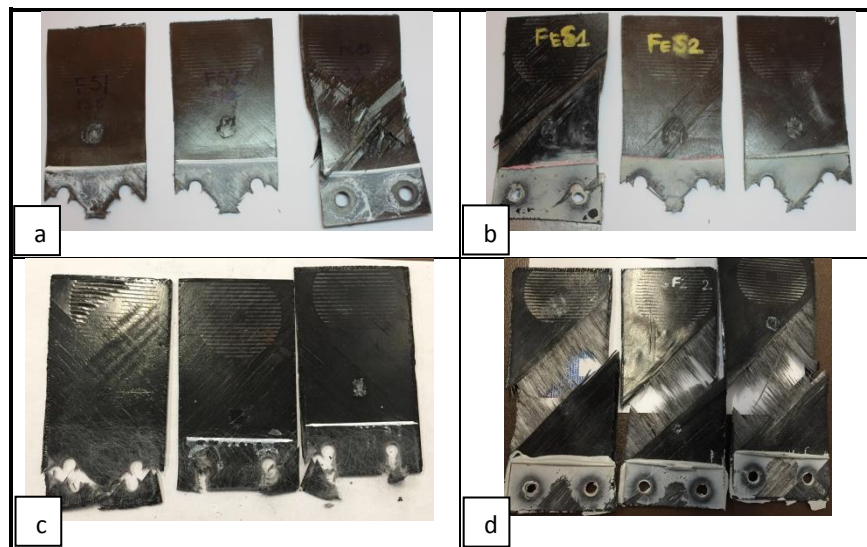


Figure 3.8 a) CF1 b) CF2 c) GF1 d) GF2 specimens after testing.

As a summary groups of specimens can be categorised in the following modes of destructions:

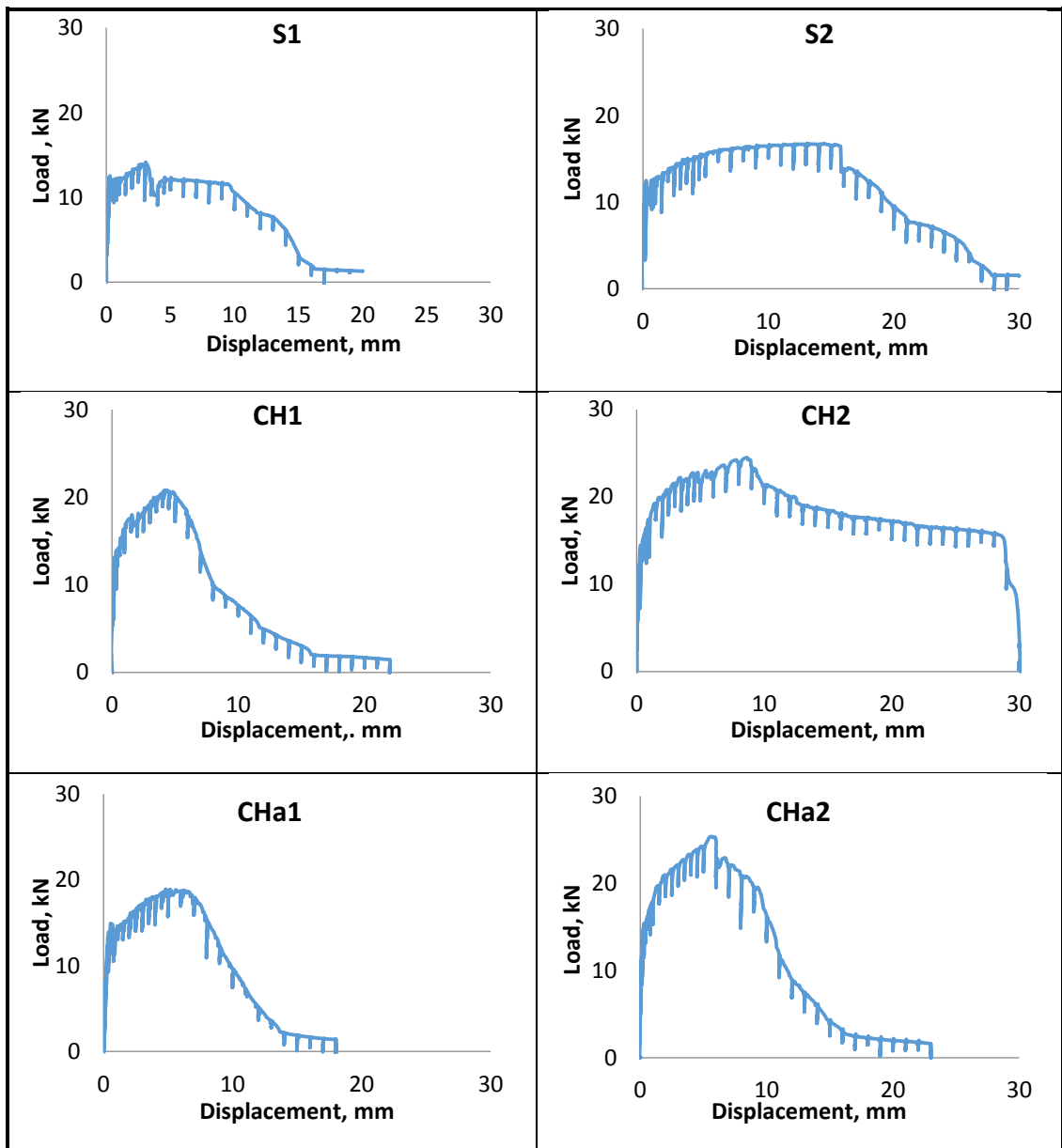
- Failure in the zone of connection only: CH1, GH1, CHa1, GHa1.

- Failure in the zone of the plate outside connections: CH2, GH2 and GF2.
- Mixed failure in the zone of the connection and outside connections: CHa2 and GHa2.

### 3.4 Small connections experimental results

Analysis of the results was made based on the load vs displacement graphs.

Examples of the load vs displacement graph are shown in Figure 3.9 for each type of specimens. Displacement in the graph is shown as a combination of the movement between the connection and elongation of the inner plate.



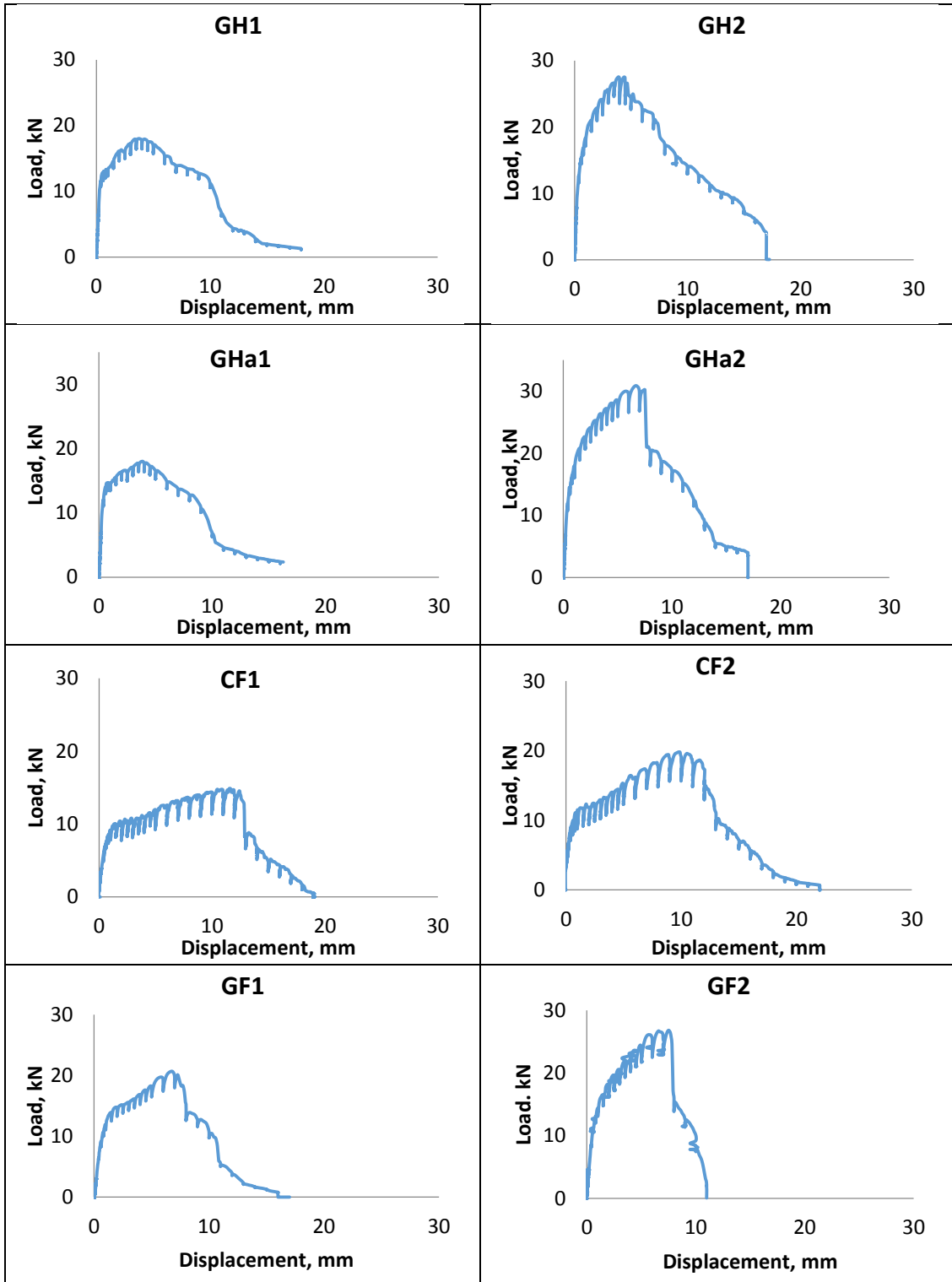


Figure 3.9. Load vs Displacement graphs each type of the specimens

### 3.5 Analysis of experimental results

Comparison between values of theoretical and experimental  $F/\Delta l$  is shown in Table 3.2. Theoretical  $F/\Delta l$  ratio is calculated with Young modulus values from tensile testing for FRP material (Table 4.3), example of calculation is shown in Appendix A. Experimental  $F/\Delta l$  ratio is obtained from Load vs Displacement graphs (Figure 3.9). Based on the theoretical values, hybrid specimens have higher values in comparison to steel specimens. Pure specimens have lower values in comparison to steel specimen due to the lower Young Modulus. Correspondence between theoretical and experimental values for steel specimens is within 10%, hybrid and pure specimens have bigger differences in values. Differences for hybrid and pure specimens are explained by slight slippage in the bolted connections with FRP material due to reduced friction in comparison to steel-to-steel type connection. These variations can also be caused by estimation and transformation of Young Modulus for the inclined fibers to Young Modulus of longitudinally placed fibers in the specimen design configuration.

Table 3.2. Comparison of  $F/\Delta l$  values for specimens

<i>Specimens</i>	<i>Theoretical <math>F/\Delta l</math> [kN/mm]</i>	<i>Experimental <math>F/\Delta l</math> [kN/mm]</i>
S1	91	84
CHa1	119	94.1
GHa1	105	51.8
CF1	45	21.4
GF1	23	17.3

Based on Figure 3.9, it can be seen that specimens with type 2 connection (bolted and adhesive) had increased load capacity. By estimating the area under load vs displacement graphs to the same displacement, all specimens with type 2 had more ductile behaviour. Specimens with bolted and adhesive connections increased in the area of more than 20%, with the highest increases for CHa and GHa specimens of 64% and 72%

respectively. The average ultimate capacity of three specimens from each type of the specimens is plotted in Figure 3.10. All types of the specimens with type 2 connections had an increase in the ultimate load of more than 20%.

Hybrid specimens GH2 and GHa2 had the highest increase in ultimate load in comparison to other specimens. CH2 and CHa2 specimens had an average increase in ultimate load of 30% in comparison to CH1 and CHa1 specimens respectively. Ultimate load of GH2 specimens increased by 56% and the ultimate load of GHa2 increased by 76% in comparison to the corresponding ultimate load of the same type inner plates with a bolted connection only.

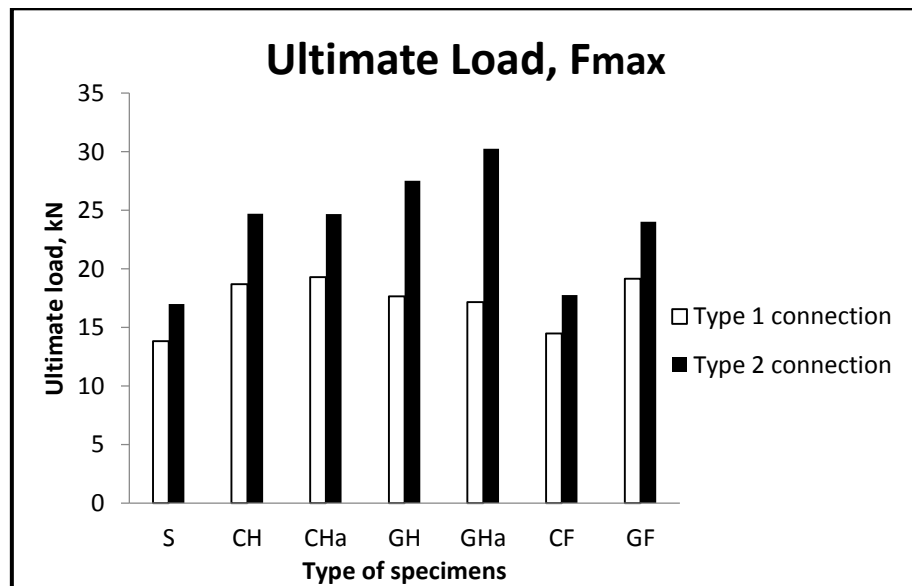


Figure 3.10. Ultimate load for small scale specimens.

Hybrid specimens achieved higher ultimate load in comparison to other specimens. For type 1 bolted connection hybrid specimens with CFRP had highest ultimate load results, 19.3 kN for CHa1 specimen. For type 2 connections, adhesive hybrid specimens with GFRP had the highest ultimate load results, 27.5 kN and 30.24 kN for GH2 and GHa2. It is important to note that the addition of the adhesive film between steel inner plate and FRP layers did not increase the ultimate load capacity of the specimens significantly. The

biggest difference of 8% between specimen with and without adhesive film was noted for GH2 and GHa2 specimens.

Steel specimens (S2), pure specimens (CF2) and GF2 had an average increase in ultimate load of 24% in comparison to the same type specimens with type 1 connection. Pure CF specimens with type 1 and type 2 connections had similar ultimate load in comparison to steel specimens. Ultimate load results of GF2 specimens were higher than S2 and CF2 specimens - its value reached 24 kN.

### 3.6 Conclusions to Chapter 3

Testing of steel, hybrid and pure FRP specimens with *bolted only* and *bolted with adhesive* connections demonstrated that it results in different modes of destruction: in the zone of connection, in the zone outside connections or mixed when damage was occurring in zones in the area of connection and outside connections. Hybrid specimens (CH2 and GH2) without adhesive layer between steel plate and FRP layers resulted in inner plate failure. For hybrid specimens (GHa2 and CHa2) adding a layer of adhesive increased the capacity of the inner plate and resulted in the mixed mode of failure. Based on the results and analysis, the following conclusions can be drawn:

- Applying adhesive in the connection increases the capacity of the specimen for all groups of tested specimens; the highest increase was achieved for GHa2 specimens.
- The average increase in ultimate load of 24% was achieved for S2 and pure FRP specimens. For hybrid CFRP specimens 30% increase and for hybrid GFRP 66% increase in ultimate load was recorded.
- The highest ultimate capacity is monitored for hybrid specimens GH2 and GHa2, which was 27.52 kN and 30.24 kN respectively.

## **Chapter 4: Experimental test setup for shear wall specimens**

Chapter four describes the setup used in the experiments of newly developed shear wall specimens and strengthened specimens. The testing equipment was re-developed and calibrated. This Chapter provides a description of the testing equipment, laboratory instrumentation; specifications for shear wall specimens and guidance about test procedure necessary for implementation for each specimen.

### 4.1 Experimental set-up for shear walls

Single-storey medium-scale samples were constructed and tested under quasi-static loading. The same set-up was used for testing newly developed shear wall specimens and strengthened shear wall specimens as well.

A horizontal displacement was applied via a screw jack and controlled by linear variable differential transformers (LVDTs) and cable displacement sensors (CDSs). A computer testing programme was designed to conduct an experiment with prescribed amplitudes, number of cycles and frequency. Experimental investigations were conducted to evaluate the seismic characteristics of shear wall systems. The seismic characteristics/parameters investigated include:

- Maximum ultimate lateral load capacity
- Stiffness of the system
- Energy absorption capacity
- Failure modes of the system

A description of the failure modes and analysis of the seismic parameters is described in Chapters 5 and 6.

### 4.2 Description of the equipment

The shear wall specimens were tested under quasi-static cyclic displacement controlled loading in the in-plane horizontal direction. The testing equipment used to test specimens was initially designed by Ahmed Maleki, PhD student at Kingston University London (Maleki, 2014). Computer and measuring systems were modified and calibrated prior to each test.

The set-up of the testing equipment and testing of the specimens was carried out in Structures Laboratory at Kingston University. Preparation of the hybrid steel/FRP and pure FRP infill plates was done in Composite Laboratory at Kingston University London.

The testing system (Figure 4.1) shows different components, which can be divided into four main groups:

- Testing Rig: reaction frame, lateral supports
- Loading equipment: inverter, screw jack, electric motor, gear box
- Computer system: datataker (DT85G), multiplexers CEM20 and laptop
- Measuring system: load cell, LVDT, CDS, DTI and strain gauges

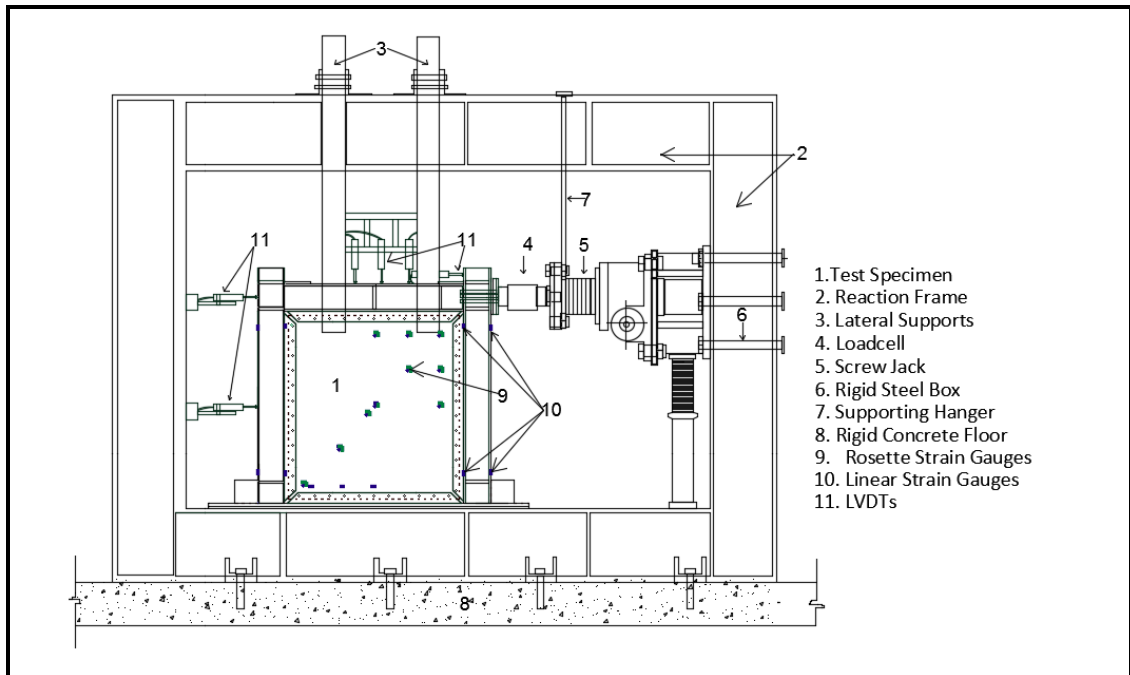


Figure 4.1. Diagram of testing equipment.

#### 4.2.1 Testing Rig

The testing rig consisted of a reaction frame and lateral supports (Figure 4.2). The main function of the reaction frame was to provide a stable and secure position for the assembled mechanism in a controlled environment. It was built from welded rectangular hollow cross-section steel columns with dimensions of 308 x 320 mm and steel I-beam

sections of 308 x 328 mm, with a flange width of 25 mm and web thickness 15 mm. Webs of upper and lower I-beams were stiffened at both sides every 500 mm along the beam.

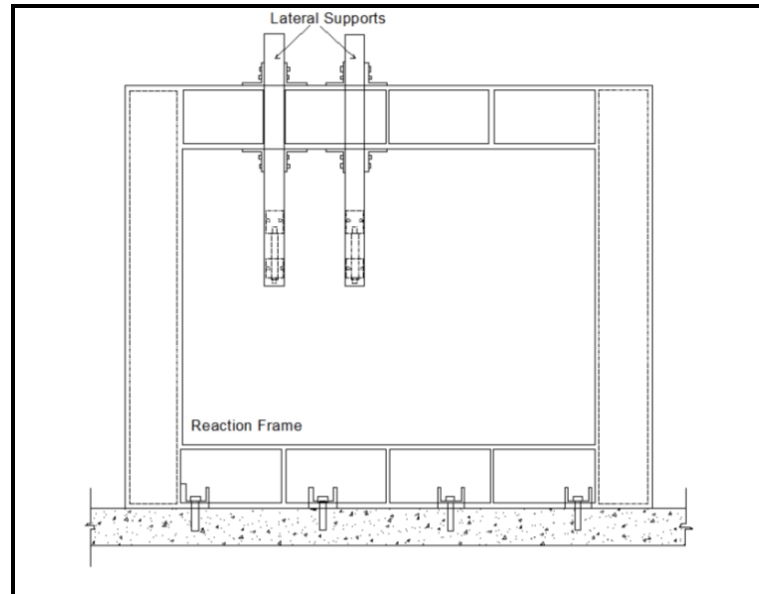


Figure 4.2. Testing rig.

The rigidity of the frame prevents any possible movements or outside factors occurring during experimental testing, which could affect the accuracy of the results. The stability of the frame was also checked with simulation conducted with ABAQUS software. The strong frame was modelled with shell elements; the analysis concluded that deformations of the frame during the test will not affect measurements of the deflections of test specimens (Maleki, 2014). The reaction frame was clamped and bolted firmly to the existing reaction strong floor with an anchor type connection to secure from sliding displacement, shifting or overturning.

The lateral bracing system consisting of lateral supports was introduced. It was made from four HS rectangular steel hollow cross-section beams with dimensions of RHS 120 x 120 x 12 mm. They were firmly bolted to the upper I-beam of the reaction frame with two rollers on each side of the specimen being fixed with angle bars (Figure 4.3). The main purpose of the lateral supports was to prevent the out-of-plane buckling of the sample as it was moving smoothly and freely between the steel rollers throughout the test. In total four

steel rollers were placed between the brackets with their position being adjusted for each specimen.

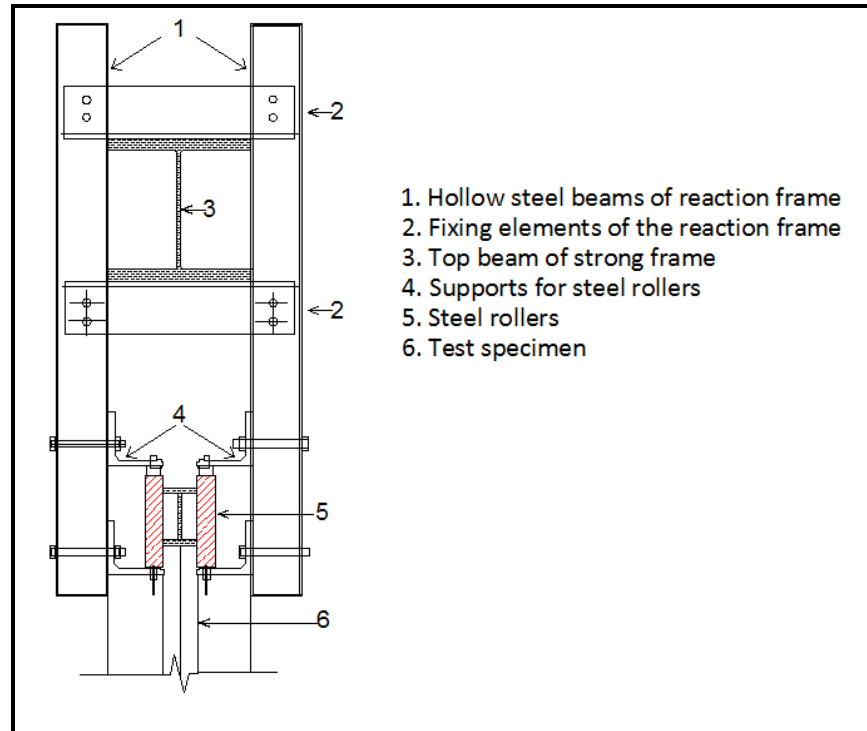


Figure 4.3. Lateral support system.

#### 4.2.2 Loading Equipment

The loading system consisted of a screw jack, an electric motor, a gear box, a cooling system and an inverter. Figure 4.4 shows the arrangement of the equipment used to apply quasi-static loading.

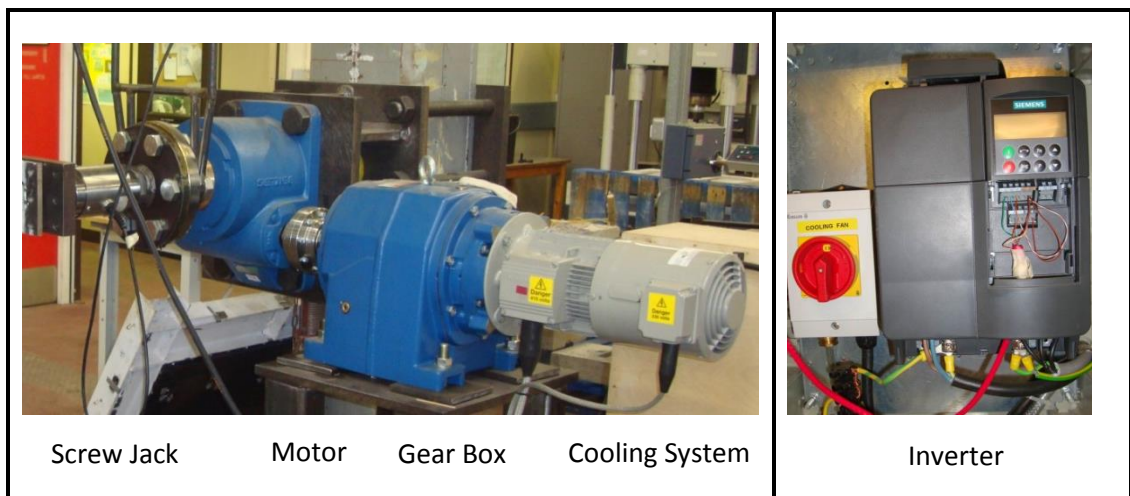


Figure 4.4. Loading system.

The screw jack Radicon/David Brown Series (Benziler Screw Jack model BD) plays an important role in the system, which require quasi-static loading. It has a maximum capacity of 500 kN force. Movement of the screw jack allows pushing and pulling of the frame in a cyclic mode. The screw jack was connected to the rigid box using four HSFG bolts M42. The rigid box is made from 35 mm thick square flat plates tightly fastened to the reaction frame with six HSFG bolts M42 (Figure 4.5).



Figure 4.5. Screw jack support.

A Siemens inverter Micromaster 420 (Figure 4.4) was used to apply screw jack's stroke via sending signal to the motor. A sinusoidal horizontal load was applied in both directions for the quasi static test. The inverter can be operated manually to move forward and reverse frame, however to move the specimen in a controllable manner, a computer user-defined programme was made. The inverter was connected to a datataker as a digital connection.

The electric motor used for the test is "Radicon/David Brown Series M". It can produce 121 HP (90 kW) power, which is adequate for the screw jack to operate at the desired rate and force. It was individually mounted perpendicular to the strong frame. To prevent overheating of the motor due to long and frequent use, a cooling system was installed. A gear box was used to reduce the speed of the motor to the appropriate level. It

was placed between the motor and the screw jack with a flexible gear type coupling connection (series X).

### 4.2.3 Logging equipment

The logging equipment consisted of the datataker DT85G, multiplexers channels expansion modules (CEM) with additional 20 channels and a laptop (Figure 4.6). The datataker DT85G series 2 was used as the acquisition and logging system during the testing. It was connected to a laptop with an Ethernet cable and a DtUSB package was installed. Three CEM20 were used to provide 20 additional analog terminals each.

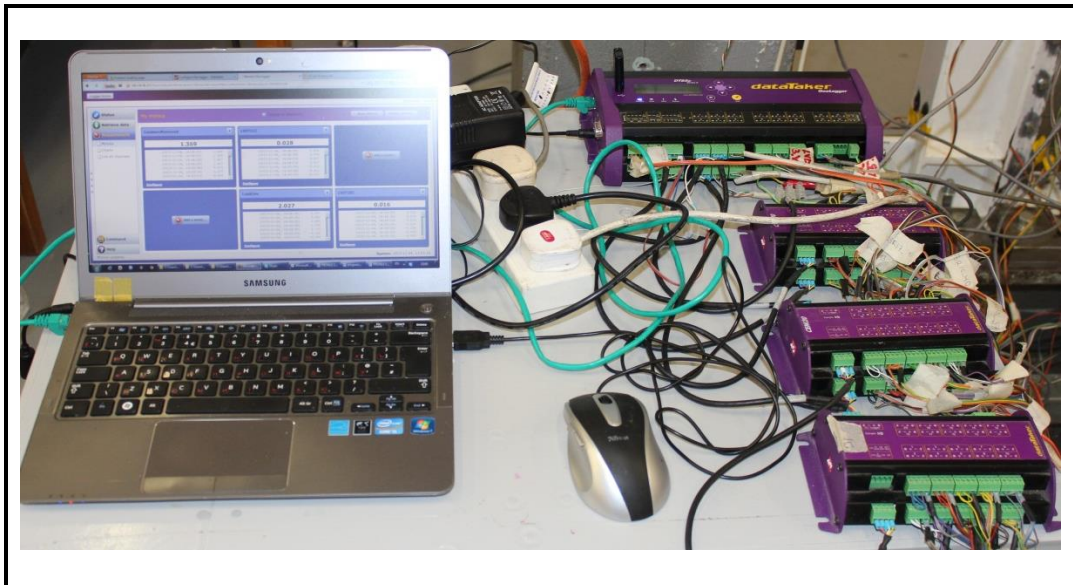


Figure 4.6. Datataker DT85G and three multiplexers CEM20.

The datataker was used to develop a programme to simultaneously control and monitor the testing rig and to measure and record specified data. The user's Manual DT85/85G (2011/2012) provided important information how to operate the datataker and to create a programme. A technical specialist from Grant Instruments (Cambridge) Ltd was consulted about specific questions in regards to the programme.

Initially, a software called DeLogger was used for the testing, which was later replaced by software called DeX as it provided a simpler connection to the datataker and

gave more options to modify the programme. DeX is a user friendly web-interface based software used to configure a test programme.

DeX was used as a configuration builder with inbuilt graphical controls. Each measurement was defined as a schedule and channel, for each piece of equipment their required parameters and terminals were defined. Each programme contained BEGIN and END commands to run and complete the cycle. It was designed to operate the equipment, to control the loading amplitude and at the same time to collect and record results such as loading level and strain gauges data.

The inverter was connected to a datataker as a digital terminal to control the movement of the screw jack. Cables from the CDSs, LDSs and strain gauges were connected as analogue terminals to the datataker and three CEM20 multiplexers. Prior to test set up the equipment was calibrated. The required scaling factors were introduced in the datataker DeX programme. Programme for datataker and channel types and wiring configurations can be found as Appendix C. Measurements obtained during the testing were recorded and saved as CVS files.

#### **4.2.4 Measuring instruments**

Measuring equipment was used to obtain several parameters and data during the testing. The load was measured with a loadcell; the displacements were measured with the aid of LVDT, CDS and dial test indicator (DTI), strain gauges were used to obtain the strain data from the specimen.

##### **4.2.4.1 Loadcell**

A NovaTech (F204) universal bi-directional loadcell was used for experiments with a maximum capacity of 500 kN. It was used to measure the applied load for any specific displacement during the experiment. It was placed between the screw jack and the shear

wall frame, the connection is shown Figure 4.7. From one side the loadcell is welded to a circular plate with locking nuts, which is bolted to the screw jack system. This flexible connection is supported with a hanger and transverse movements can be applied avoiding vertical displacements of the loading device. From the other side, it is welded to a rectangular plate, which is bolted to the frame connection plate when the specimen is installed. The position of the frame connection plate was levelled and welded accordingly for each specimen.

Centrally transmitted load is applied to avoid generation of out-of-plane loading. A secure and fix position of the loadcell prevents the occurrence of any gaps between screw jack and frame, eliminating breakages and buckling.

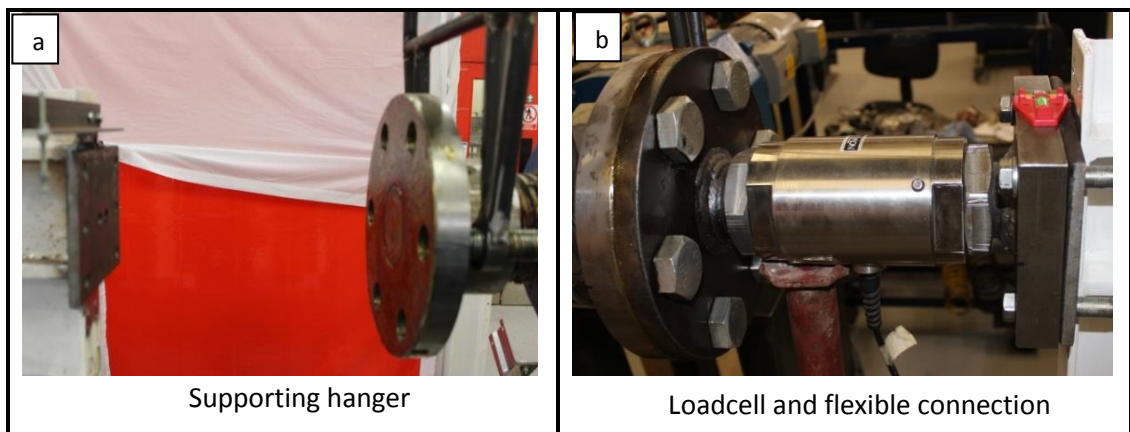


Figure 4.7. Loadcell configuration a) location for loadcell b) levelling of loadcell.

The loadcell was scaled under compression and tension (Figure 4.8a and b). The load was applied with Mayes tensile machine and signal was measured with datataker (Figure 4.8c and d), to introduce scaling factors. The difference between applied load and datataker was within 5%.

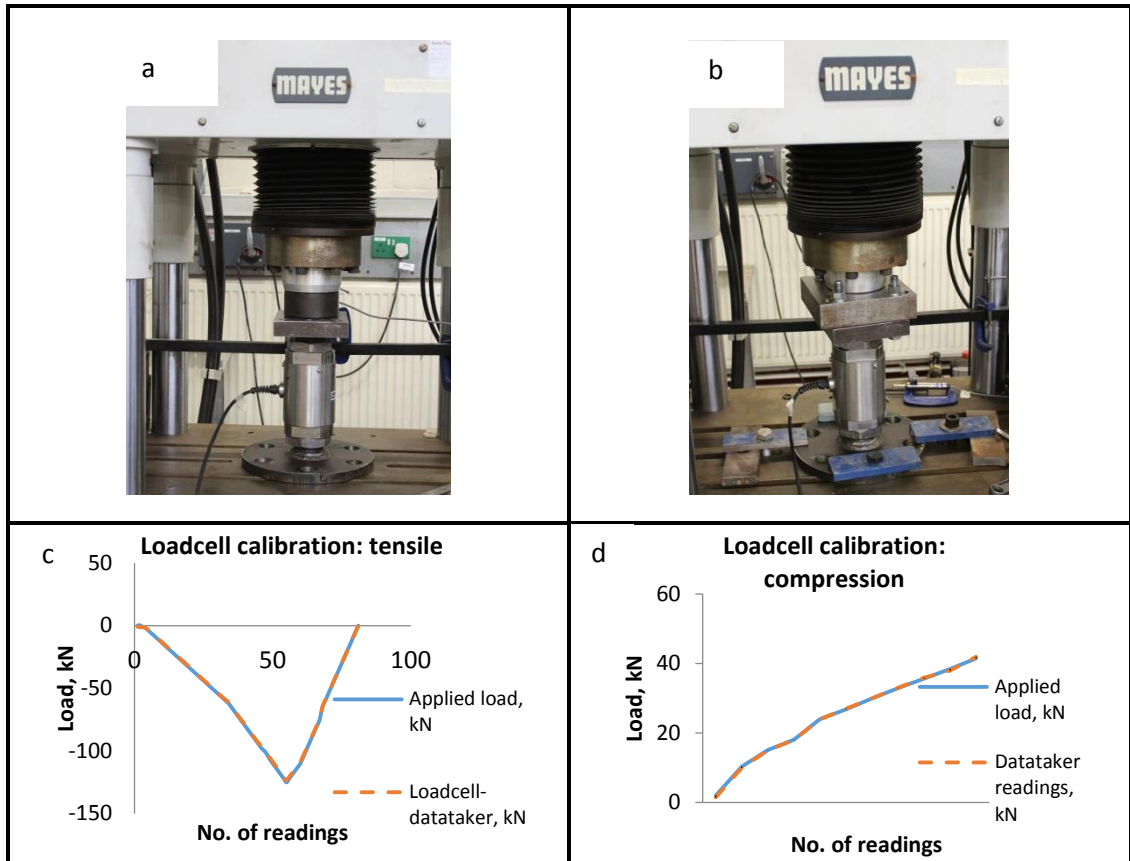


Figure 4.8. Calibration of loadcell a)&c) tension b)&d) compression.

#### 4.2.4.2 Linear Displacement Sensors

The measurement of the horizontal displacement was used as a control parameter for a test. Two types of the LVDTs were used manufactured by Vishay Micro Measurements and Schreiber. The Schreiber SM40-7 LVDT has a maximum range of 120 mm. To provide a constant voltage input during a test, an amplifier with a 22.2V excitation was connected to the datataker and wired to the LDVT.

Linear variable displacement transducer- LVDTs- (Vishay HS-25) were used for small measurements with a full displacement range of 26 mm. Model HS-25 LVDT's non-linearity is 0.35% of the full scale (FS), which is less than 0.091 mm (Vishay, 2014). A fully active 350-ohm strain-gauge bridge is used to identify spindle displacement displaying an infinite resolution and excellent linearity. Its bridge excitation is from 2 to 10V.

Four measurement devices were installed to the plate attached at the top of the column where loading is applied (Figure 4.9). LVDT-1 (manufacturer by Schreiber SM40-7) was used to measure larger displacements, LVDT-2 (manufacturer by Vishay) was used to measure displacement up to 5 mm. A mechanical dial test indicator (DTI) was used for manual control of applied displacement.

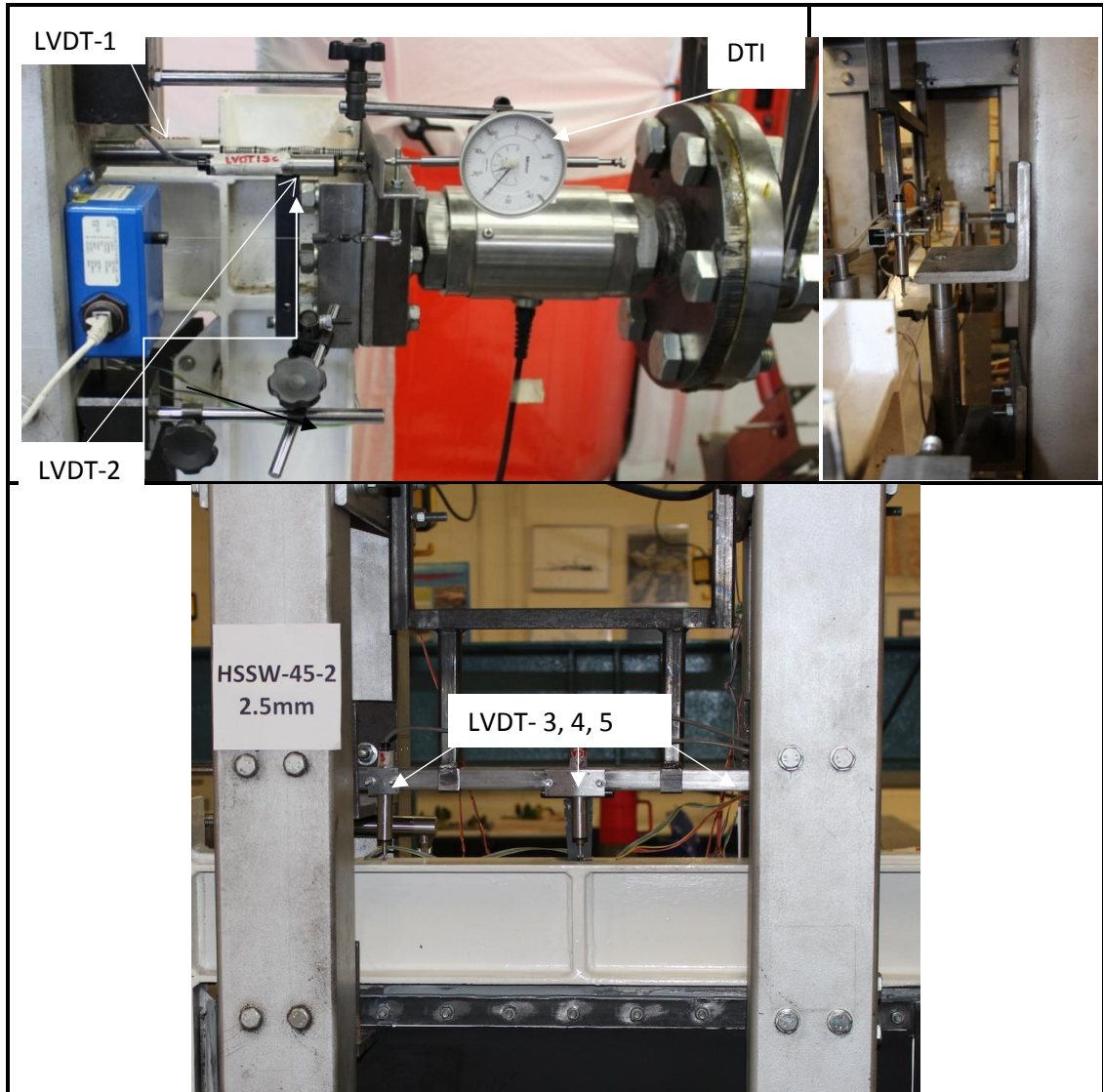


Figure 4.9. Displacement measurement.

To measure vertical displacements, which are experienced by the top beam of the shear wall during testing, three LVDTs (3, 4, 5) were fixed in the frame which allows measurement of vertical movement to the specific points of the top flange during the process of testing. Other LVDTs were installed to measure displacement on the side of the

column where load is applied and at the middle of the columns of the SW, their location is indicated in Figure 4.9.

Prior to testing, the LVDTs were calibrated and scaling factors were obtained to input them in the datataker programme. To obtain scaling factors, the LVDTs were connected to the datataker as a bridge connection, then they were placed in a specially designed testing rig. Output voltage signals were taken for a few readings with a known thickness of slip gauge blocks. Graphs with physical and signal coordinates were plotted as a linear relationship, to obtain scaling factors. Then polynomial scaling factors were introduced in the datataker programme

#### 4.2.4.3 Cable- Extension Displacement Sensor

CDSs were used as additional displacement measuring equipment. Model CDS-10 produced by Vishay Micro- Measurements provided a maximum cable extension of 10 inches or 254 mm. The accuracy of CDS is 0.15% of FS, which corresponds to 0.381 mm. When retractable stainless steel cable is extended, it exhibits linearly proportional voltage signal. Their resistance and maximum supply voltage are  $500\Omega$  and 30V respectively, which are specified in the datataker programme.

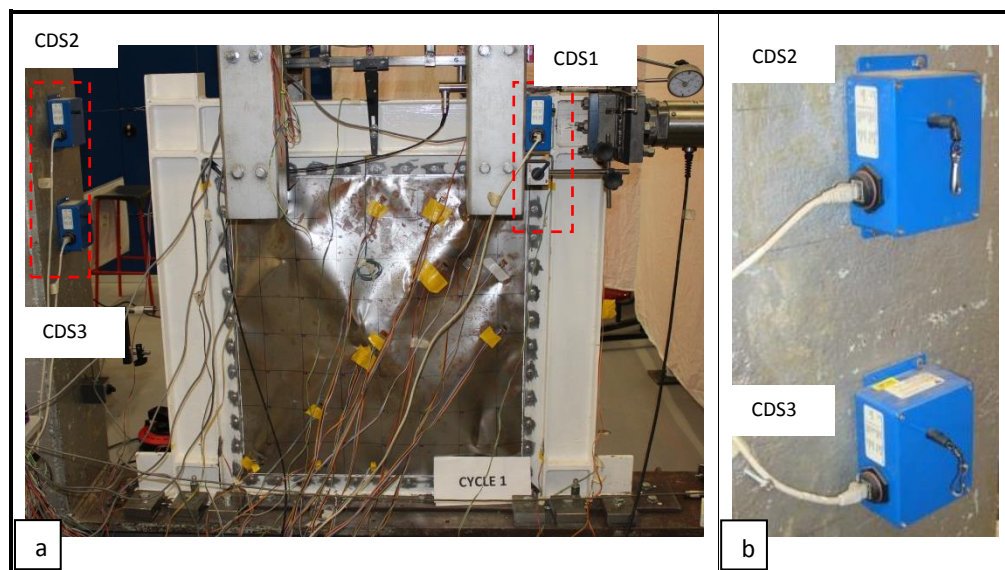


Figure 4.10. Positioning of the CDS. a) test set-up b) CDS Positioning.

Three CDSs (Figure 4.10) were connected to the datataker and programmed to measure the original position of the frame and the readings during the test in order to calculate the final change in displacement. One of the CDSs was attached to the lateral support next to the loading equipment; other two CDSs were located on the other side of the specimen to measure the corresponding horizontal displacement.

A similar procedure was used to calibrate CDS 1, CDS 2 and CDS 3 as measuring horizontal displacements. They were connected to the datataker as a voltage signal. Several output signals were taken for 0 mm measurement and maximum displacement to determine the scaling factors.

#### 4.2.4.4 Strain gauges

Linear and rosette strain gauges were used during the testing to obtain strain data: CEA-06-240UZ-120 (linear), CEA-06-120CZ-120 (rosette), CEA-06-250UR-350 (rosette). These strain gauges have encapsulated grids and exposed solder tabs. CEA series gauges manufactured by Vishay have large, copper-coated tabs allow soldering leadwires directly to the gauge. Properties of strain gauges used according to Vishay specifications (Vishay, 2014c).

Linear and rosette strain gauges were attached to the frame and infill plate using the same technology. Firstly, the position of the strain gauges was marked with a cutting knife. Then the surface where strain gauges were to be attached was prepared. The surface was roughened with sand paper, and then it was cleaned with an IPA cleaner and dust remover. The strain gauge was placed with the aid of tweezers to the surface layered with instant adhesive. The strain gauge's position was adjusted when wax paper was placed at the top of it and left to cure for 30 min. After that, the terminal of the strain gauges was cleaned to remove their protective layer. Terminals to wire strain gauges were prepared and soldered with a soldering instrument. To make sure that wire would not disconnect later, the wire

was secured via sealer tape to the surface of the shear wall. Finally, the resistance was checked with a digital multimeter. The scheme for application of strain gauges is shown in Figures 4.11, 4.12 and 4.13.

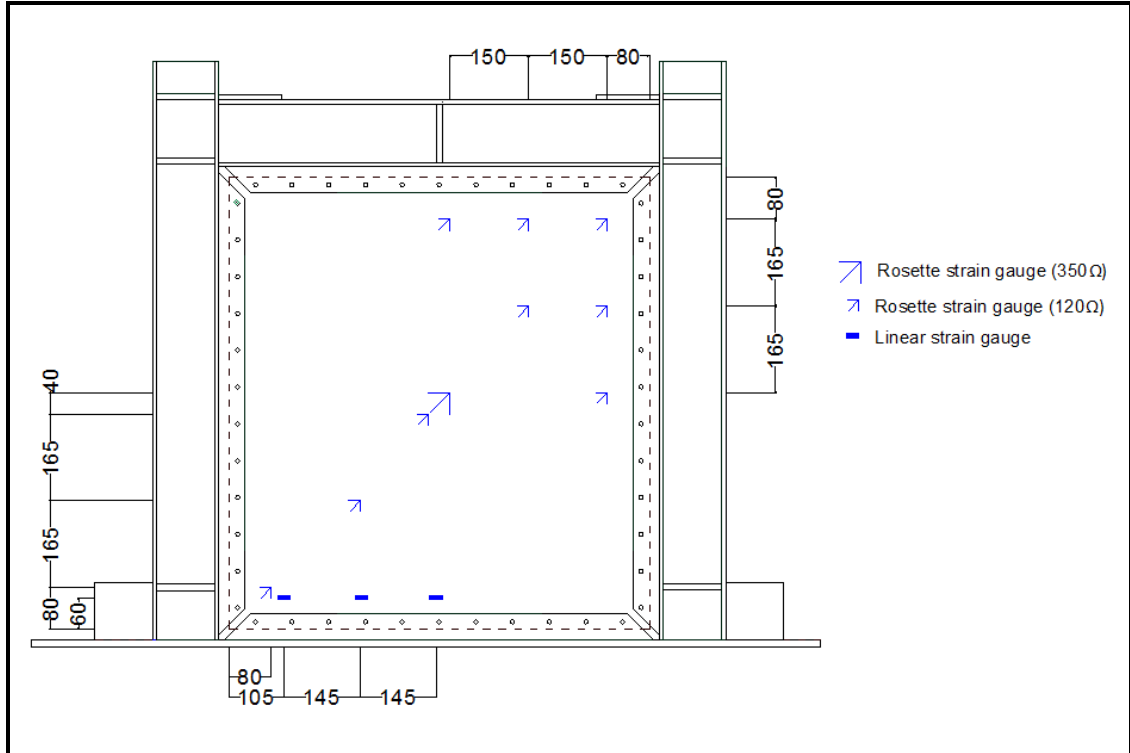


Figure 4.11. Strain position on the infill plate.

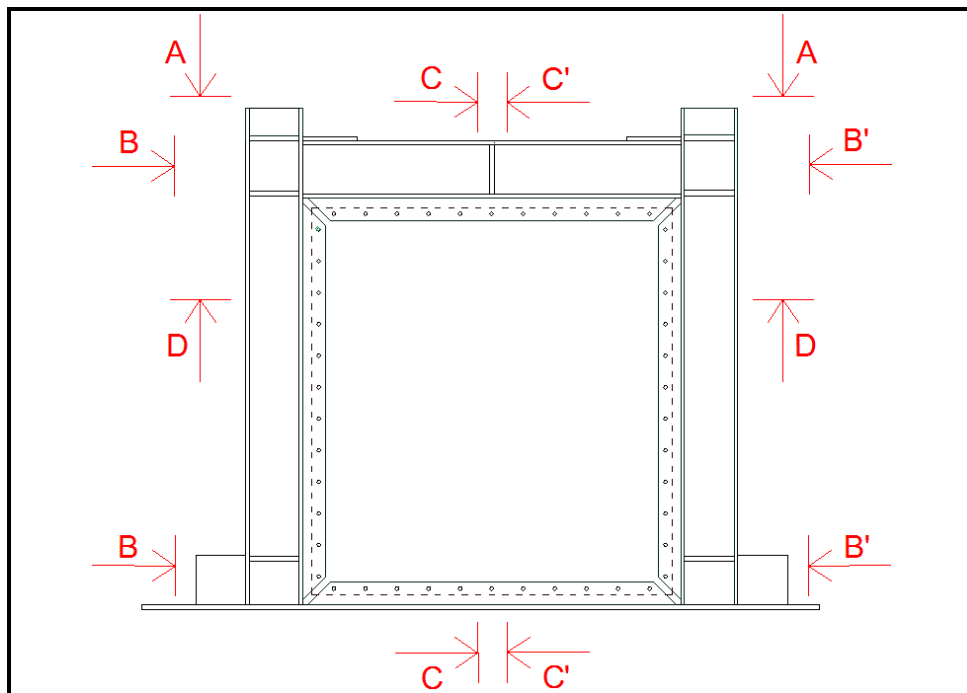


Figure 4.12. Scheme for strain gauge attachment on the frame.

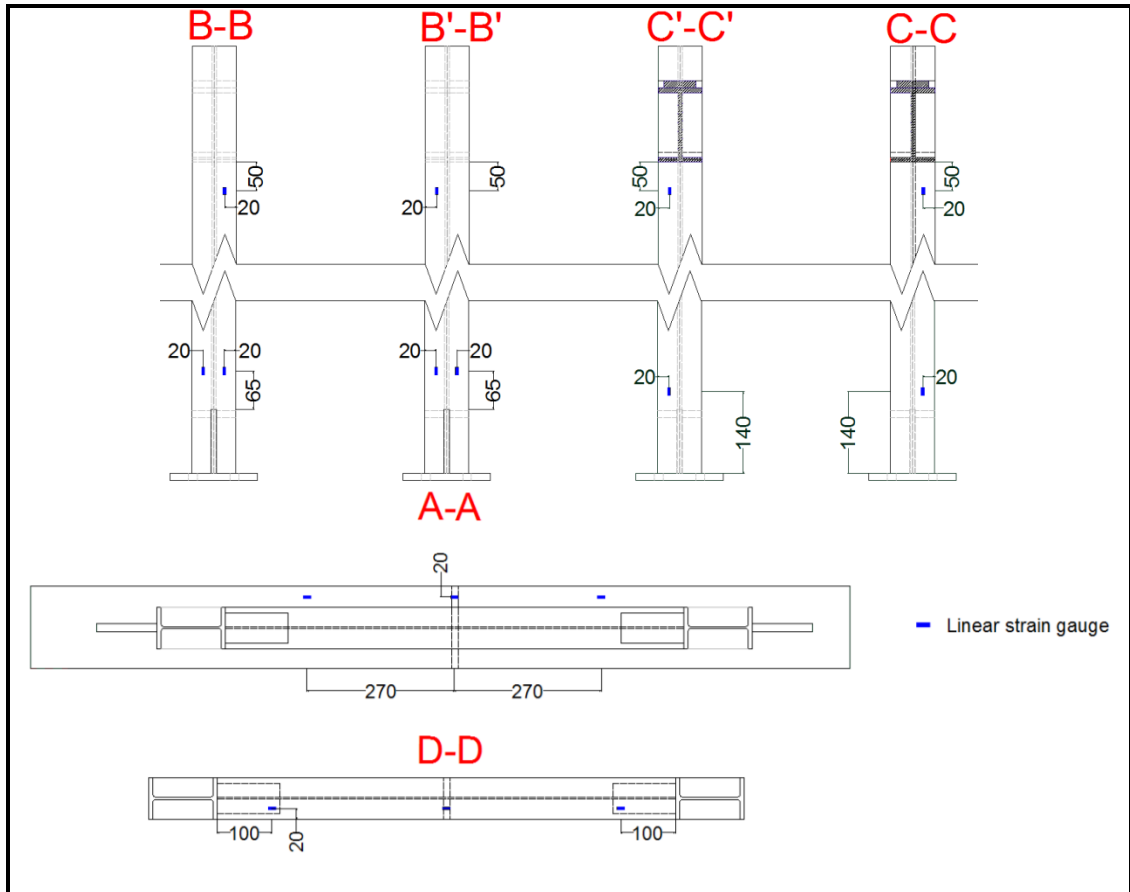


Figure 4.13. Scheme for strain gauge attachment on the frame (top and side section).

### 4.3 Shear wall specimen specification

Single-storey medium scale specimens were tested in the project (Figure 4.14). The steel frame and infill plate were made from cold reduction steel; the length between centre to centre of the column was 965 mm. Shear wall scaled models were designed at Kingston University London and manufactured by Cannon Steels Ltd. Primary fish plates were welded continuously to the steel frame. Prior to the test, the shear wall specimens were prepared in several stages: preparation of the steel frames and preparation of different types of infill plates.

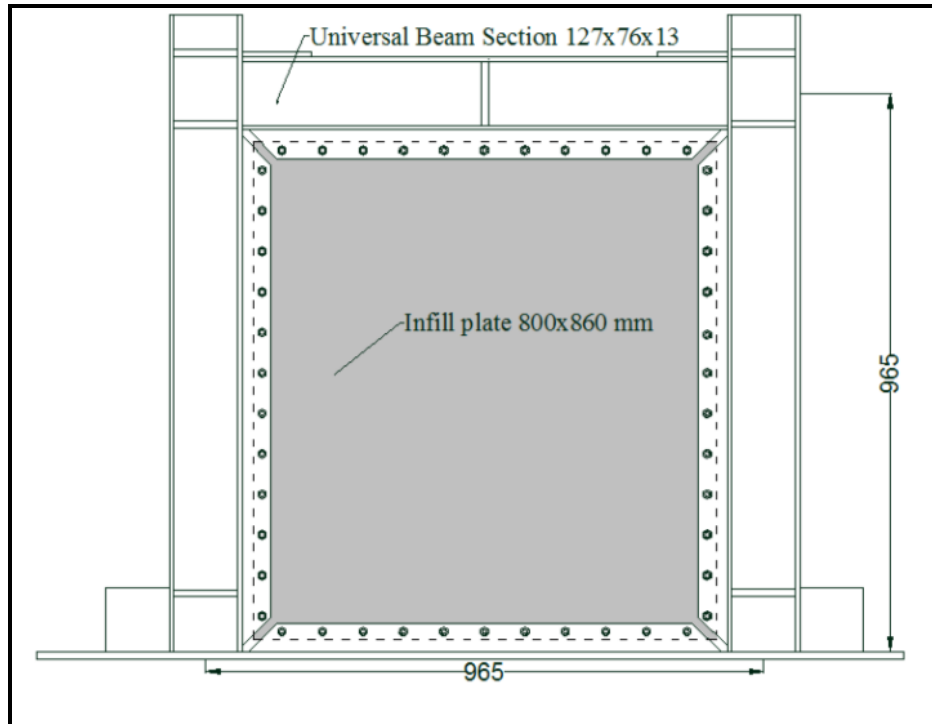


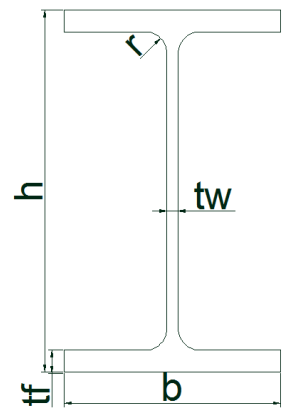
Figure 4.14. Dimensions of single-storey shear wall specimen.

#### 4.3.1 Steel frames specification and preparation for testing

The steel frames tested in this study were 1/3 scaled model of a shear wall with a height of 1025 mm and width of 1090 mm. The steel frame members consisted of two columns and beam made from Universal Beam Section 127 x 76 x 13 mm (S355 grade). They were fabricated, assembled and welded by Cannon Steels Ltd. Properties of British Universal Beam UB 127 x 76 x 27 mm section are shown at Table 4.1.

Table 4.1. Properties of UB 127 x 76 x 13 mm (After British Standards Institution, 2005c).

<i>Dimensions</i>					
Section Depth [h] (mm)	Section Width [b] (mm)	Web thickness [tw] (mm)	Flange thickness [tf] (mm)	Sectional Area (cm <sup>2</sup> )	Weight/ mass per metre (kg/m)
127	76	4	7.6	16.5	13
<i>Static Parameters</i>					
Moment of Inertia		Section Modulus			
I <sub>x</sub> (cm <sup>4</sup> )	I <sub>y</sub> (cm <sup>4</sup> )	W <sub>x</sub> (cm <sup>3</sup> )	W <sub>y</sub> (cm <sup>3</sup> )		
473	55.7	74.5	14.7		



Three types of stiffeners were used to increase the bending resistance of the steel frame, which were welded with a custom weld to the position shown in Figure 4.15.:

- type A (110x35x15 mm) x 14No. stiffening flanges of the I-beam
- type B (115x55x10 mm) x 2No. stiffening two top flanges of the I-beam
- type C (110x110x15 mm) x 2No. welded to the columns and base plates.

The steel frame columns and stiffeners of the shear wall were welded to the base plate, which was used to fix the shear wall specimen to the strong frame. In addition to high tensile bolts (8.8 N-m) M14 and M10, four clamps were used with M16 bolts to provide additional fixing.

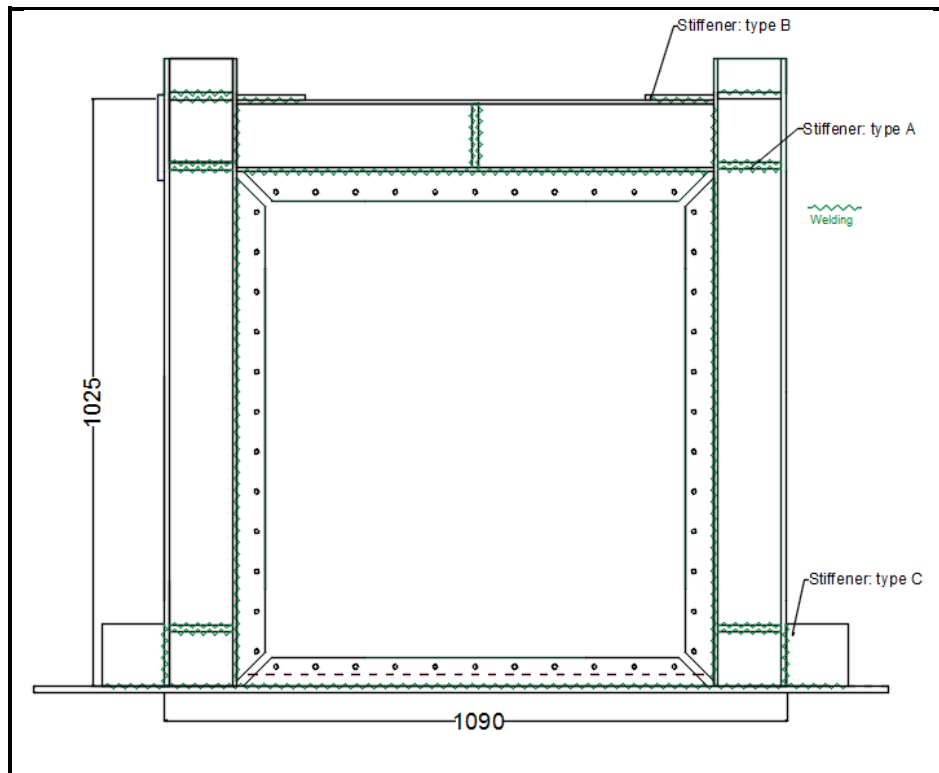


Figure 4.15. Dimensions of sample.

Prior to the testing, the steel frames were cleaned by removing rust with a Bosch angle grinder and a wire brush. For fine removal of rust finishing sand paper was used. IPA cleaner/white spirit was used to prepare the surface for painting and removing dirt and oil stains. Hammerite metal smooth white paint was coated on the boundary elements,

stiffeners of steel frame to prevent rust and did not require priming agent or an undercoat. The strain gauges were attached and wired, as it was specified in section 4.2. Seven steel frames were prepared for testing.

### 4.3.2 Infill plates

Three types of plates were prepared: steel only, hybrid and pure infill plates. Their dimensions are 800 by 860 mm.

#### 4.3.2.1 Steel infill plates

A control infill plate was made from cold rolled steel sheet. The thickness of the infill plate was 0.8 mm. S275JR grade steel infill plates were used, with a characteristic yield strength of 275 MPa and a guaranteed tensile strength of 400-410 Newtons per m<sup>2</sup>. Pre drilled holes of 10 mm were made by Cannon steel for M8 bolted connections with spacing of 70 mm. Steel infill plates (Figure 4.16) were cleaned with acetone. A grid of 100x100 mm was drawn on the surface of the infill plate to observe out-of-plane buckling. The position for strain gauges was marked.

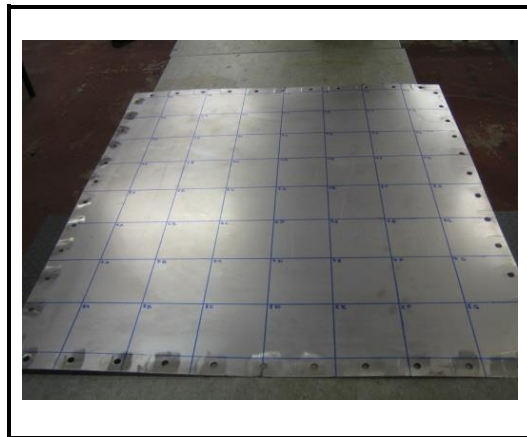


Figure 4.16. Steel infill plate.

#### 4.3.2.2 Hybrid infill plates: steel/GFRP and steel/CFRP

In the hybrid specimens the same steel frames were used but the infill plates were prepared by symmetrically laminating a steel plate (0.8 mm thick) with two layers of unidirectional (UD) FRP prepreg material. Unidirectional fibre orientations were placed at

$\pm 45^\circ$  relative to the loading direction on both sides of the steel infill plate. The use of the UD FRP prepreg allowed the customization of the infill plates according to design requirement in terms of the fibre orientation and number of FRP layers.

The following FRP were used:

- CFRP: unidirectional CFRP prepreg type Medium Temperature Molding MTM 28-1 series - MTM28-1/T700(12k)-160-35%RW
- GFRP: unidirectional GFRP prepreg with epoxy resin E722-02 (produced by TenCate Advanced Composites Ltd)- E722-02 UGE400-02 32%rw

CFRP materials were supplied by Cytec Industrial Material Ltd. MTM28-1 series prepreg is based on the  $120^\circ\text{C}$  curing technology of epoxy matrix resins with a density  $1.22\text{ g/cm}^3$ . CFRP was supplied in a roll of 600 mm wide. Specifications for MTM-28-1 prepreg  $0^\circ$  configuration provided by the supplier are indicated in Table 4.2.

Table 4.2. MTM-28-1 prepreg  $0^\circ$  configuration (cured 1 hour at  $120^\circ\text{C}$  and tested at room temperature).

Test	Units	Value
Interlaminar shear strength	MPa	75
Flexural strength	MPa	1450
Flexural modulus	GPa	41
Tensile strength	MPa	1050
Tensile modulus	GPa	38
Tensile strain-to-failure	%	2.75
Compression strength	MPa	790
Compression modulus	GPa	37
In-plane shear strength	MPa	72
In-plane shear modulus	GPa	4.35

Medium temperature prepreg GFRP system was supplied by TenCate Advanced Composites Ltd company. CFRP was supplied in a roll of 500 mm wide with GFRP density of density  $1.21 \text{ g/cm}^3$ .

Prior preparation of the hybrid plates, tensile testing was conducted in accordance to D3039/D3039M-08: Standard Test Method for Tensile Properties of Polymer Matrix Composite Materials (ASTM, 2000); D3518/D3518M-94: Standard Test Method for In-Plane Shear Response of Polymer Matrix Composite Materials by Tensile Test of a  $\pm 45^\circ$  Laminate (ASTM, 2007a) and D3518/D3518M-94: Standard Test Method for In-Plane Shear Response of Polymer Matrix Composite Materials by Tensile Test of a  $\pm 45^\circ$  Laminate (ASTM, 2007b).

Prepreg vacuum/oven curing cycle was used to prepare the specimen and same procedure was followed as described further for preparation of the hybrid infill plates. After CFRP or GFRP plates (110x260 mm) were cured, individual specimens were cut using a guillotine and then sharp edges were removed using a sanding belt. Steel end tabs were attached using adhesive. For each test, four specimens with each angle configuration:  $0^\circ$ ,  $90^\circ$ ,  $45^\circ$  were prepared. Specimen configurations are shown in Figure 4.17.

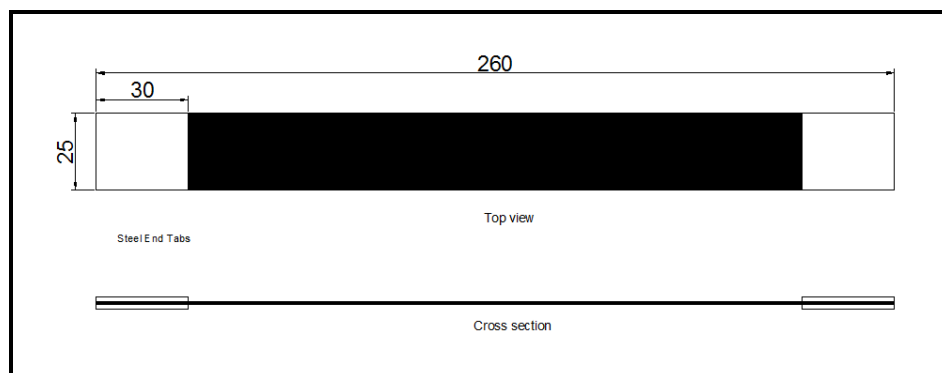


Figure 4.17. FRP Specimen for tensile testing.

Following properties were found:  $E_{11}$ ,  $E_{22}$ ,  $G_{12}$ ,  $V_{12}$ , which were calculated from stress vs strain graphs. Graphs for CFRP specimens are demonstrated in Appendix A, tensile test results for GFRP have been part of a separate MSc project. The mechanical properties of these prepreg are summarised in Table 4.3.

Table 4.3. Properties of the FRP materials used.

	Unidirectional CFRP type MTM 28-1 series prepreg (produced by Cytec Industrial Material Ltd)	Unidirectional GFRP prepreg E722-02 (produced by TenCate Advanced Composites Ltd)
Young's Modulus E11, GPa	140	40.95
Young's Modulus E22, GPa	8.5	10.5
Shear Modulus G12, GPa	5.8	3.3
Poisson's ratio $\nu_{12}$	0.319	0.311

For the preparation of all hybrid infill plate, FRP layers were applied according to the manufacturer's recommendations. The infill plates were prepared by thoroughly cleaning the steel plate with smooth sand paper followed by acetone. EF72 adhesive film (manufactured by TenCate Advanced Composites Ltd) with area weight of  $100 \text{ g/m}^2$  was placed between the steel plate and FRP prepreg to create a strong bond between FRP laminate and core steel infill plate. The additional adhesive film delays the delamination of FRP prepreg during cyclic loading. Then FRP prepregs were laid according to the design specifications with fibre orientations at  $\pm 45^\circ$  angle of fibres, two layers on both sides of plate (Figure 4.18).

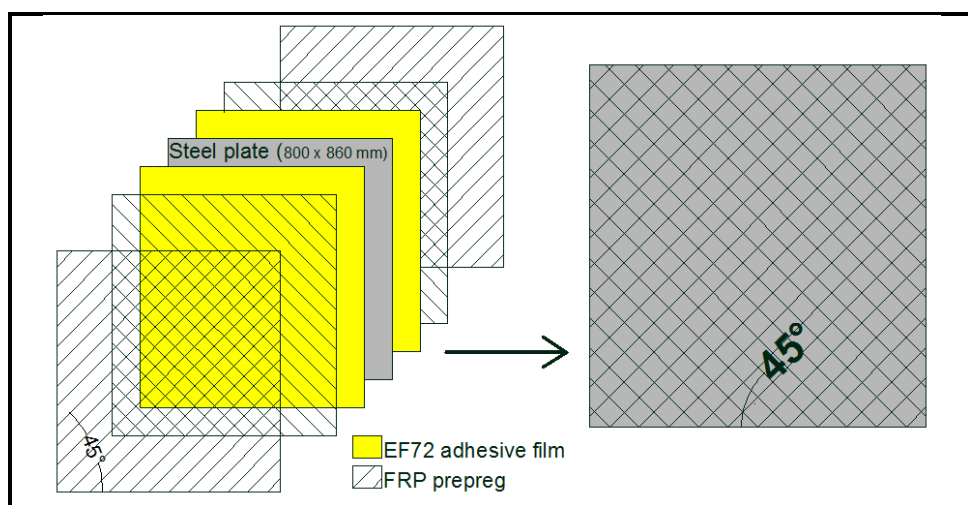


Figure 4.18. Design specification for hybrid specimens.

A roller was used to remove air traps between layers and to make the stacking sequence. The position of the drilled holes was marked and punched with a nail after

application of each layer to be able to identify bolt holes after curing. Two steel plates that match in size of the sample size were sanded flat, cleaned and covered with polytetrafluoroethylene (PTFE) sheet. A vacuum breather cloth was wrapped around the specimen, then the specimen was sealed, vacuum bagged and cured inside an oven under vacuum (Figure 4.19). The curing temperature increased at a rate of  $3^{\circ}\text{C}$  per minute until  $120^{\circ}\text{C}$  and an even pressure up to 980 mbar was applied to the laminate by using a vacuum pump. Then the temperature was kept constant at  $120^{\circ}\text{C}$  for 1 hour and finally the temperature decreased to  $60^{\circ}\text{C}$  during the cooling down cycle. The sample was then left to cool to room temperature outside the oven (Figure 4.19).

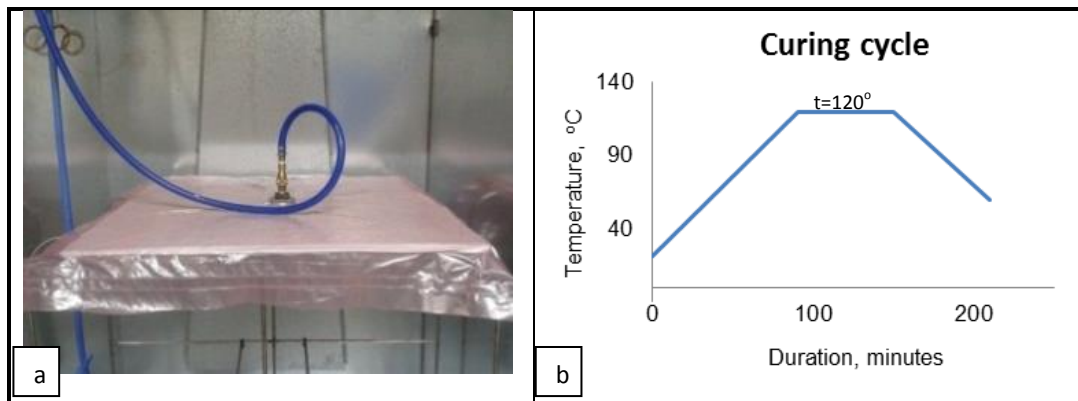


Figure 4.19. a) Oven/vacuum curing b) curing cycle.

#### 4.3.2.3 Pure FRP plates: GFRP and CFRP

The pure FRP plates were prepared with the same oven/vacuum method described above. For carbon and glass composite specimens, FRP layers were made by layering them between two plates used as moulds. The first layer of the FRP material was rolled on the cover steel plate mould, then the rest were laid in accordance to design specifications.

### 4.3.3 Assembling specimens

#### 4.3.3.1 Connection between steel frame and infill plates

The connection between fish plates and infill plates is demonstrated in Figure 4.20. Forty six M8 bolts were used to connect fish plates and infill plates. Two types of fish plates (primary and secondary) were used to connect the frame of the shear wall and infill plate.

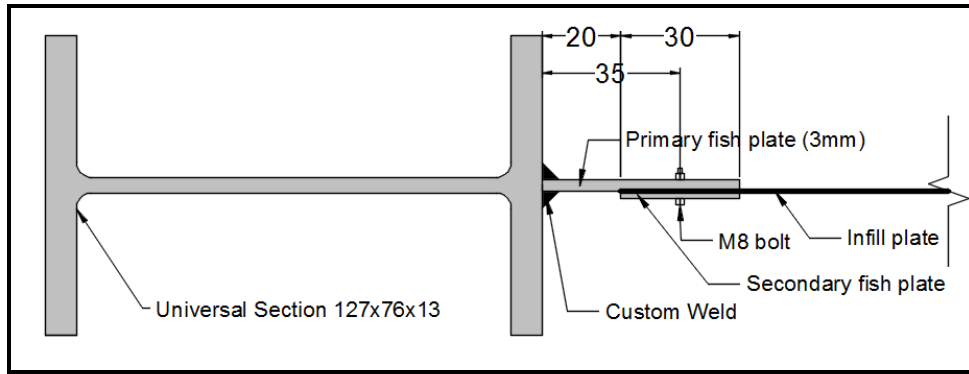


Figure 4.20. Connection between infill plate and fish plates- top view of the I-beam of the frame and infill plate.

Primary fish plates 50 mm wide and 3.5 mm thick were welded to the beam, columns and base plate of shear wall specimen. Four secondary (edge) fish plates 30 mm wide and 2 mm thick were also used. The spacing between bolts was 70 mm, 46 M8 bolts are used to clamp infill plate between fish plates (Figure 4.21).

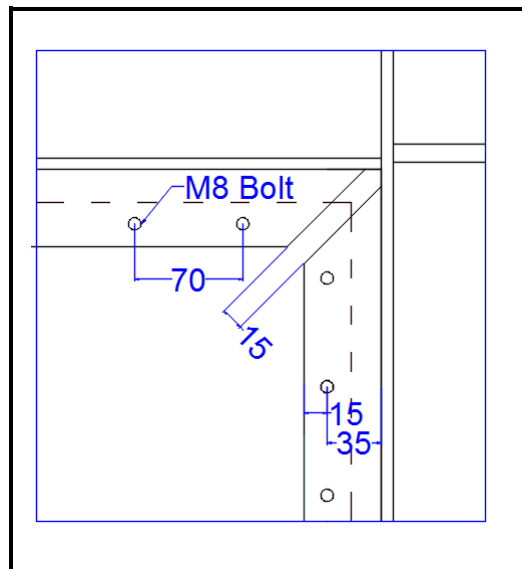
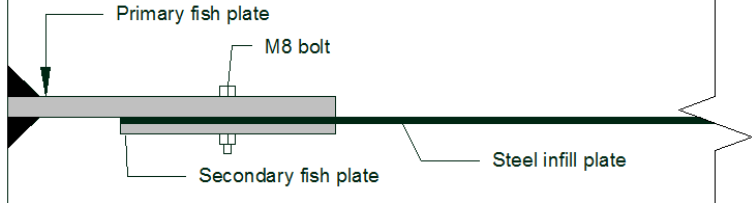
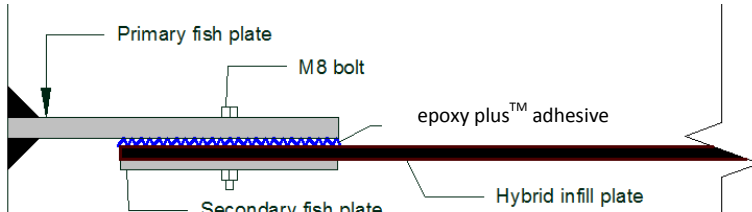
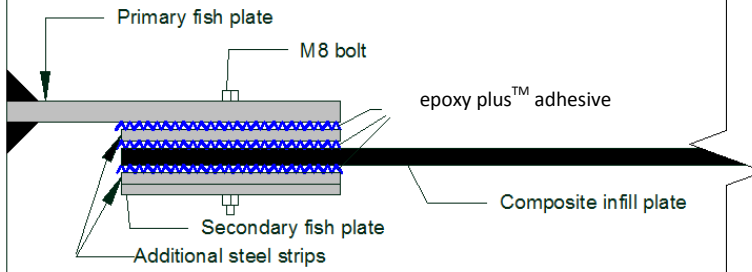


Figure 4.21. Plan view of the frame showing connection between infill plate and fish plates.

Three types of the connection were used to join infill plates and frames of the shear wall, illustrated in Table 4.4, which are type A, type B and type C connections. Type A and Type B connections were tested as part of the small connection tests and described in Chapter 3. Type C connection was developed and introduced at final stage for large-scale specimens to solve the problem of weaker connections for pure FRP plates.

Table 4.4. Connection between fish plates and infill plates.

Connection	Scheme for connections between infill plate and fish plate
Type A: bolted connection	 <p>Primary fish plate M8 bolt Secondary fish plate Steel infill plate</p>
Type B: bolted and adhesive	 <p>Primary fish plate M8 bolt Secondary fish plate epoxy plus™ adhesive Hybrid infill plate</p>
Type C: bolted and adhesive + additional steel strips	 <p>Primary fish plate M8 bolt Secondary fish plate Additional steel strips epoxy plus™ adhesive Composite infill plate</p>

Type A was a bolted connection used for steel shear wall specimen. Once the primary and secondary fish plates were cleaned with a wire brush, they were roughened with sand paper. The edges of the infill plate were cleaned with sand paper. Before tightening bolts all surfaces were cleaned with IPA cleaner. Then the M8 bolts were tightened with torque wrench to torque of 25 N-m for A4 steel grade class. M8 bolts had a minimum breaking torque of 32 N-m for A4-70 stainless steel grade class, corresponding to a grade of 316 or 18/8/3, where “A” means cold worked austenitic stainless steel and “70” represents a minimum tensile strength of 700 N/mm<sup>2</sup>.

For type B connection, in addition to the bolted connection, toughened epoxy plus™ adhesive (manufactured by Devcon ITW Polymers Adhesive) with a shear strength of 20 MPa was applied between the primary fish plates and the infill plate. The epoxy plus™ is a room cured adhesive (1:1 combined epoxy hardener and epoxy resin) with a setting time of 25 minutes.

This connection was used for hybrid specimens. Similarly to type A connection preparation, surfaces of fish plates and infill plates were roughened and then cleaned by removing grease, dust and moisture. The FRP surfaces were abraded until they lost gloss. Then an adhesive was applied evenly on edges of infill plate and primary fish plates, the surfaces were connected and were bolted together with M8 bolts to the specified torque. Any excessive adhesive coming out from the edges was removed. To achieve good bond, the specimen was cured at room temperature for at least 24 hours before testing.

An additional layer of adhesive at the connection was proved to be extremely beneficial from previous investigations for small scale specimens (Chapter 3). The benefit of adhesive applications is very important considering the governing role of the connections capacity for such elements and the fact that reduced friction at the surface of FRP material results in a dramatic reduction of the capacity of the connection.

A type C connection was used for pure FRP specimens. In order to provide a stiff connection to the infill plate, an additional steel strip 30 mm wide and 1.5 mm thick was attached with adhesive to both sides around the edges of the infill plate. Holes were drilled after the strips were attached. Finally, the infill plate with steel strips was attached to the fish plate with M8 bolted and adhesive.

#### **4.3.3.2 Fixing frame in the position**

When the infill plates and steel frames were prepared, the test specimens were assembled. The surfaces of primary and secondary fish plates were cleaned with sand paper and acetone, then the infill plates were fixed to the steel frame via bolts or bolts with adhesive. The specimen was then placed in position in the strong frame. Centering of the specimen and the loadcell was done with a level, and then the plate for the loadcell was welded. The specimen was firmly fixed to the reaction frame with bolted and clamp connection.

#### 4.4 Specification of the newly developed shear walls specimens

The specifications of all specimens that were tested in this study with thicknesses and weights are described below in Table 4.5.

Table 4.5. Specimen description and characteristics.

Name of the specimen	Design configuration of the infill plate	Weight of the infill plate, kg	Thicknesses of the infill plate, mm	Connection between infill plate and fish plates
Steel Shear Wall (SSW)	Steel [S]	4.08	0.80	TYPE A: bolted
Hybrid Carbon FRP Shear Wall (HCSW*)	[-45/+45/S/+45/-45]	5.20	1.64	TYPE A: bolted
Hybrid Carbon FRP Shear Wall (HCSW)	[-45/+45/A/S/A/+45/-45]	5.53	1.70	TYPE B: bolted + adhesive
Hybrid Glass FRP Shear Wall (HGSW)	[-45/+45/A/S/A/+45/-45]	5.95	2.40	TYPE B: bolted + adhesive
Carbon FRP Shear Wall (CSW)	[-45/+45/-45/+45/+45/-45/+45/-45]	2.24	1.68	TYPE C: bolted + adhesive
Glass FRP Shear Wall (GSW)	[-45/+45/-45/+45/+45/-45/+45/-45]	3.26	2.52	TYPE C: bolted + adhesive

NOTE: S- steel; A- adhesive film (EF72), -45/+45- angle of the fibres inclination

The control SSW contained steel infill plate with a thickness of 0.8 mm. The hybrid specimens, HCSW\* and HCSW, are steel framed with infill plates which were prepared by laminating a steel plate (0.8 mm) with two layers of prepreg CFRP fabric on each side of the infill plate. HCSW\* specimen was without adhesive film layer between steel plate and FRP layers and Type A connection.

The HGSW specimen was prepared by laminating prepreg GFRP fabric as it was described in section 4.3.2 CSW and GSW specimens were prepared by laminating eight layers of the carbon FRP or glass FRP respectively. The types of the connection specified in Table 4.4 are described in Section 4.3.3.

#### 4.5 Testing protocol

Different testing techniques have been established in the field or laboratory to test specimens in earthquakes engineering to find different parameters. These methods can have dynamic, pseudo dynamic or slow cyclic manner of applying load. Each method has its advantages and disadvantages. The conducted studies in this work have been based on slow cyclic experimentation. "Slow cyclic" or "quasi static" experimentation implies that displacement is applied in a slow and controlled manner. Dynamic effects and the rate of applying displacements are not taken into account.

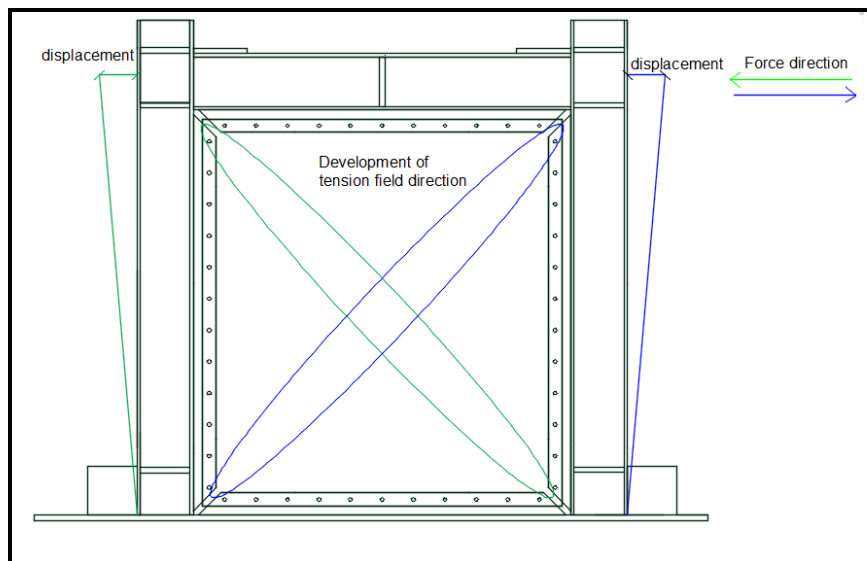


Figure 4.22. Illustration of the frame being subjected to push and pull loading.

The shear wall specimen was subjected to the same displacements in both directions: push and pull regarding the position of the loadcell. Applied force was measured with a loadcell as it was described above. The corresponding development of the diagonal tension field within the infill plate in the direction of the applied force is indicated in Figure

4.22. The testing procedure of the application of the loading was according to ATC-24 protocol from Applied Technical Council (ATC-24, 1992).

Figure 4.23 shows cyclic sinusoidal loading designed for these specific types of specimens and applied for a range of different amplitudes varying from 0.4 mm to 35 mm displacement. The application of the same displacement in both directions completes one cycle of loading. Initially, three cycles at each amplitude were applied, and then above 15 mm displacement, the number of cycles was decreased to two cycles per amplitude according to the ATC-24 protocol.

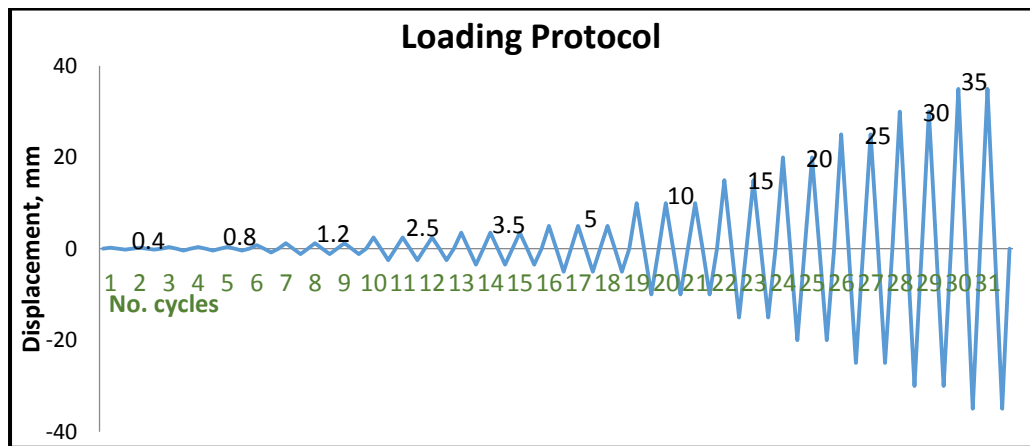


Figure 4.23. Cycling loading in accordance to ATC- 24 protocol.

The rate of the applying displacement varied from 0.05 mm/min between 0.4 mm and 10 mm displacement to around 2.2 mm/min between 10 mm and 35 mm displacement.

As a result of the applications it can be concluded that the developed testing equipment and testing procedure allowed the investigation and comparison of the behaviour of the newly developed specimen (Chapter 6) and the behaviour of the strengthened specimens (Chapter 7).

## **Chapter 5: Experimental results of newly developed shear walls**

This Chapter contains experimental results obtained for the medium scale specimens of shear walls. The description and schemes of the damage and defects occurring during the test is shown for each specimen. The following graphs and figures are included for each specimen:

- Load vs Displacement hysteresis curve
- Average load vs displacement data
- Photos of significant destruction occurring to specimens
- Delamination levels for specimens with FRP material.

### 5.1 Testing of the SSW\* and SSW specimens

The SSW\* was tested with an infill plate of thickness of 0.8 mm. This specimen was tested as a trial specimen to ensure that the equipment worked well and was calibrated correctly. Amplitudes from 0.4 mm to 25 mm were applied to the tested specimen (Figure 5.1). The load vs displacement graph is demonstrated in Figure 5.1. The first sign of out-of-plane buckling started at the first cycle of loading 0.4 mm displacement, out-of-plane deformations did not fully recover after the end of the 2.5 mm loading cycle.

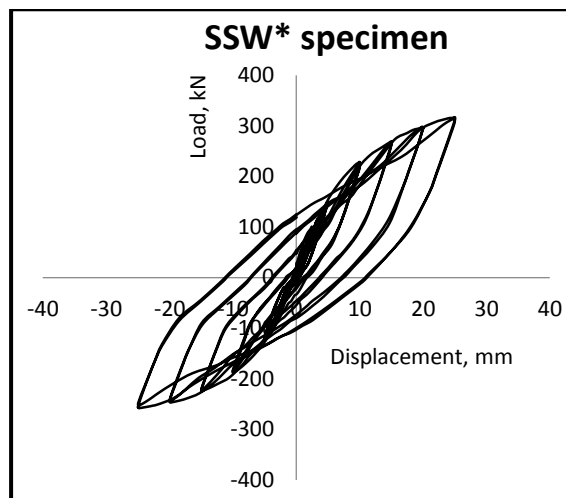


Figure 5.1. Load vs displacement graph for SSW\*.

Movement of the infill plate from its original position started at 10 mm. At this level of displacement because of the significant stress concentration in the corners of the infill plate, there was damage in the corners of the infill plate and fish plates. Due to the layer of paint coated at the primary fish plates and low surface friction at the connections, it caused earlier failure of the connections. It was seen as unstable behaviour at early stages of loading and pinching on the graph.

Pinching was detected via visual inspection of deformed shape development on the infill plate. At 15 mm displacement, "pinching" of the steel plate started through buckling of the steel plate and twisting at the places where diagonal tension field action changed its direction. "Pinching" of the steel plate further increased at 20 mm displacement. At 25 mm

displacement, development of plastic hinges at the bottom of the columns was observed. Primary and secondary fish plates buckled due to the wave action of the diagonal tension field. Small holes developed in the infill plate due to the “pinching” of the plate (Figure 5.2).



Figure 5.2. SSW\* specimen at 25 mm displacement.

Results of SSW\* specimen demonstrated that the loading system of the testing equipment and the programme for testing needed modifications. Thick plate bolted connections between the load cell and the frame were adopted to reduce the differences in the load in both directions of application. It was also found that the plate connecting the loadcell and screw jack needed to be thicker to avoid deformations in the connections.

As specimen SSW\* was used for calibration and development of the testing set-up, results of this specimen are not included in further analysis in this Chapter.

After introducing modifications to the loading system, the control SSW specimen was tested. The SSW specimen was made from steel frame and a steel infill plate with a thickness of 0.8 mm. For SSW specimen proper treatment of the connection between fish plates and infill plate was undertaken. The results of this specimen are compared with

other specimens to identify differences in seismic behaviour in terms of the stiffness, ultimate load and energy absorption in Chapter 6.

The steel shear wall specimen SSW was loaded up to 35 mm displacement and the load of the SSW was still increasing at 35 mm displacement in comparison to 30 mm displacement (Figure 5.3b). However, during the last cycle of loading at 35 mm displacement (Figure 5.3a), there was a more significant drop in comparison to the first cycle that was not noticed at previous levels of displacement. The SSW specimen also underwent significant damage at high levels of displacement, as described below.

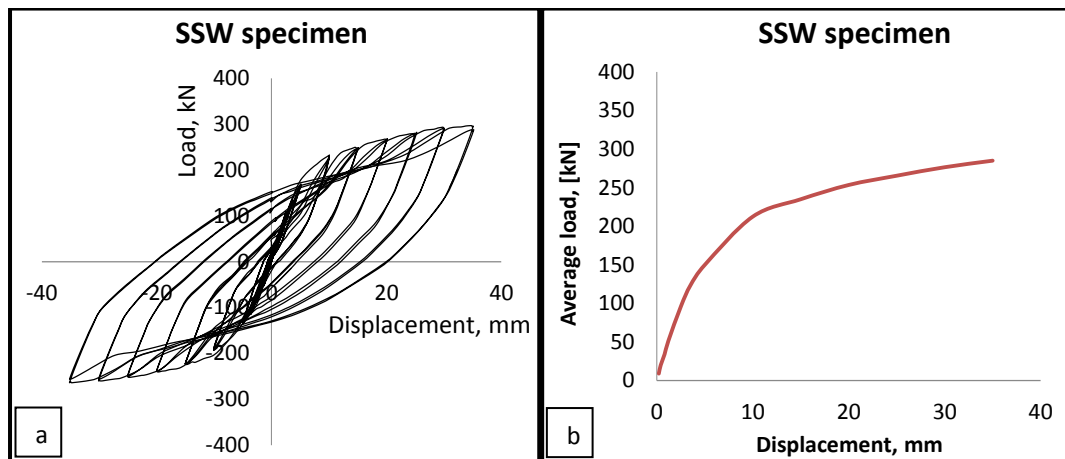


Figure 5.3. SSW specimen a) Hysteresis curve b) Load vs Displacement.

One side of the infill plate was coated with black matte paint to avoid reflections while taking readings for infrared thermography. In order to check sliding movements and tearing of the infill plate at the connections, the original position of the infill plate and fish plate border was marked with a white colour. Appearance of sliding was detected via visual inspection of the border line.

The first signs of buckling of the infill plate occurred at 1.2 mm displacement with corresponding noise. Until displacement of 3.5 mm, diagonal tension action was with elastic deformations and the initial shape of the plate was recovering at the end of the cycles. However, when the infill plate had undergone plastic deformations for

displacements above 3.5 mm, out-of-plate deformations were more visible and the initial shape did not recover at the end of the cycle. The number and amplitude of diagonal tension field waves were increased at higher displacements (Figure 5.4a).

At displacements higher than 10 mm, enlargement of holes around bolts in the connections between fish plates and infill plates started. It led to the yielding of the steel infill plate and it tearing around its bolt holes, corresponding noise occurred when tearing started. Sliding of the infill plate progressed with the increase of the displacement. After the 15 mm displacement cycle, 3-4 mm displacement from the original position of the border of the infill plate to the new position at the top border was noticed between fish plate connections.

The initial pinching of the infill plate along diagonal tension field started at a displacement of 15 mm, which further progressed to development of small holes at displacements higher than 30 mm (Figure 5.4c). Development of plastic hinges at the bottom of the columns of the steel frame was noticed at displacements above 15 mm, which increased in size at higher displacement (Figure 5.4b) and appeared at the top of the columns above 30 mm displacement. A summary of the damage occurring at 35 mm displacement is demonstrated in Figure 5.4d. At 35 mm displacement, sliding of the plate reached 15 mm and bolt holes were visible at fish plate section. Due to the concentrations of stresses in corners of the infill plate and fish plates, steel snapped along the folding line of the plate.

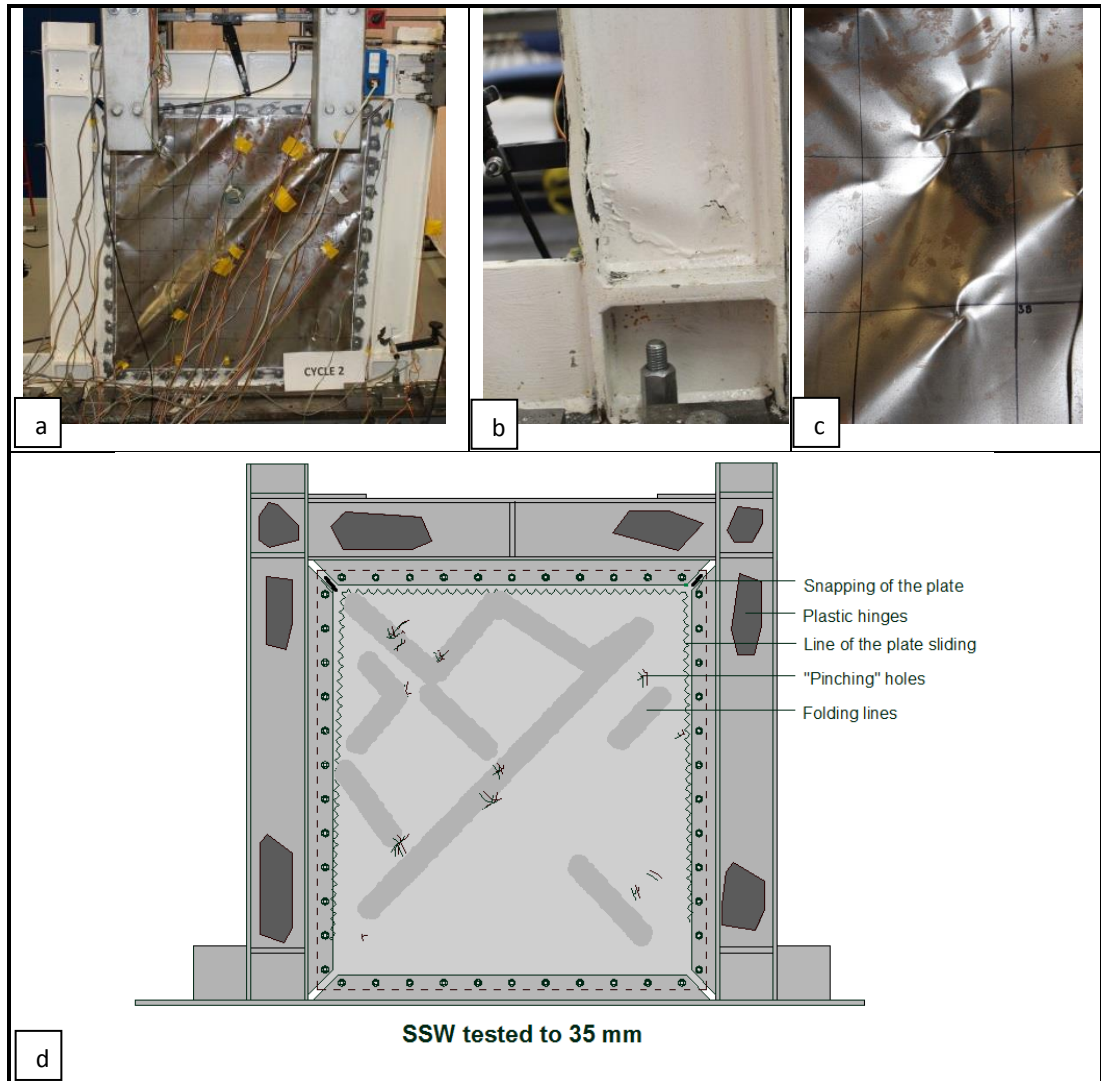


Figure 5.4. SSW specimen after 35 mm displacement a) diagonal tension field development b) plastic hinges c) twist holes along diagonal lines d) summary of damages to the SSW at 35 mm displacement.

The final failure of the steel shear wall specimen (Figure 5.4a) occurred through the development of the plastic hinges around the bottom and top areas of the column and tearing of the steel plate around bolt holes.

## 5.2 Testing of the HCSW\* and HCSW specimens

As a first stage of development HCSW specimens, the HCSW\* specimen was prepared as a hybrid specimen with two layers of CFRP fabric on both sides of the steel infill plate with an angle of inclination  $45^\circ$ . The connection between hybrid infill plate and steel fish plates for HCSW\* was bolted only (without application of adhesive) and no adhesive film was placed between steel plate and FRP layers. The surface of the hybrid

specimen was the same as for steel specimen SSW coated with black matte colour to eliminate reflections while obtaining IRT data.

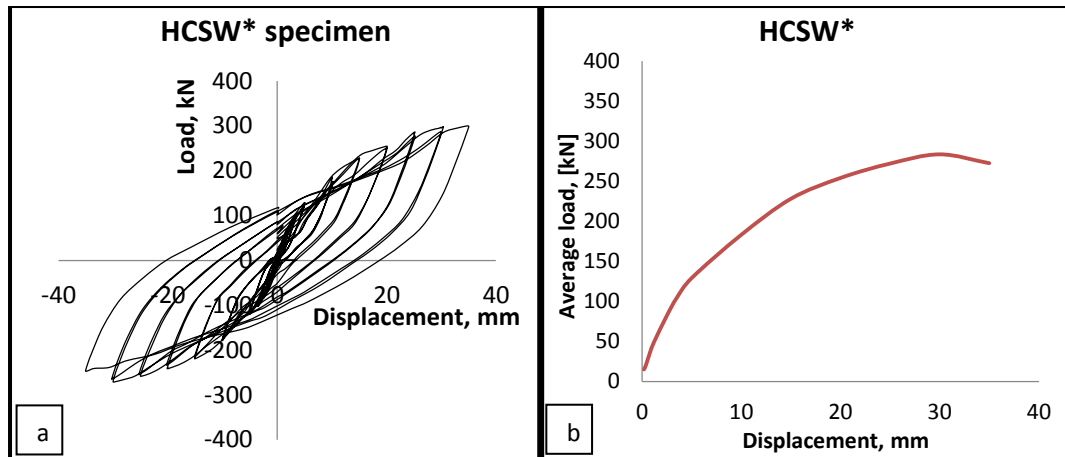


Figure 5.5. HCSW\* specimen a) Hysteresis curve b) Load vs Displacement.

Figure 5.5a shows that the HCSW\* specimen had unstable hysteresis curve and a pinching effect was noticed at the initial stages of loading due to FRP fractures. The HCSW\* was subjected to 35 mm displacement and load values started to decrease after reaching an ultimate load capacity at 30 mm displacement (Figure 5.5b). Only one cycle was applied at the 35 mm displacement due to the local damage of the beam-column connection.

The visible out-of-plane deformations started to develop at the 1.2 mm cycle, which did not recover fully at the end of the cycle. For the HCSW\* specimen, the main damage occurring to the specimens were de-bonding of the FRP from the infill plate and delamination between the FRP layers and steel plate. Furthermore, these two modes of failure are referred to as the delamination process.

The first delamination of the FRP appeared in top corners of the infill plate at 5 mm displacement, as the stress concentration was high in the corners through the diagonal tension field action. Further delamination along diagonal field action in both directions increased with subsequent increase of the loading cycle and a crack in FRP layers occurred in one of the corners of the infill plate. With the increase of the loading, development of

delamination was not uniform in push/pull directions with more significant delamination developing in the push direction.

For the HCSW\* specimen, the connection between hybrid infill plate and steel fish plates was bolted only (without application of adhesive) and sliding of the plate at the upper parts of the shear wall was observed after 10 mm displacement cycle. At 15 mm displacement, sliding of the infill plate increased and movement of 5 mm was noticed at the top of the infill plate, further increasing when tested at higher levels of displacements.

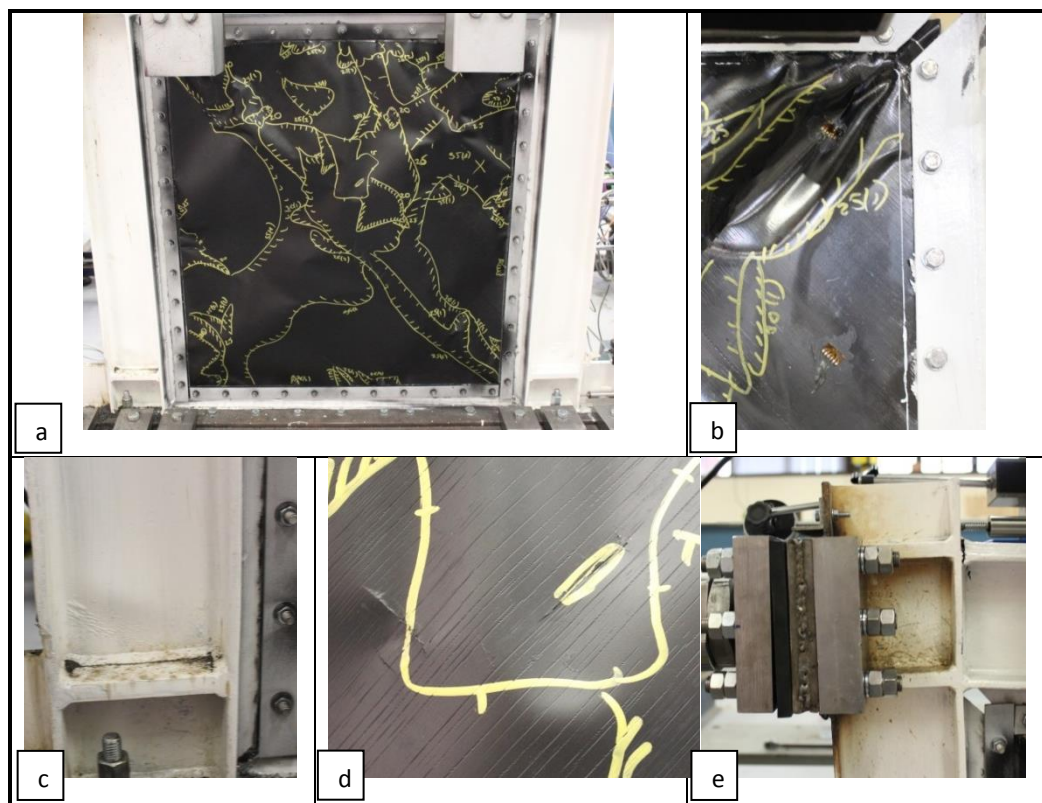


Figure 5.6. Damages to HCSW\* specimen after 35 mm displacement a) delamination level b) failure in connection c) plastic hinges d) tearing in FRP layers e) crack in the beam-column connection.

Development of plastic hinges in the bottom part of the columns was noticed after 20 mm displacement cycle (Figure 5.6c), and the top part of the column at 30 mm displacement. At 30 mm displacement, around 40% of the FRP fabric delaminated (Figure 5.6a), tearing in FRP layers was also noticed at high levels of displacement (Figure 5.6d). Bolt holes were visible near the surface of fish plates (Figure 5.6b), fibres and plate cracked in the corner of the infill plate. At 35 mm displacement, a large crack between the beam

and column connection of the shear wall (Figure 5.6e) appeared near the loading equipment, therefore the specimen was subjected to only one loading cycle.

Early failure of the connections, progressive delamination and low stiffness, resulted in the change of the design specifications - placing layer of the epoxy film and improving the connection between fish plates and infill plate for hybrid specimens HCSW and HGSW.

The HCSW specimen was prepared with two layers of CFRP fabric on each side of infill plate with an angle of inclination  $45^\circ$ . As mentioned above, in order to achieve better bond between steel infill plate and FRP layers and to prevent early stage delamination, a layer of EF72 adhesive film was applied before placing first layer of FRP. In addition, a layer of epoxy plus<sup>TM</sup> adhesive was added to improve connection between fish plates and infill plate (Chapter 3).

The HCSW specimen achieved its ultimate load values at 15 mm displacement (Figure 5.7b). This specimen was tested until 30 mm displacement and the last cycle at 30 mm had a significant drop in load and energy absorption in comparison to previous cycles (Figure 5.7a).

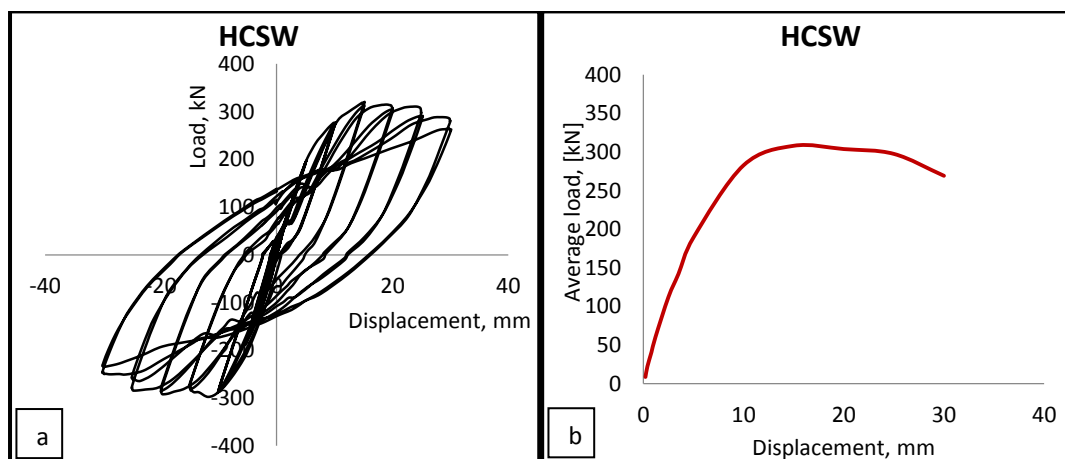


Figure 5.7. HCSW specimen a) Hysteresis curve b) Load vs Displacement.

In the HCSW specimen the first sign of buckling of the infill plate through the development of wave-type deformations was noticed at 1.2 mm displacement. Out-of-

plane deformations did not recover fully at the end of the applied 2.5 mm displacement cycle.

At 10 mm displacement, delamination between FRP and steel plate started at the top corners of the plate. Additionally, a crack along the diagonal tension field action appeared, which developed at 10 mm displacement and grew further at higher levels of displacement. At 15 mm displacement cracks in the adhesive layer at the border of the fish plate appeared, sliding and tearing in the connections between fish plates and infill plate started at displacements higher than 15 mm.

At 20 mm, loading cracks in the FRP fabric grew in the direction of diagonal tension field action on one side of the plate and the fabric started to de-bond from the steel plate near corners of the fish plates on other side (Figure 5.8 a, c and d). Above 25 mm, delamination between CFRP layers and the steel plate along the full length of diagonal tension field action and in the corners were observed for HCSW at displacement. Delamination levels for the HCSW specimen at 20 mm and 30 mm displacements were considerably less than for the HCSW\* specimen at the same levels of loading (Figure 5.6).

At 25 mm loading, the infill plate snapped in the top corners near primary fish plates with occurrence of holes and delamination of the FRP. Visible formation of plastic hinges was noticed at 25 mm displacement and above. The infill plate continued to slide with the increase of the displacement; elongated bolt holes were visible at a displacement of 30 mm (Figure 5.8 c and d). A hole in the steel plate and FRP fabric near fish plate corners increased in size considerably at 30 mm displacement (Figure 5.8d).

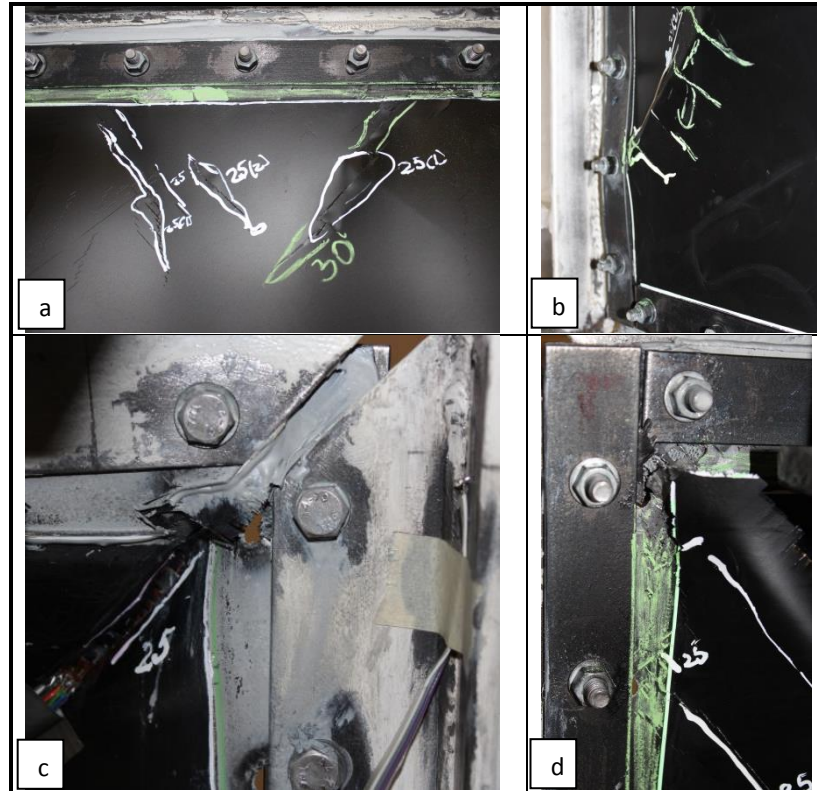


Figure 5.8. Damages to HCSW specimen after tested to 30 mm displacement a) delamination and cracking of fibres b) buckling of the fish plate c) sliding of the plate d) development of hole in the corners.

### 5.3 Testing of the HGSW

The HGSW specimen was prepared with the same design specifications as HCSW specimen, with two layers of GFRP fabric on each side of infill plate with an angle of inclination  $45^\circ$ . To connect the fish plate and infill plate, a bolted connection with adhesive was used.

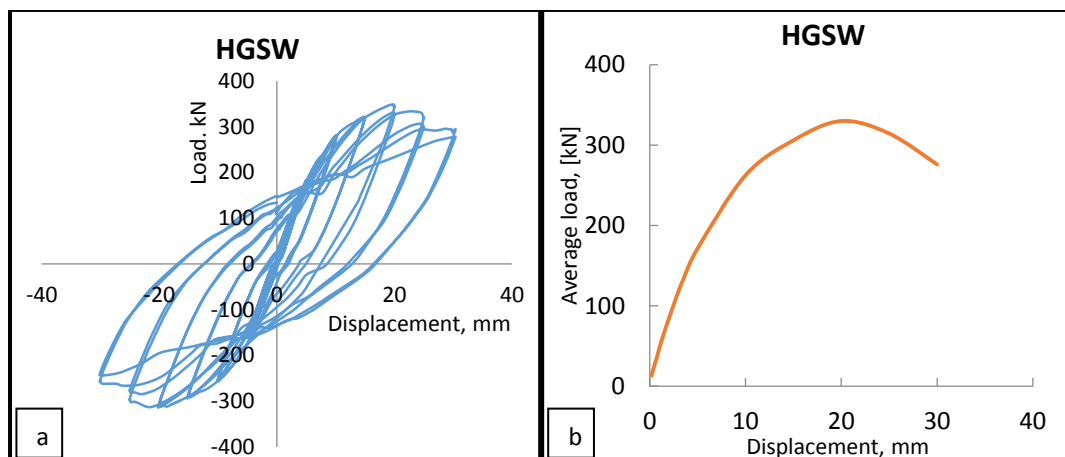


Figure 5.9. HGSW specimen a) Hysteresis curve b) Load vs Displacement.

Figure 5.9a shows the load vs displacement curve for the HGSW specimen. Measured load values started to decrease between 20 mm and 30 mm displacement (Figure 5.9b). The main mode of destruction for hybrid specimens HGSW was delamination and buckling of the plate. In HGSW specimen, visible diagonal tension field development started at the displacement of 1.2 mm in both directions, deformation did not fully recover after the end of 2.5 mm loading cycle.

At displacement higher than 10 mm, development of tension field residual deformations in both directions led to the delamination of GFRP fabric from steel plate. Small delaminated areas in both corners of the infill plate on the front side of the sample appeared; at the back of the sample delamination was recorded in one corner with tearing of the fibres. Cracking in the adhesive layer between fish plates and the infill plate was noticed. The first signs of the development of plastic hinges at the bottom of the columns were recorded at 15 mm displacement and at the top part of columns at 20 mm.

Testing at 20 mm displacement, further delamination in the corners developed, however the extent of delamination was smaller compared to HCSW specimen at the same level of loading. A vertical gap in the adhesive started to develop with the sliding of the infill plate. The tearing gap of the adhesive increased between fish plate and infill plate. At 25 mm testing, further delamination occurred, mainly tearing of the FRP in the corners (still very small). At 30 mm displacement, the top corners in the infill plate around fish plates snapped and the elongation of the bolt holes of the infill plate became visible.

The specimen was tested to 30 mm displacement loading, delamination levels on front and back sides are shown in Figure 5.10a and b. Less progression and extent of the development of FRP delamination and higher deformability of the plate allowed more effective utilization of the capacity of the steel frame.

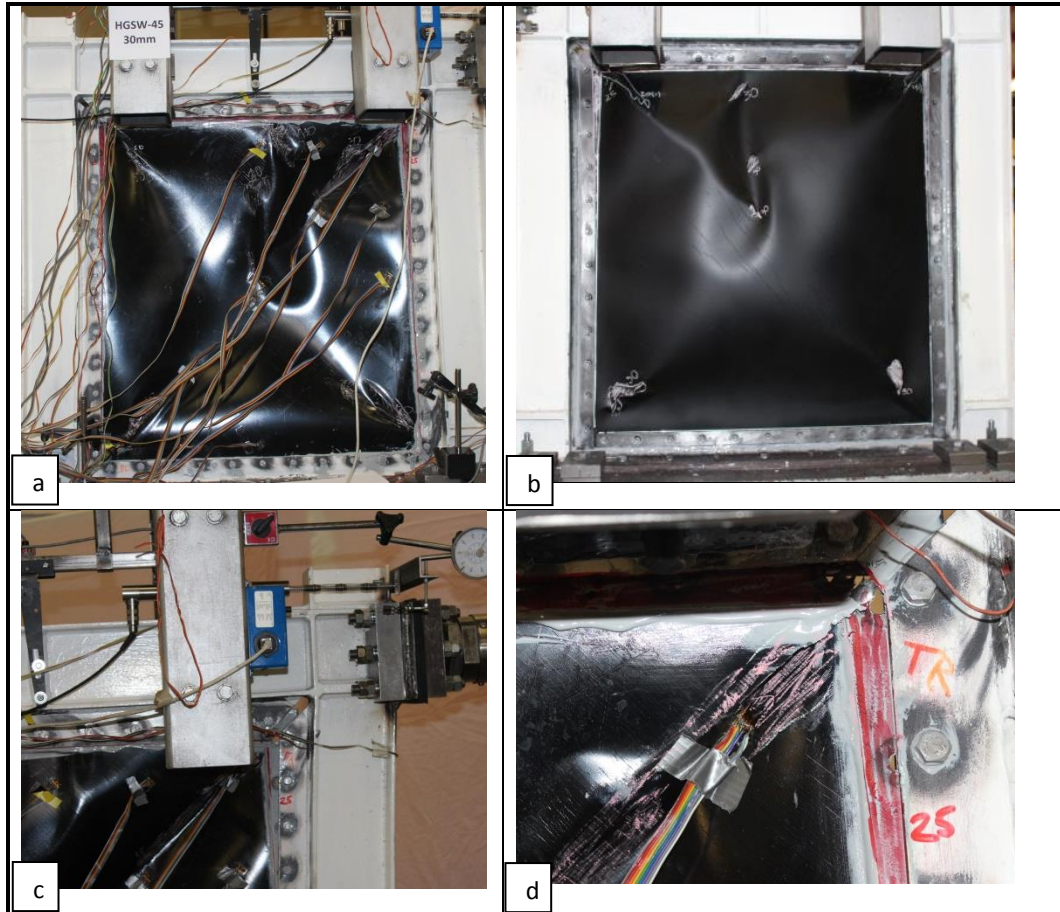


Figure 5.10. HGSW specimen tested to 30 mm displacement a) front b) back side of plate c and d) failure in connection.

## 5.6 Testing of the CSW

The CSW consisted of a pure carbon infill plate. Eight layers of CFRP were placed at  $45^\circ$  inclination. In order to provide a stiff connection for infill plate, a type C connection (Chapter 4) was used. An additional steel strip 30 mm wide and 1.5 mm thick was attached with adhesive on both sides around the edges of the plate.

Figure 5.11a shows hysteresis loops for CSW specimen, in comparison to other specimens, the loops are shallow at high displacements. During the last cycle at 25 mm displacement, load values were decreased due to the development of a significant crack in the infill plate.

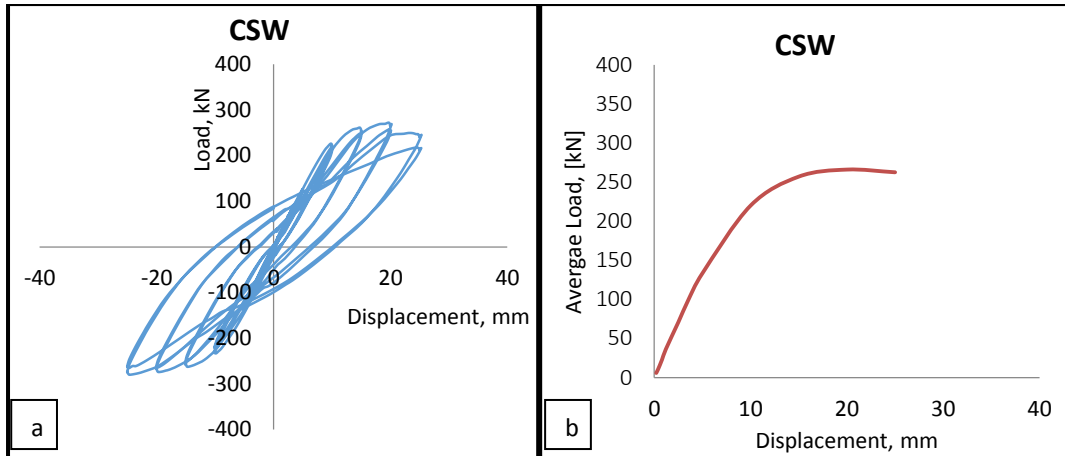


Figure 5.11. CSW specimen a) Hysteresis curve b) Load vs Displacement.

For the CSW specimen diagonal tension field action through the development of out-of-plane deformations was noticed at 2.5 mm displacement. They recovered at the end of loading cycle to the displacement of 5 mm.

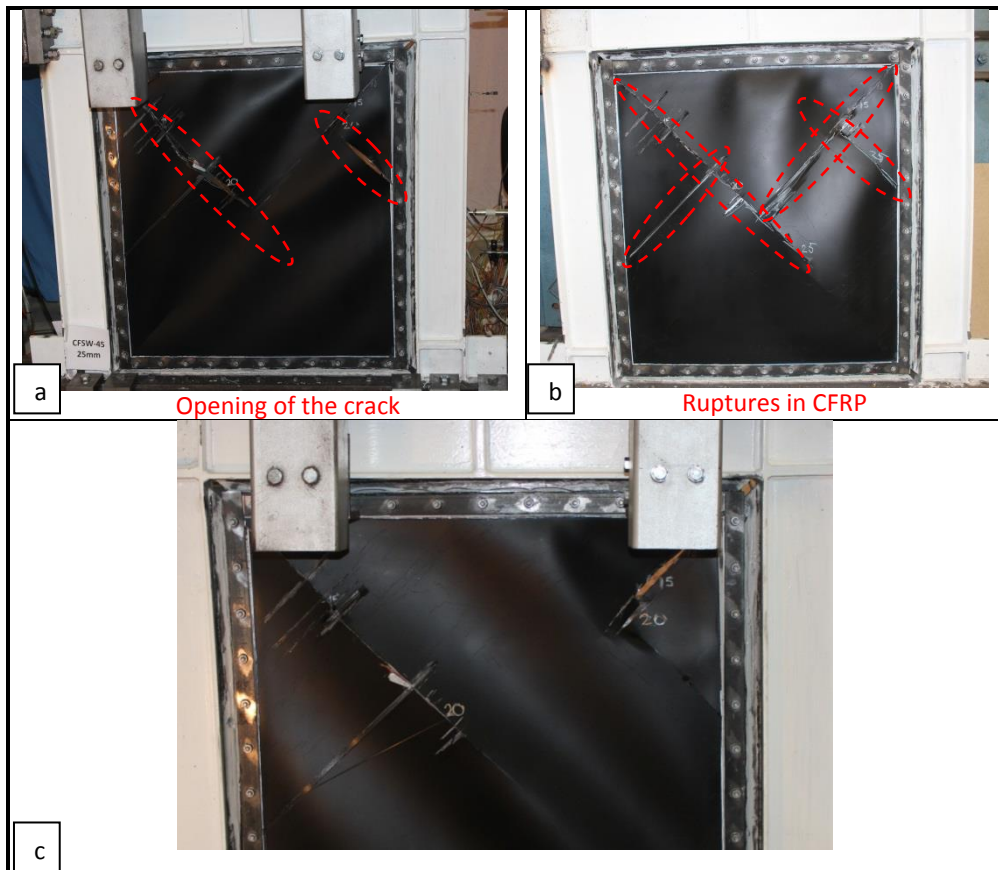


Figure 5.12. CSW specimen with a) opening of the crack during 1<sup>st</sup> cycle of 25 mm displacement testing b) ruptures in the specimen tested to 25 mm displacement c) delamination of thin strips of CFRP.

Tearing and appearance of the first cracks of the CFRP layers in the corners developed when the specimen was tested to a displacement higher than 10 mm. These

cracks in FRP fabric increased longitudinally in size at higher displacements. When displacements increased to 15 mm displacement and higher, thin strips of the CFRP perpendicular to the cracks (Figure 5.12c) started to delaminate in top corners of the infill plate.

At 20 mm displacement, a crack through the whole thickness of the CFRP plate developed. The layer of the adhesive of the connection between fish plates cracked when the specimen was tested to 20 mm displacement, however due to the stiff steel plate at the connection no visible movement of the plate was recorded. Development of the plastic hinges was noticed at 20 mm displacement in the steel boundary elements. Carbon specimen failed at 25 mm displacement at the level of the deformations when the maximum load was exceeded with significant cracks developing in the direction of diagonal tension field (Figure 5.12a and b).

### 5.7 Testing of the GSW

The GSW consisted of a pure glass FRP infill plate within steel framed boundary elements. Eight layers of GFRP were placed at 45° inclination. The Same stiff connection for the infill plate as for CSW specimen was applied for GSW specimen.

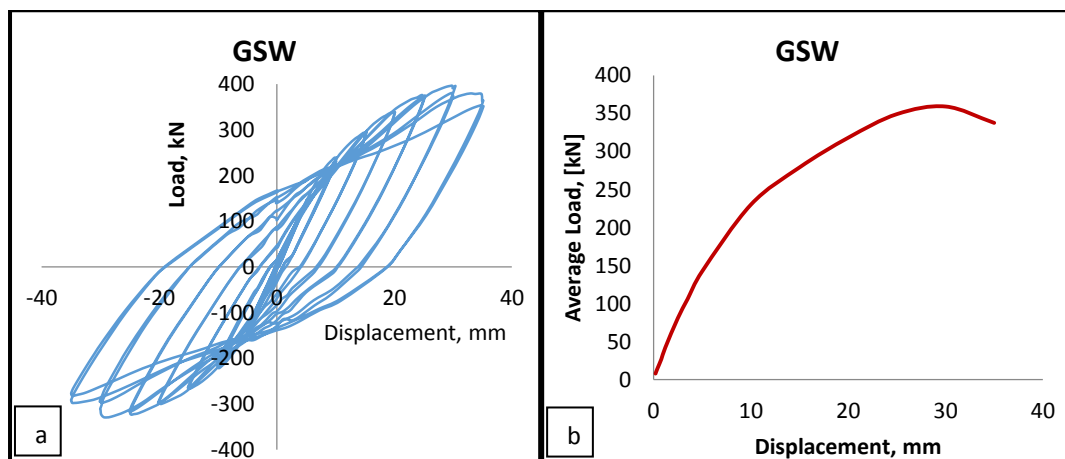


Figure 5.13. GSW specimen a) Hysteresis curve b) Load vs Displacement.

Figure 5.13a shows the hysteresis curve for the GSW specimen, the hysteresis loops were wider in comparison to CSW specimen at the same level of displacement. The decrease of the load was recorded at a displacement higher than 30 mm (Figure 5.13b). At 0.8 mm and 1.2 mm displacements, out-of-plane buckling of the infill plate was noticed; this was recovered at the end of the cycle. After 2.5 mm displacement, out-of-plane buckling of the plate was not fully recovered at the end of the cycle, no other changes were noticed to the specimen up to 15 mm displacement.

At 15 mm displacement, further buckling of the plate and crack in the layer of adhesive at the connections was observed near top section of the plate. With the increase of displacement, a crack in adhesive elongated and the plate started to slide. At 20 mm displacement, further buckling of the plate continued. Delamination and tearing of the FRP in corners of the infill plate started when the specimen was subjected to 20 mm displacement cycle. Development of the plastic hinges occurred at the bottom of the shear wall columns. The glass FRP infill plate was torn in one of the corners (40-50 mm long crack in FRP layers). After 25 mm displacement loading, further delamination and tearing in the top corners of the infill plate was noticed. Plastic hinges at the top external flanges of the shear wall columns (close to stiffeners) also developed.

At 30 mm displacement, further delamination of the GFRP developed in the corners of the infill plate (Figure 5.14a). For GSW specimen cracks did not through go all layers of the GFRP fabric, as they were developed for the CSW specimen. At 30 mm displacement, the infill plate slid and a significant gap developed between infill plate and adhesive layer in the corners (Figure 5.14b). Due to the diagonal tension field action, fish plates buckled as is seen in Figure 5.14c.

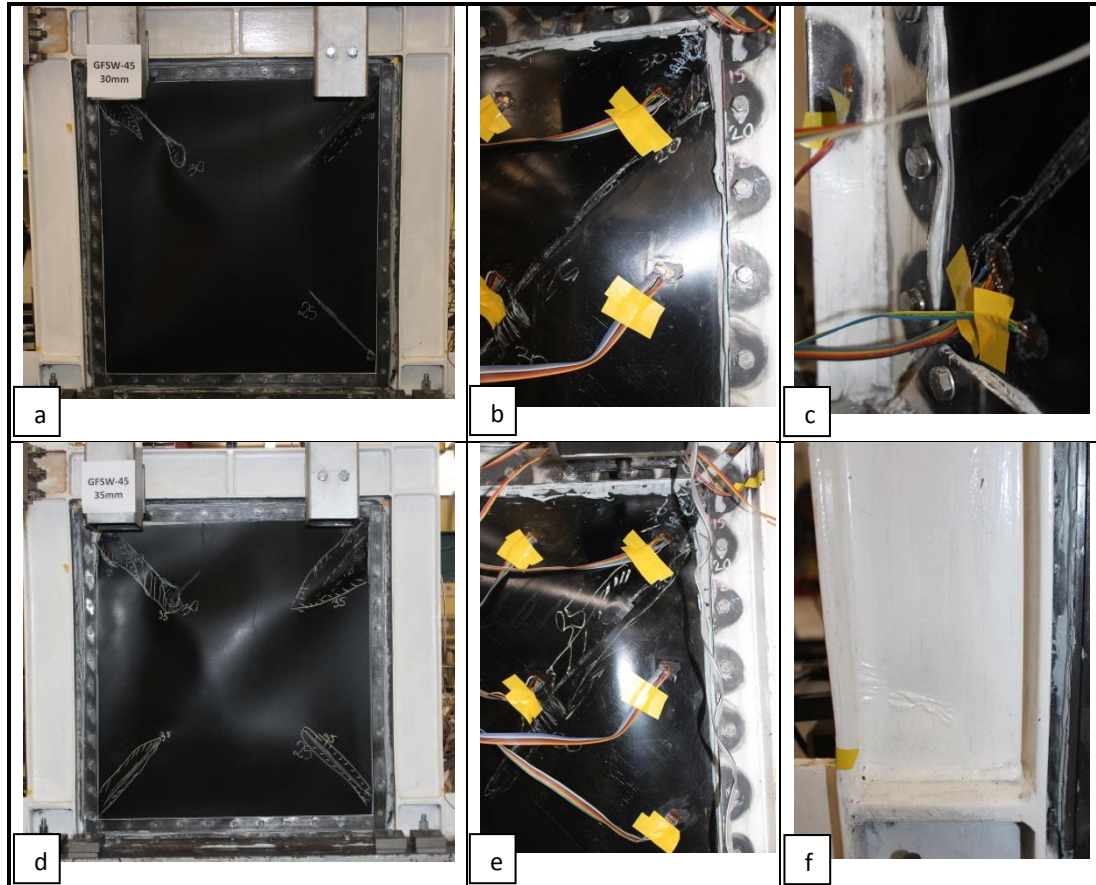


Figure 5.14. GSW specimens tested to 30 mm displacement a) delamination b) damages to connection c) buckling to fish plates. GSW tested to 35 mm displacement d) delamination e) damages to connection f) plastic hinges.

With the increase of the displacement to 35 mm displacement, in the GSW specimen, areas of the delamination were widened in the corners (Figure 5.14d). Further sliding of the plate occurred, and elongated bolt holes were visible, which happened at a later stage in comparison to other specimens (Figure 5.14e). Sections where plastic hinges developed further buckled at high displacements (Figure 5.14f).

## 5.8 Modes of the destruction for all specimens

### 5.8.1 Damages identified by IR thermography

Damage of the specimens was additionally monitored with the use of the IRT camera through passive and active data collection and analysis. IR camera was set up on one side of the shear wall specimen and two sets of data were obtained: passive thermography without external heat and active thermography with external heat, which are described

further. In order to avoid reflection of the surface of the infill plate both steel and hybrid, the surface of the plates was coated with matt black colour.

To conduct test VarioCAM high resolution infrared (IR) camera was used which is capable to measure temperatures between  $-40^{\circ}\text{C}$  to  $1200^{\circ}\text{C}$ . This camera is used for a long wave infrared spectral range (LWIR) of  $7.5\text{--}14\ \mu\text{m}$  and measurement accuracy is  $\pm 1.5\text{K}$  or  $\pm 15\%$ . A detector size of  $640 \times 480$  pixels and the maximum image resolution is  $1280 \times 960$  IR pixels. To record data and analyse results Irbis software was used. Figure 5.15 shows an IR camera set-up for recording data.



Figure 5.15. IRT camera set-up during testing.

### 5.8.2 IRT passive data

Passive thermography was used to measure surface temperature of the specimen continuously and recording images at 30 seconds interval during the testing. No external heat was applied for this method during the test. As the displacement was increasing, IR camera was recording temperature changes due to the developed plastic deformations occurring in the specimen.

IRT passive data images recorded during the test without external heat allowed confirmation of the development of the failure in the connections for specimens in addition to the registration of the corresponding physical noise.

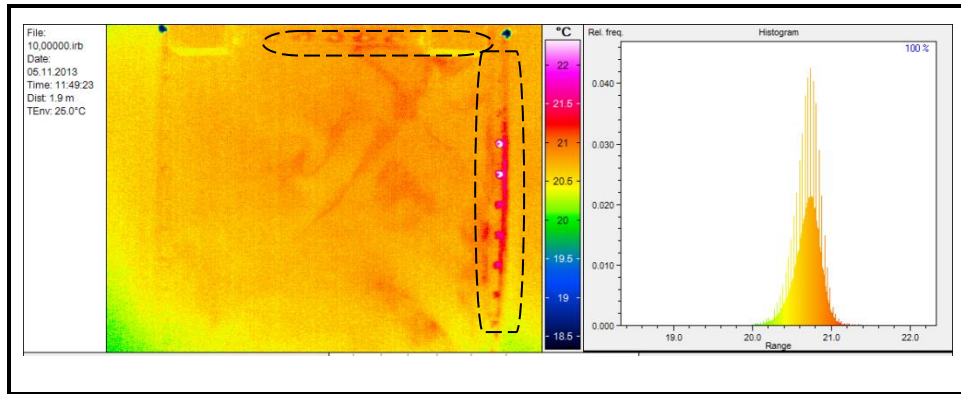


Figure 5.16. IR images demonstrating temperature distribution for SSW specimen.

Figure 5.16 shows damages in the connection area for SSW specimen occurring at 10 mm displacement cycle. IRT image shows warmer temperatures at the top and sides of the steel shear wall and increases of the temperatures along the changes of diagonal profile. Warmer areas around bolts indicated friction and plastic deformations around bolted connection between shear wall frame and infill plate.

During testing of specimens, IR images also allowed to record temperature distribution with increase of the temperature in the direction of the diagonal tension field. The IRT images reflected the changes in the diagonal tension field action. Figure 5.16a shows HCSW\* specimen subjected to 30 mm displacement in horizontal direction in regards to neutral position to of the sample and Figure 5.16b corresponding IR image.

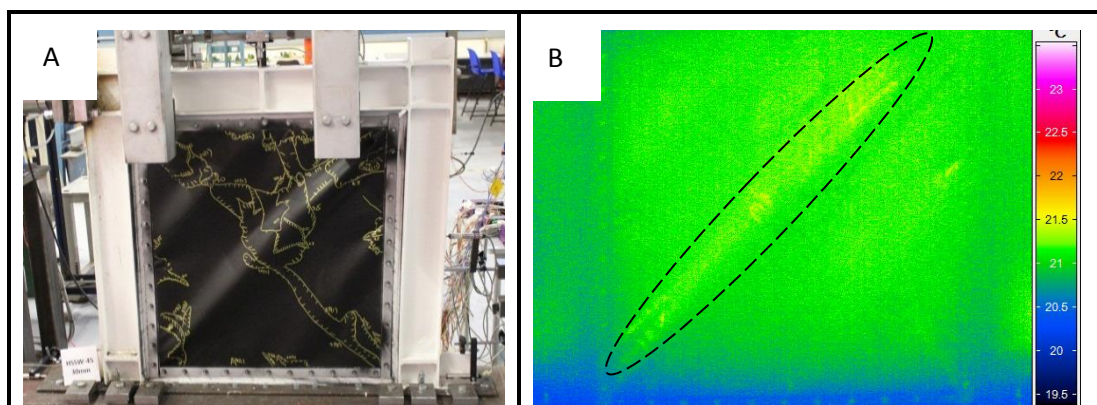
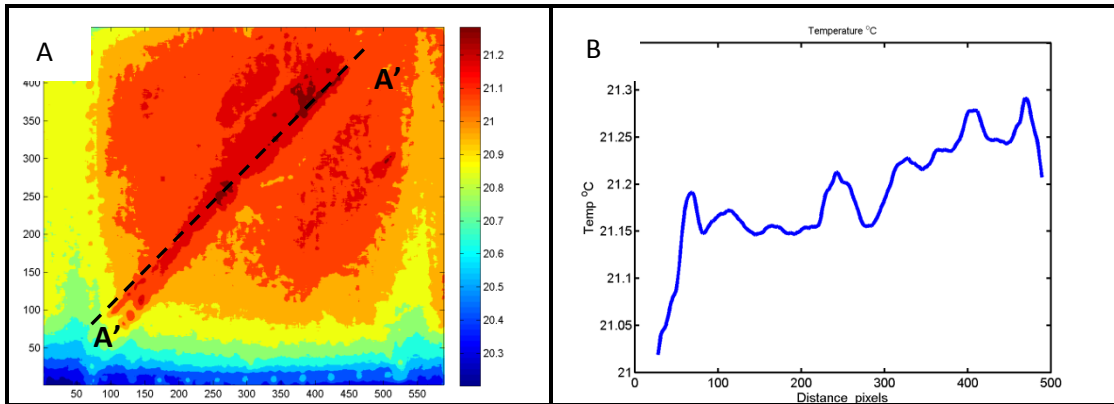


Figure 5.17. Heat releases at maximum 30 mm displacement in horizontal direction for HCSW\* specimen a) shear wall photo b) IR image.

By processing data further in the programmer developed in MATLAB software, a temperature profile (Figure 5.18a) and diagonal tension field action profile was identified as line A'-A' (Figure 5.18b). This method can be used for estimation of the temperature

increase along the diagonal tension field for applied displacements and to assess the distribution of plastic deformations in the infill plate.



**Figure 5.18.** IR images of HCSW\* specimen at 30 mm displacement after MATLAB processing a) demonstrating temperature distribution and tensile field profile b) temperature distribution along A'-A' line.

The results from passive IRT are clearly defining the opportunity to assess the increased plastic deformations on basis of generated temperature differences for steel and hybrid structural elements and the connections between them during the process of testing. Connections between frame and infill plate elements are crucial in shear wall design, IR camera allowed to detect when friction in the bolt area begins and to monitor further development of plastic deformations till failure of the connection.

### 5.8.3 IRT active data

Active thermography was used to measure the surface temperature of the specimen after exposure to external heat. Heat guns were used to apply additional thermal excitation. Due to irregular geometry of the sample heat gun was adopted as more appropriate source of heating than some alternative sources like thermal blanket.

The active thermography was conducted after application of the certain range of the displacement to the shear wall specimen. An external heat provided a thermal contrast between the areas of bonding of the steel and FRP materials and characterizing bond's integrity and estimate delamination for hybrid specimens. Further analysis of the results was done via processing data in the programme developed in MATLAB software. Both

visual inspection and infrared thermography camera images were used to estimate delamination after significant displacements.

For the HCSW\* specimen, Figure 5.19a and d shows image of the plate and the line made by gold marker indicates area of the delamination identified via visual inspection after loading specimen to 20 mm and 30 mm displacement correspondingly. The blue colour in Figure 5.19b and Figure 5.19e shows delamination via visual inspection and blue colour in Figure 5.19c and Figure 5.19f delamination via IRT data. The analysis of the results from IRT was conducted limiting the area of the sample to part with similar thermal mass (internal zone of the infill plate) and assuming 1°C as the temperature difference between the areas with damaged and undamaged bonding within this zone.

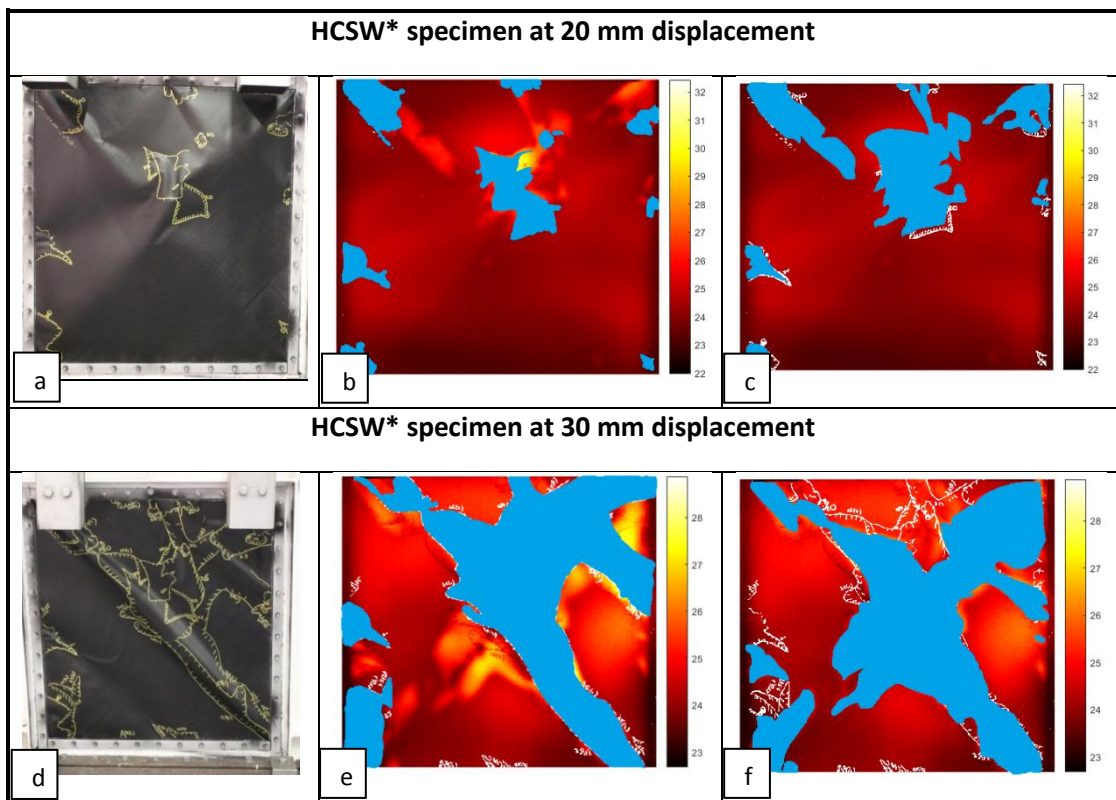


Figure 5.19. IRT active data analysis for HCSW\* a) 20 mm image b) 20 mm visual delamination c) 20 mm IRT delamination d) 30 mm image e) 30 mm visual delamination f) 30 mm IRT delamination.

Via visual inspection the estimated areas of FRP debonding from the steel plate were 10% and 38% at 20 mm displacement and 30 mm displacement respectively. Corresponding results for the same level of displacement as for visual inspection are 16% at 20 mm and 40% at 30 mm displacements, which indicates good correspondence. IRT

results are considered as more reliable in view of lower precision of visual inspection and further development of damaged zones as a result of higher levels of loading.

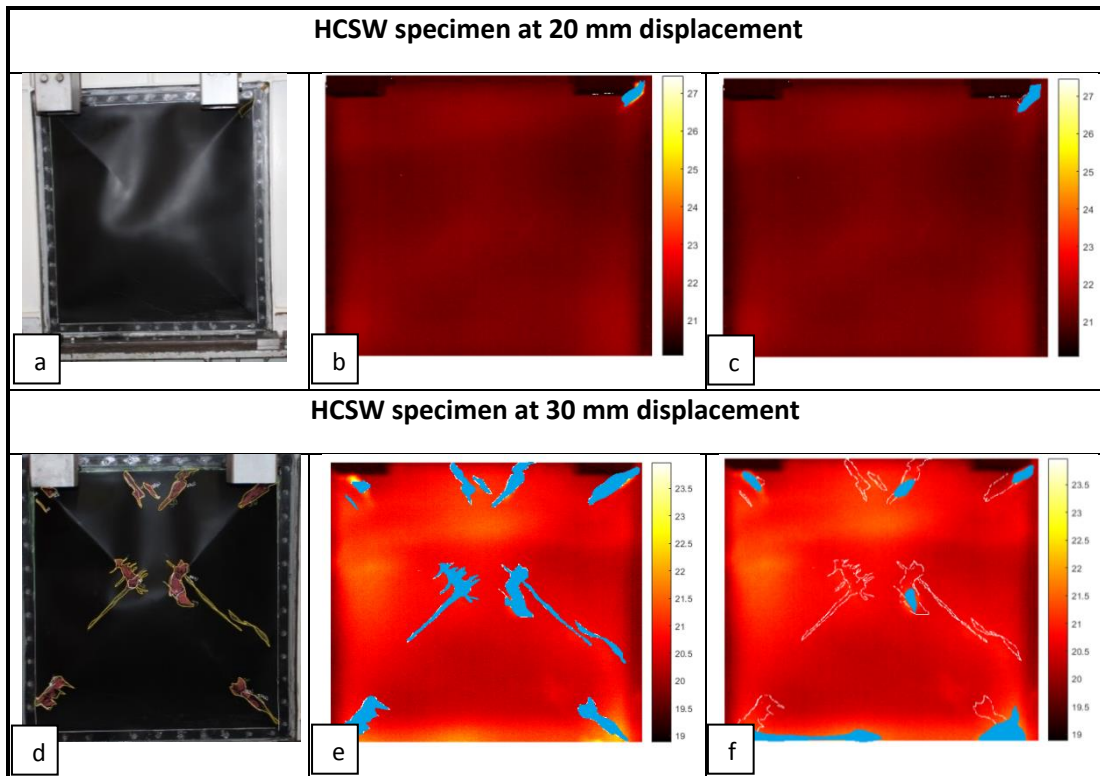


Figure 5.20. Delamination of the HCSW specimen. a) 20 mm image b) 20 mm visual delamination c) 20 mm IRT delamination d) 30 mm image e) 30 mm visual delamination f) 30 mm IRT delamination.

For the HCSW specimen, comparison of the images 5.19b and 5.19c shows good correspondence between visual and IRT data inspection of level of delamination at 20 mm displacement. A small area of 0.3% was delaminated in the corner. At 30 mm displacement, the delamination level identified by IRT method (Figure 5.19e) was considerably less in comparison to visual inspection (Figure 5.19f). Insufficient temperature difference was obtained during heating of the specimen where damage of the FRP fabric occurred as FRP crack development. At 30 mm displacement, 6.21% of the area was delaminated with visual inspection, 3% of the delaminated via IRT data. More precise IRT data analysis could be conducted via processing series of consecutive photos taken during the test at different stages of heating.

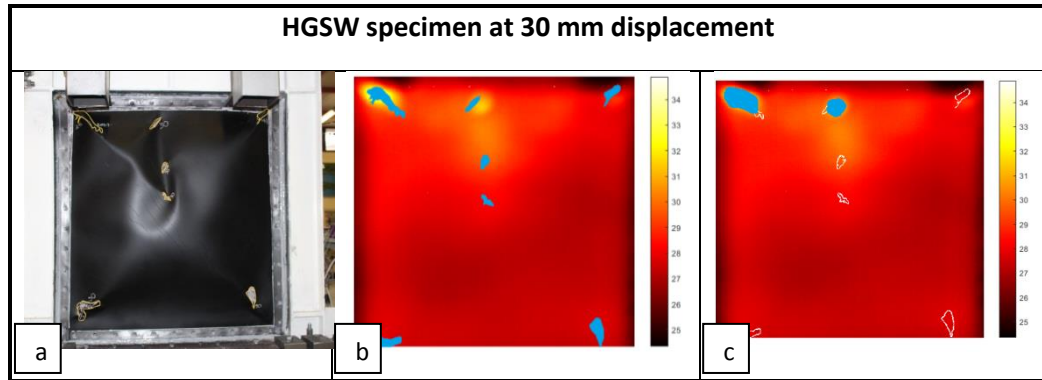


Figure 5.21. Delamination of the HGSW specimen a) 30 mm image b) 30 mm visual delamination c) 30 mm IRT delamination.

For the HGSW specimen, as described before, areas of delamination between FRP and steel plate were less in comparison to other specimens. Figure 5.21 shows delamination level at 30 mm displacement. Only small areas at the top of the specimen were registered. Delamination area was calculated as 1.8% via visual inspection and 1.3% via IRT data.

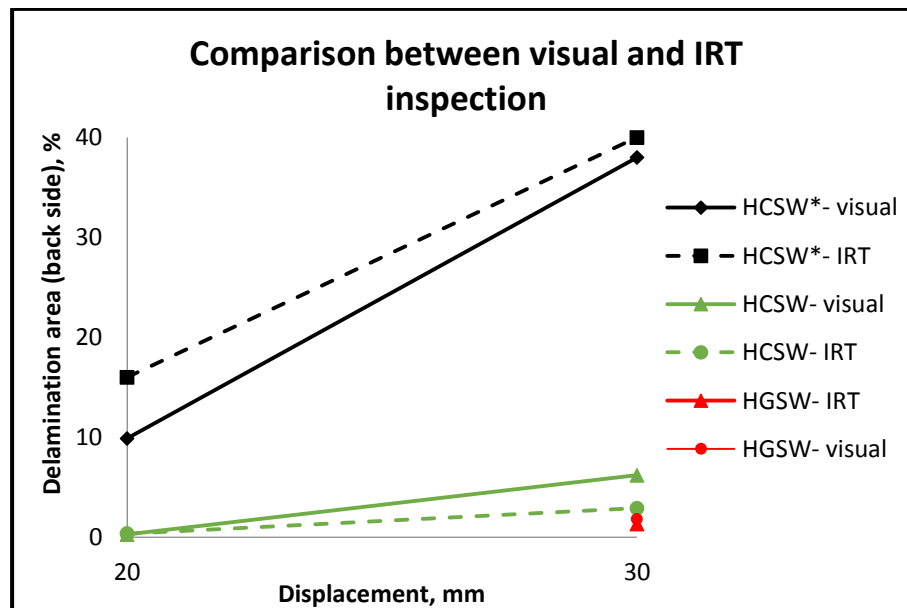


Figure 5.22. Delamination area for HCSW\*, HCSW and HGSW specimens.

A summary of the delamination areas for HCSW\*, HCSW and HGSW specimens is shown in Figure 5.22. For the HCSW\* specimen delamination was significant at 20 mm displacement and it increased significantly at 30 mm displacement. Therefore, for the HCSW and HGSW specimens epoxy film was added in between steel plate and FRP layers as described before in Chapter 4. Addition of the epoxy film proved to be effective and

eliminate delamination considerably, delaminated area on the back side of the plates was under 10% for both specimens at 30 mm displacement.

Data between visual and IRT inspection of the delaminated areas shows good correspondence. However, to introduce temperature difference for the whole specimen simultaneously, more uniform heating method or analysis of the series photos for small elements of the sample could improve results as an IRT practical application.

#### 5.8.4 Summary of the damages for all specimens

Tested specimens experienced different destruction at different levels of loading. Three levels were introduced as level 1: \*, level 2: \*\* and level 3: \*\*\* to assess the extent of damages.

Table 5.1. Description of different damages.

Damage level Damage type	Level 1: *	Level 2: **	Level 3: ***
<b>No.1: Damage due to the buckling of the plate (diagonal waves)</b>	Residual deformations through the wave-length of the infill plate	Pinching of the plate	
<b>No.2: Connection: widening of bolt holes</b>	Enlargement of the bolt holes	Visible damage to the connections through bolt holes appearance near fish plates	Snapping of the infill plate near connection
<b>No.3: Connection: sliding of infill plate</b>	0-5 mm	5-10 mm	More than 10 mm
<b>No.4: Delamination and de-bonding of FRP</b>	0%-10%	10%-20%	More than 20%
<b>No.5: Cracking of the infill plate in diagonal direction</b>	Appearance of cracking	Up to 100 mm long cracks	More than 100 mm long cracks
<b>No.6: Appearance of plastic hinges</b>	Appearance at the vertical steel frame elements	Appearance at the horizontal steel frame element	

A summary of damages is shown in Table 1.1, which were development of out-of-plane deformations due to the diagonal tension field, changes to the connection and to steel infill plate, delamination and cracking in the FRP layer, and appearance of the plastic hinges.

Damages were compared at displacements: 10 mm, 20 and 30 mm. At 10 mm displacement (Table 5.2), all specimens experienced out-of-plane deformation of the infill plate due the diagonal tension field action. At this level of displacement, damages to the connection started to appear for SSW specimen and all hybrid specimens. No changes to connections were identified for pure only specimens. Delamination and cracking in the FRP area developed for all specimens except GSW specimen. No appearance of the plastic hinges was identified via visual inspection.

Table 5.2. Damages for all specimens at 10 mm displacement.

Damage type Specimens	No.1: Damage due infill plate	No.2: Connection: widening of bolt holes	No.: 3 Connections: sliding of infill plate	No.4: Delamination and de- bonding of the FRP	No.5: Cracking of FRP in diagonal direction	No.6: Plastic hinges
SSW	*	*	*	N/A	N/A	-
HCSW*	*	*	*	*	*	-
HCSW	*	*	*	*	*	-
HGSW	*	*	*	*	*	-
CSW	*	-	-	*	*	-
GSW	*	-	-	-	-	-

Changes in the damage level at 20 mm displacement (Table 5.3) in comparison to 10 mm displacement are indicated in green colour in Table 5.2. At 20 mm displacement, for

SSW specimen further damages to the infill plate occurred through the development of pinching areas. For GSW specimen crack in the adhesive bond developed, which indicated sliding of the plate and widening of the bolt holes. Further sliding of the HCSW\* continued at 20 mm displacement, no further changes for connections were recorded for other specimens.

Significant changes for hybrid and pure FRP specimens occurred by the increase of the delaminated areas and development of the cracks in FRP fabric. HCSW and CSW had highest level of damages- 3, whereas GSW specimen experienced less extent of damages of this type. Development of the plastic hinges was visible for all specimens except HCSW specimen.

Table 5.3. Damages for all specimens at 20 mm displacement.

Damage type Specimens	No.1: Damage due infill plate	No.2: Connection: widening of bolt holes	No.: 3 Connections: sliding of infill plate	No.4: Delamination and de- bonding of the FRP	No.5: Cracking of FRP in diagonal direction	No.6: Plastic hinges
SSW	**	*	*	N/A	N/A	*
HCSW*	*	*	**	**	**	**
HCSW	*	*	*	*	***	-
HGSW	*	*	*	*	**	*
CSW	*	-	-	*	***	*
GSW	*	*	*	*	*	*

At 30 mm displacement (Table 5.4), significant damages to the connections occurred to hybrid specimens, elongated bolt holes were visible near fish plate surfaces and infill plate cracked in the corners through FRP and steel. Delaminated areas increased for all

specimens, however HCSW\* specimen had more progressive development. HCSW\* specimen similar to SSW specimen, developed pinching areas on the infill plate surface. This effect was not recorded for other specimens. For SSW, HCSW\* and GSW specimens, plastic hinges appeared in the horizontal section of the shear wall as well. For HCSW and HGSW specimen plastic hinges developed in vertical elements of the shear walls.

Table 5.4. Damages for all specimens at 30 mm displacement.

Damage type Specimens	No.1: Damage due infill plate	No.2: Connection: widening of bolt holes	No.: 3 Connections: sliding of infill plate	No.4: Delamination and de- bonding of the FRP	No.5: Cracking of FRP in diagonal direction	No.6: Plastic hinges
SSW	**	*	**	N/A	N/A	**
HCSW*	**	***	***	***	**	**
HCSW	*	***	***	*	***	*
HGSW	*	***	***	*	***	*
GSW	*	*	**	*	**	**

Assessment of the damages of SSW and HCSW\* specimens allowed to improve the design of the hybrid shear walls HCSW and HGSW specimens. Analysis also shows the rate of the development of damages in different types of specimens.

In addition to the above presented qualitative analysis of the damages and corresponding behaviour of the samples, further quantitative detailed analysis of the experimental results is presented in Chapter 6.

## **Chapter 6: Analysis of experimental results of newly developed shear walls**

This Chapter contains experimental analysis for the tested shear wall specimens: SSW, HCSW\*, HCSW, HGSW, CSW and GSW. The analysis of the results was made on the basis of the parameters and properties described in this Chapter: ultimate load capacity, stiffness values, energy absorption.

## 6.1 Introduction to the analysis of the results

This chapter describes experimental results for newly developed shear wall specimens and their failure modes. The six shear wall specimens: SSW (control specimen), HCSW\*, HCSW, HGSW, CSW and GSW were tested under quasi-static cyclic loading until the corresponding modes of destructions. The infill plates of CSW and GSW specimens were made of corresponding CFRP and GFRP laminates using the same steel boundary elements as the other specimens. They will be further referred to as *pure FRP* group in the text.

All the specimens were at least tested to displacement of 25 mm. Subsequently specimens, which have not reached to their ultimate capacity were subjected to additional displacement loading. CSW specimen was tested to 25 mm, HCSW and HGSW to 30 mm and GSW, SSW, HCSW\* to 35 mm ultimate displacement. Hysteresis loops for displacements up to 25 mm for all above mentioned specimens are shown Figure 6.1 (a- f), respectively.

## 6.2 Parameters for the analysis and failure modes of the specimens

In Chapter 5 the different failure modes of the shear wall specimens were discussed. These modes are delamination and de-bonding of the FRP material from the steel infill plate (as it was demonstrated in Chapter 3), yielding of the steel infill plate, elongation of the bolt holes and tearing of the infill plate around the connection between steel boundary elements and infill plate. The most important parameters which will be measured for comparison of the different shear wall specimens are:

- $F_{avg}$  [kN]- **Magnitude of the average load at each displacement level.** This load is calculated by taking the average of the extreme loads of all cycles at any specific

level of applied displacement. The average load,  $F_{avg}$  is referred to load capacity at the applied displacement.

- $F_{max}$  [kN]- **Ultimate load**, is the maximum load achieved by each specimen and referred to as the capacity of the shear wall system.

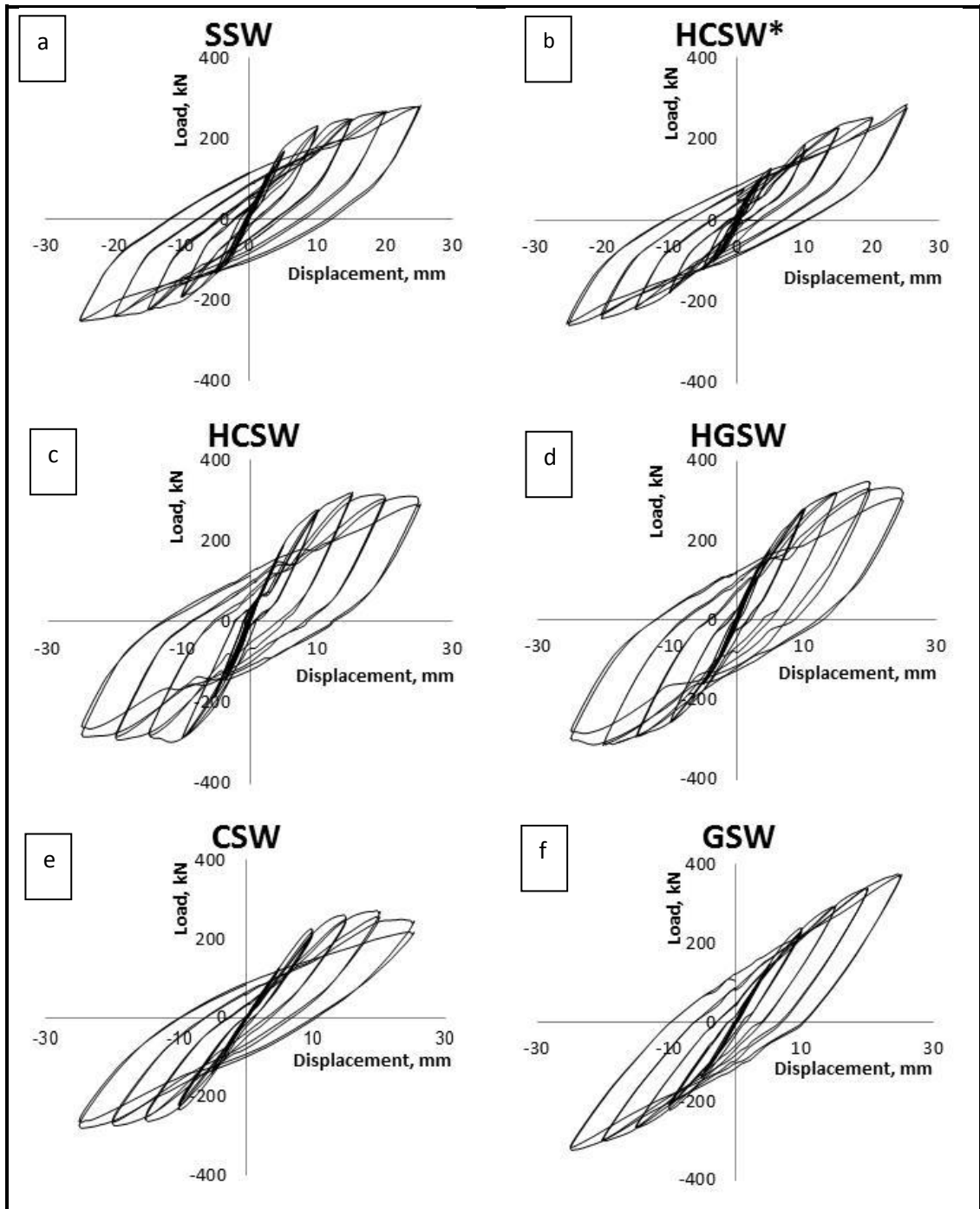


Figure 6.1. Cyclic load - displacement for a) SSW b) HCSW\* c) HCSW d) HGSW e) CSW f) GSW during cyclic loading.

- $K_0$  [kN/mm]- **Initial stiffness**, is the slope of the load- displacement curve in the linear region. It was calculated by dividing changes in the load by displacement for initial level of loading where relationship between load and displacement is approximately linear.
- $K_D$  [kN/mm]-**Dynamic stiffness**, measured as the slope between the extreme pull and push displacement values.
- $\Delta_{NL}$  [mm] and  $F_{NL}$  [kN]- are the load and displacement at the start of the nonlinear behaviour.

### 6.3 Comparison of average load values, $F_{avg}$ , for all specimens

From the hysteresis loops shown in Figure 6.1 (a-f), load - displacement curves were estimated by taking the average of the extreme loads for each of the samples over the cycles at the same amplitude as shown in Figure 6.2. Note that the thickness of the steel infill plate for all specimens is 0.8 mm. The same number of FRP layers (two layers on both sides of the infill plate) was applied in the hybrid specimens. Pure FRP specimens were designed with eight layers aiming to achieve similar thicknesses to the corresponding hybrid specimens with steel plate and four FRP layers.

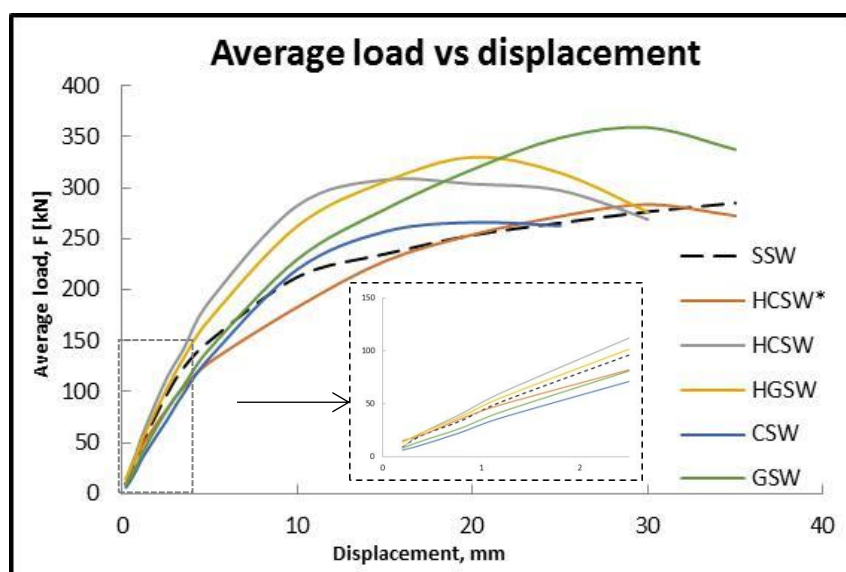


Figure 6.2. Variation of average load- displacement for five newly developed and SSW (control) shear wall specimens.

### 6.3.1 Comparison of HCSW\* and HCSW behaviour

As a first stage of the development of hybrid shear wall system, in the HCSW\* traditional bolted connection between the primary fish plates welded to steel frame and the infill plate was used. Because of the lower friction between the steel surface and the surface of FRP material, in HCSW\*specimen a dramatic reduction of the capacity of the connection was observed. In addition to the early failure of the connections, significant delamination and de-bonding of the CFRP layers from the steel infill plate occurred for displacements above 5 mm.

As a result of the conducted tests on small scale specimens described in Chapter 3, adhesive bonding at the connection was proved to have a governing role for improving the connections capacity for hybrid elements. It was also found be extremely beneficial as it increases the stiffness of structural elements. As a second stage of the development of hybrid specimens, HCSW specimen was designed by bonding the fish plate to the infill plate using epoxy adhesive and also by incorporating an epoxy film between the steel infill plate and the FRP layers to enhance the quality of the bond and improve the delamination resistance of the FRP from the steel infill plate.

A comparison between two hybrid specimens HCSW\*, HCSW and control specimen SSW is shown in Figure 6.3. Up to 18 mm displacement, the HCSW\* specimen shows relatively lower load capacity than SSW. Above 18 mm displacement load capacity of HCSW\* and SSW are approximately the same. This effect was caused by the poor bonding between CFRP and steel infill plate which resulted in large scale delamination of the FRP from the infill plate at displacement of 18 mm. Up to 28 mm displacement, for HCSW\* specimen the load values are lower than for HCSW specimen.

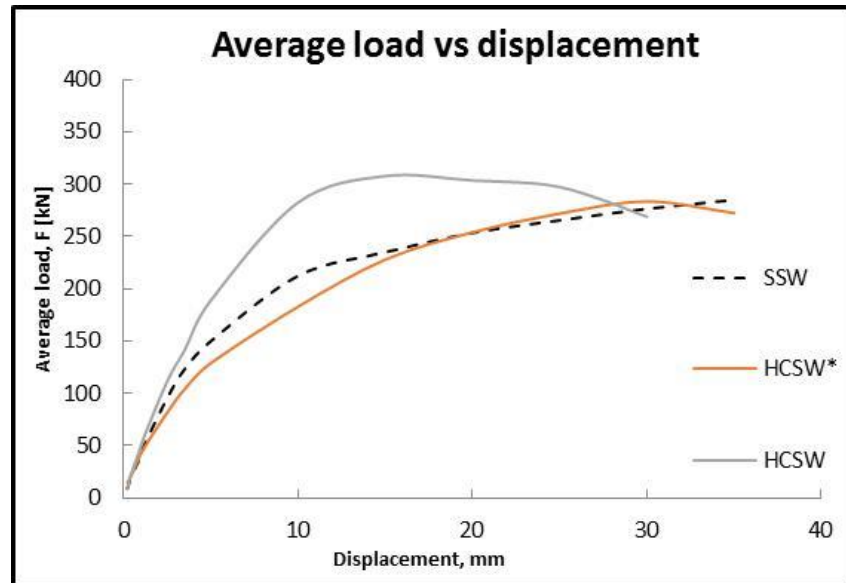


Figure 6.3. Comparison of load – displacement curves for HCSW\*, HCSW and SSW (control) specimens.

The test results of the HCSW\* specimen, proved that after the large scale delamination of the FRP layers for HCSW\* at early stages of the displacements, the FRP material did not contribute to the capacity anymore and only the steel element had a governing structural role in the HCSW\* system. The shear wall system did not act as a hybrid system and the loading capacity failed to reach the expected high magnitude. Therefore, the bond between the steel infill plate and the FRP layers needed improvement. This led to the application of an additional epoxy resin film in HCSW specimen which resulted in a better performance of the hybrid shear wall system. HCSW\* is has been discarded from further analysis.

### 6.3.2 Comparison of HCSW and HGSW behaviour

Both HCSW and HGSW specimens were designed with an additional layer of adhesive film between infill plate and the FRP layers and the fish plate was bonded to the boundary members. The behaviour of the HCSW, HGSW and SSW specimens is compared in Figure 6.4.

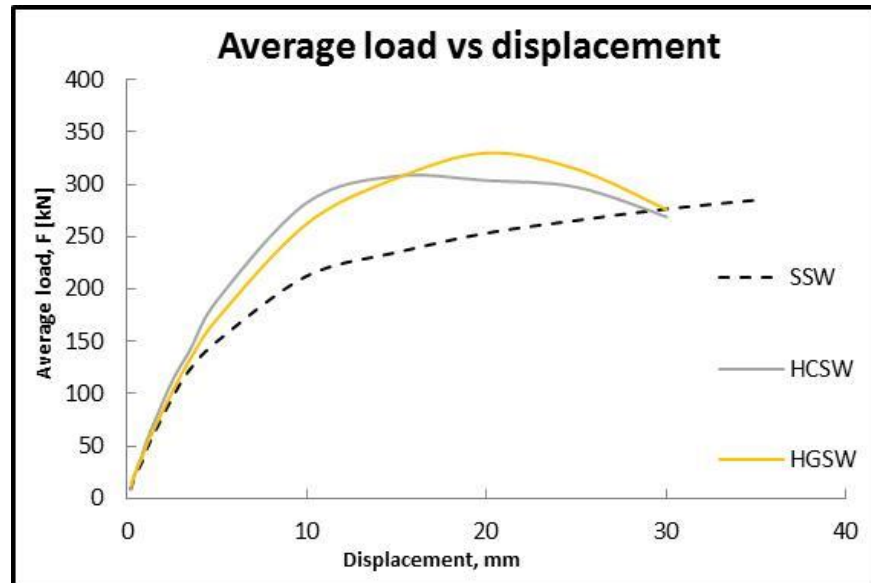


Figure 6.4. Comparison of load – displacement curves for HCSW, HGSW and SSW (control) specimens.

The load capacity for HCSW and HGSW hybrid specimens is higher at all amplitudes up to 30 mm displacements in comparison to control SSW specimen. Up to 4 mm displacement, SSW, HCSW and HGSW behaved very similarly and the graphs were close to each other. The initial stiffness of HCSW is higher than HGSW and both are stiffer than the control specimen SSW. At 15 mm displacement, the HCSW specimen reaches its ultimate capacity of 308 kN, and at this level of displacement HGSW has similar load value.

At 30 mm displacement, a significant destruction of the connection between the infill plate and the fish plates for both specimens occurred and the tests were terminated. Between 15 mm and 30 mm displacements, HGSW specimen showed higher load capacity than for HCSW specimen. The HGSW achieved ultimate load capacity of 330 kN at 20 mm displacement. After that the load started to decrease and at 30 mm displacement it was approximately the same as HCSW.

Comparing the behaviour of the HCSW and HGSW, it can be seen that the addition of GFRP to steel infill plate results in higher ultimate load. As CFRP material is stiffer than GFRP, it is a cause of the earlier failure of the connections between the infill plate and the

frame, higher extent of development of delamination and a lower ultimate load capacity for HCSW specimen.

### 6.3.3 Comparison of CSW and GSW behaviour

For shear wall systems with pure GFRP and pure CFRP infill plates (Figure 6.5), the initial load values for the same levels of displacement are lower than the control specimen SSW. Above 6.5 mm displacement for GSW specimen and 9 mm displacement for CSW specimen, both specimens showed better load capacity than the control specimen. Up to 11 mm displacement, GSW and CSW behave similarly, but above this level the difference between the two specimens starts to increase significantly. For example, the load capacity difference between two specimens is 20% at 20 mm displacement and increasing up to 33% at 25 mm displacement.

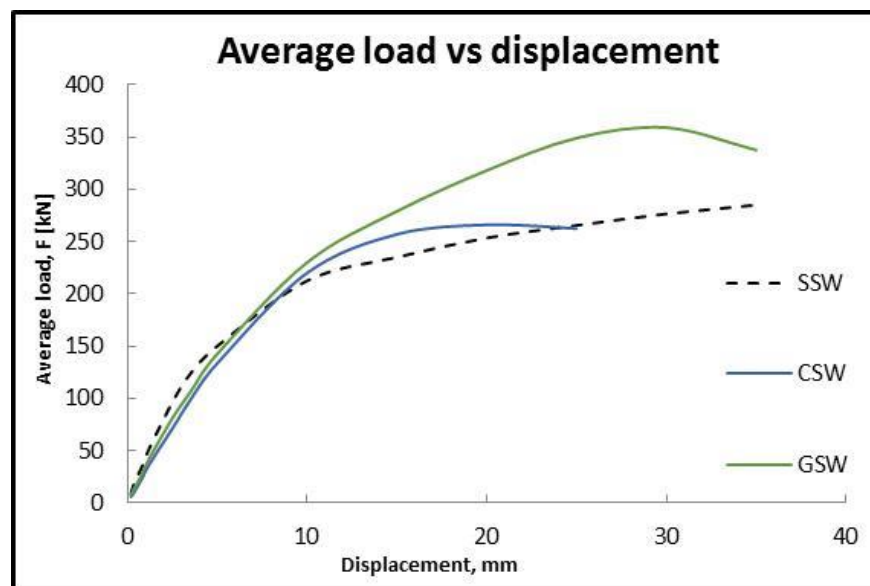


Figure 6.5. Load vs displacement results for CSW, GSW and SSW (control) specimens.

For the CSW specimen the main mode of the failure was a sudden and fast development of delamination and intensive cracking within the CFRP fabric resulting in a relatively brittle failure of the infill plate. In comparison with CSW specimen, GSW had more gradual failure of the infill plate. The connections between the infill plate and the fish

plates behaved better than for other specimens up to the termination of the test. The GSW ultimate load capacity of 359 kN was 35% higher than the CSW ultimate capacity of 266 kN.

#### 6.3.4 Comparison of hybrid group and pure FRP group behaviour

Two pure FRP specimens and two hybrid specimens have similar trends in the behaviour with very close load capacity between specimens of the same group up to 10 mm displacement (Figure 6.6). The average load capacity for the hybrid group is 21% higher than the capacity of pure FRP group specimens at 10 mm displacement. In both groups the specimens with GFRP material have higher ultimate load capacity and faster reduction of the load values, when maximum load value was achieved. However, a more significant difference in the load capacity between two specimens of the pure FRP group is noticeable above 10 mm displacement.

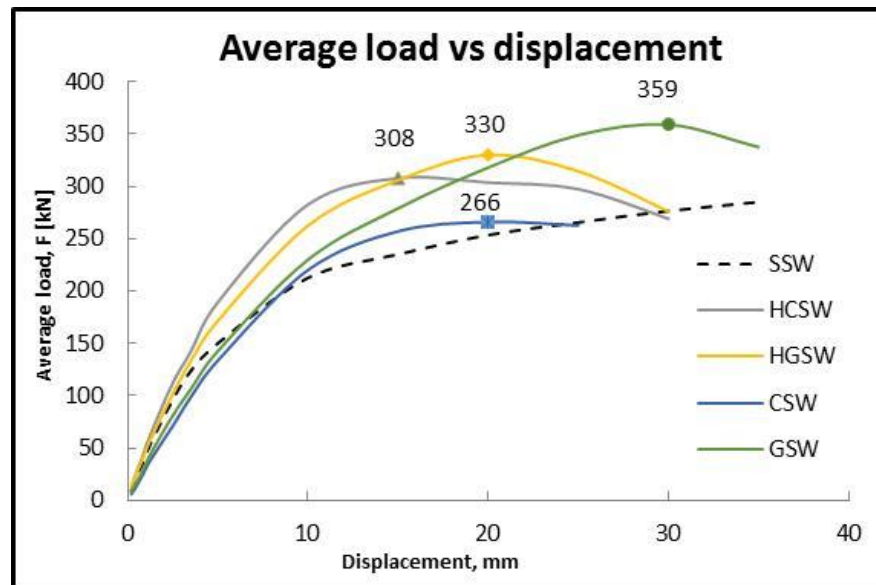


Figure 6.6. Comparison of load - displacement results for HCSW, HGSW, CWS, GSW and SSW (control) specimens.

The load values of the CSW specimen are lower than hybrid specimens HCSW and HGSW, as well as the GSW specimen. The GSW specimen performs better than the HCSW specimen above 18 mm, and HGSW specimen above 21 mm displacement, respectively. Above 21 mm displacement, load capacity of the GSW specimen is the highest compared to all other tested specimens.

### 6.3.5 Comparison of initial stiffness ( $K_0$ ), changes in stiffness for whole testing range ( $K$ ) and dynamic stiffness ( $K_D$ )

For the initial loading (Figure 6.2), all shear wall systems predominantly behave in a linear elastic way. The initial stiffness ( $K_0$ ) is calculated for the region up to 2.5 mm displacements. The experimental data from the linear region, load and displacement is approximated with linear functions. The linear functions and correlation factors between experimental results and results for analytical approximations can be found in Appendix A. For control SSW specimen initial stiffness is 37 kN/mm. The specimens with the highest initial stiffness values were for hybrid specimens. Their stiffness values are between 38 kN/mm and 44 kN/mm, which is higher than steel one. The added layer of CFRP and GFRP to the steel plate are contributing to increase of stiffness. Both GSW and CSW specimens have lower initial stiffness than control SSW due to lower values of Young Modulus. Their initial stiffness is between 29 kN/m and 32 kN/m.

The stiffness at peak load at any displacement,  $k$ , was found for all specimens by finding the slope of the “unloading” branch of the hysteresis curve at the beginning of reversing the displacement, as it is shown in the Figure 6.7 for SSW specimen.

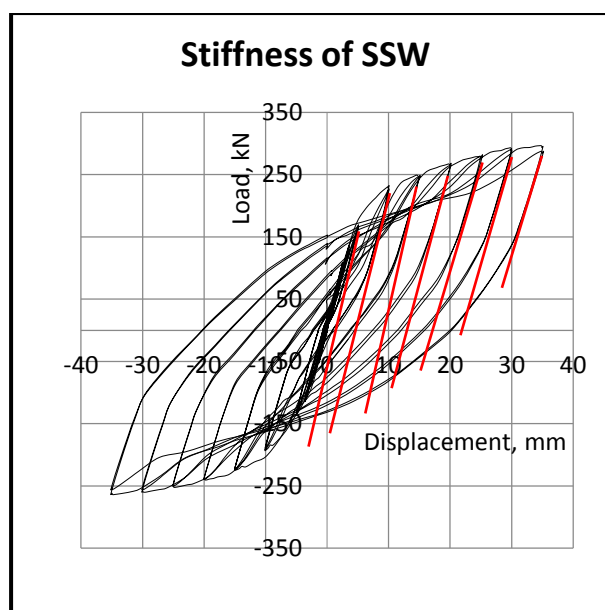


Figure 6.7. Lines showing history of variations of stiffness for SSW specimen.

The variation of stiffness values at peak load at any displacement for all specimens is shown in Figure 6.8. Hybrid specimens are the stiffest in comparison with all other specimens.

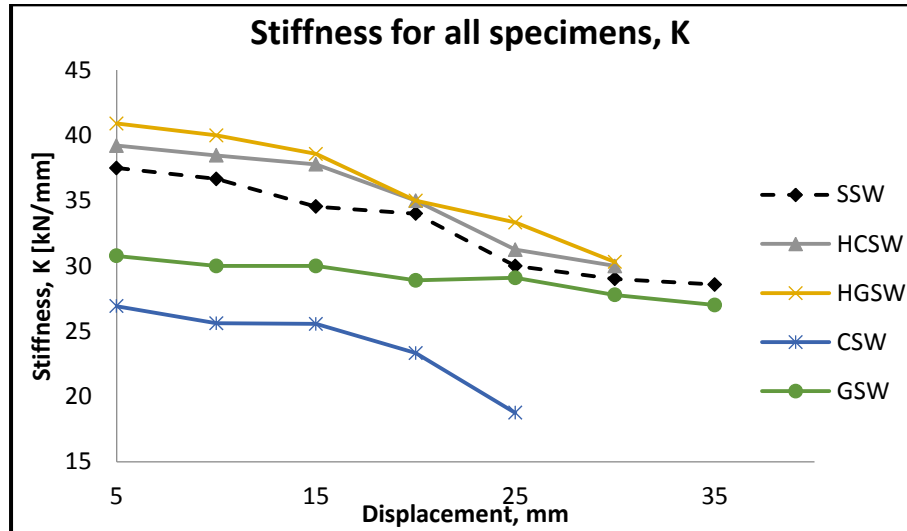


Figure 6.8. Stiffness values for all specimens.

Stiffness,  $k$ , for pure FRP specimens was lower in comparison with SSW specimen, however the rate of decreases in the stiffness values of the pure GFRP specimen is shallower in comparison with all other specimens. Stiffness of pure CFRP specimen is considerably lower than all other specimens.

The dynamic stiffness is calculated for specimens by measuring the slope between extreme pull and push force/displacement values for the first cycle of loading at each level of displacement (Figure 6.9). The evolution of the dynamic stiffness during cyclic loading for all specimens is demonstrated in Figure 6.10. Up to 20 mm displacement, dynamic stiffness for hybrid specimens HCSW and HGSW is higher in comparison with other specimens. However, at 30 mm displacement, all specimens except GSW specimens have approximately the same dynamic stiffness as SSW.

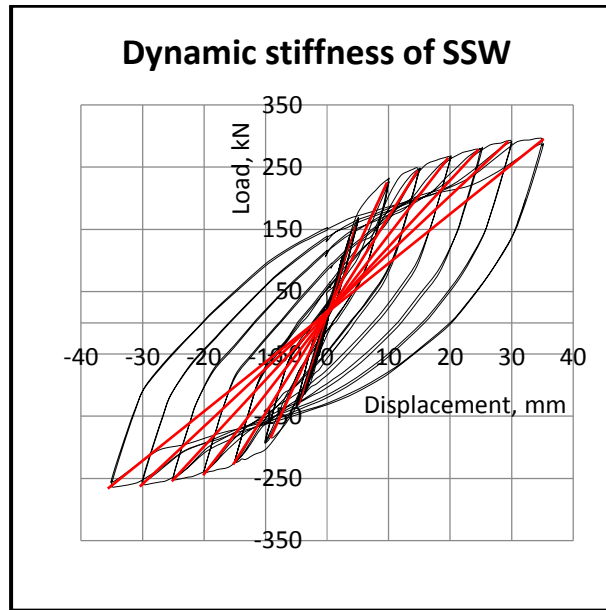


Figure 6.9. Lines showing history of dynamic stiffness for SSW specimen.

This is an evidence that for hybrid specimens at 30 mm displacement, the FRP materials do not contribute to the structure performance anymore. The GSW specimen had the smallest decrease in dynamic stiffness values up to 30 mm displacements and higher values of  $K_D$  than all other specimens above 25 mm displacement.

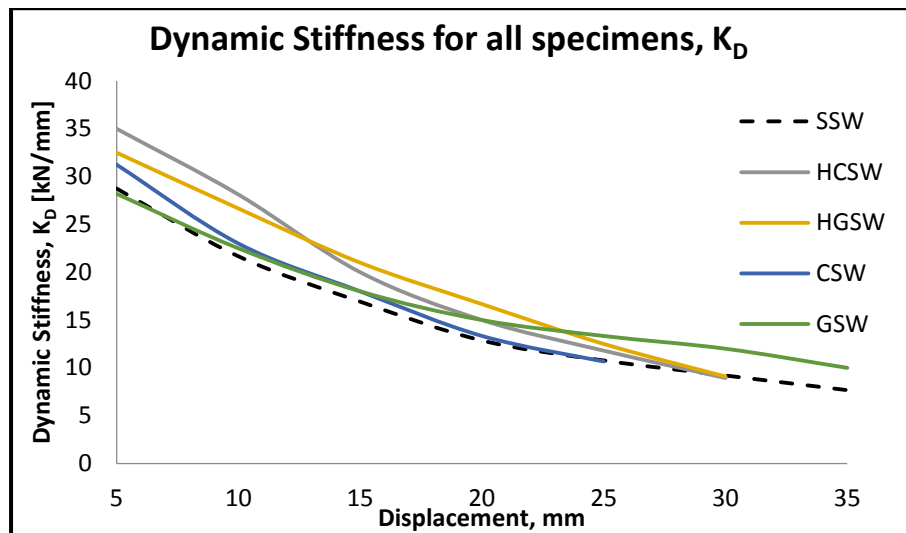


Figure 6.10. Evolution of dynamic stiffness during cyclic loading for all specimens.

#### 6.4 Deformability

Based on the Figure 6.2, a reverse analysis was conducted comparing of the displacements at the same level of loading up to 250 kN as demonstrated in Figure 6.11. As

not all specimens achieved values above 250 kN, analysis of deformability above these values will be analysed in Section 6.5.

Up to 150 kN loading, the deformations of the SSW specimen were less than for pure FRP specimens and higher than for the hybrid group. After 150 kN, the displacements of SSW increased faster and were highest in value in comparison with other specimens. Displacements increased from 2.6 mm at 100kN to 19 mm at 250 kN loading.

For all levels of loading, the hybrid HCSW and HGSW specimens showed lower deformability in comparison to the other specimens. Their displacement increased from approximately 2 mm at 100 kN to 8 mm at 250 kN. HCSW specimen is the least deformable specimen for this interval.

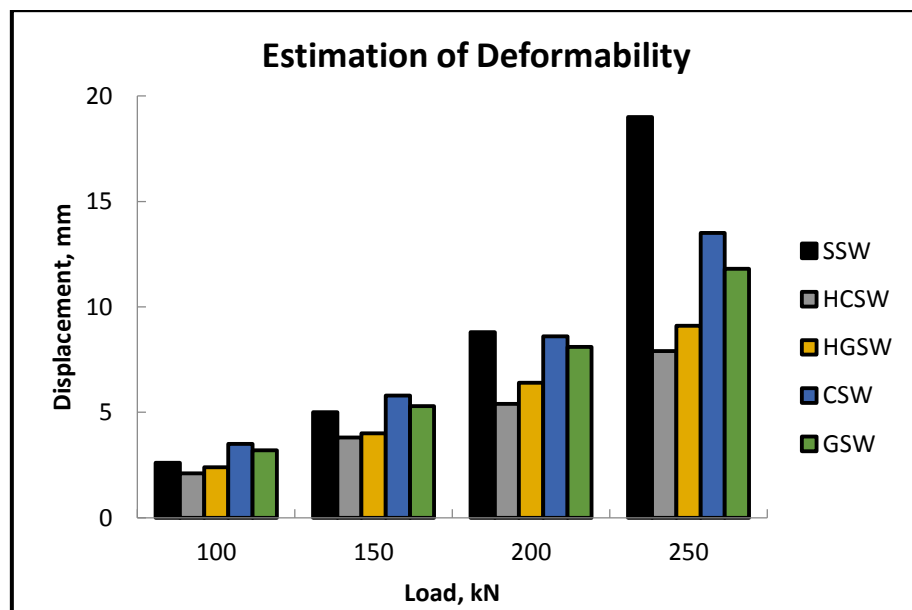


Figure 6.11. Comparison of the deformability at the same level of loading.

The pure FRP specimens had similar trend to hybrid specimens in increasing their deformability values with the increase in the load. For CSW and GSW specimens deformations were 3.5 mm and 3.2 mm at 100 kN respectively. At 250 kN for CSW and GSW specimens, they increased to 13.5 and 11.8 mm, respectively. The GSW specimen had less deformations in comparison to the CSW specimen.

### 6.5 Ultimate load capacity

Figure 6.12 shows a summary of the ultimate load capacities and their corresponding displacements achieved by all specimens. The hybrid specimens reached their ultimate load values at early stages of loading in comparison to pure FRP specimens with the same FRP material: HCSW at 15 mm displacement and CSW at 20 mm displacement; HGSW at 20 mm displacement and GSW at 30 mm displacement. The reason for this trend is that in hybrid plates in comparison to pure FRP, steel plate as a core in the infill plate has higher Young's Modulus and is contributing to high initial stiffness of HCSW and HGSW specimens.

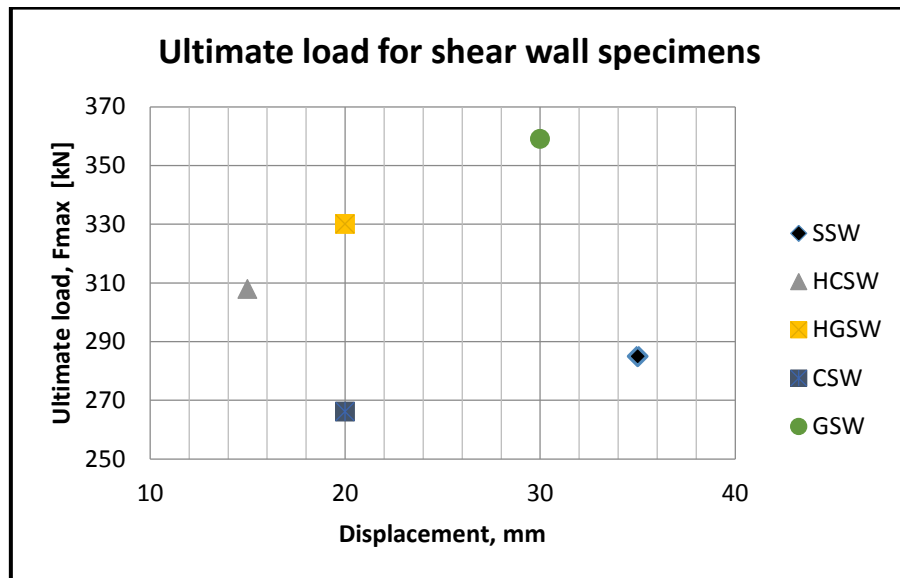


Figure 6.12. Comparison of ultimate load capacities for shear wall specimens and corresponding displacement.

In both pure FRP and hybrid group, specimens with CFRP material achieved lower ultimate load in comparison to the specimens with GFRP material. Plates with CFRP material were less deformable at higher loads, which resulted in their brittleness and intensive cracking and delamination in comparison to GFRP infill plates.

The GSW specimen achieves higher ultimate load value of 359 kN among all specimens, including the HGSW specimen. Contributing factors to such high ultimate load values of GSW is higher deformability of the specimen with pure FRP infill plate. For HGSW

specimen, the snapping of the steel plate and the cracking in the FRP in the infill plate corners did not allow it to achieve higher ultimate load. In addition, pure FRP group had connection with higher capacity. GSW and CSW specimens had 1.5 mm steel strips on both sides and 8 layers of FRP at the connection in comparison with hybrid group specimens with 0.8 mm steel plate and 4 layers of FRP.

Whereas CSW specimen achieved early ultimate load values in comparison to other specimens, despite its stiffer connections, due to the brittleness of the infill plate and development of significant delamination and cracks in the FRP plate at relatively early stages of loading in comparison to GSW.

## 6.6 Analysis of energy absorption

The analysis of the energy absorption (EA) was conducted on the basis of the following parameters:

- **EIC [kJ]- Energy absorption per individual cycle of loading.** Energy absorbed by shear wall calculated from measuring enclosed area within individual cycle of loading at the specific level of loading.
- **ESD [kJ]- Energy absorption at any specified level of displacement.** It is energy absorbed within all hysteresis loops by the shear wall system at any specific level of the displacement.
- **CEA [kJ]- Cumulative energy absorption,** - is the sum of the energy absorbed by addition of all hysteresis loops up to a specified level of loading.
- **SEA [kJ/kg]- Specific energy absorption,** - is the cumulative energy absorption (CEA) normalized to the total weight of the shear wall system for each specimen. As mentioned in the previous chapters a shear wall system consists of infill plate, fish plates and all boundary elements.

### 6.6.1 Energy absorption per individual cycle- EIC

The distribution of the EA between the individual cycles at the same level of displacement is shown in Figure 6.13. It can be seen that energy absorbed is the highest during the first cycle of any applied displacement amplitude and then decreases during the second and the third cycles at the same amplitude for all specimens.

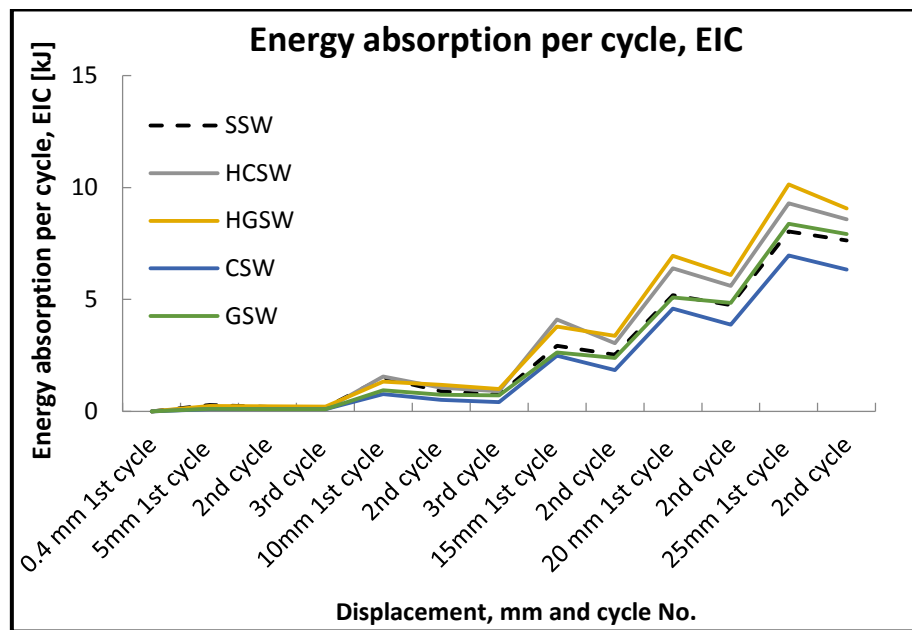


Figure 6.13. Energy absorption for individual cycles.

The highest absolute EIC difference between first and last cycles (Figure 6.14) was around 1.1 kJ for HCSW hybrid specimens at 15 mm and for HGSW at 30 mm. The GSW specimen had also high absolute difference of approximately 1 kJ at 30 mm and 35 mm displacement, whereas absolute differences for CSW specimen were between 0.63 kJ and 0.73 kJ for the specified region.

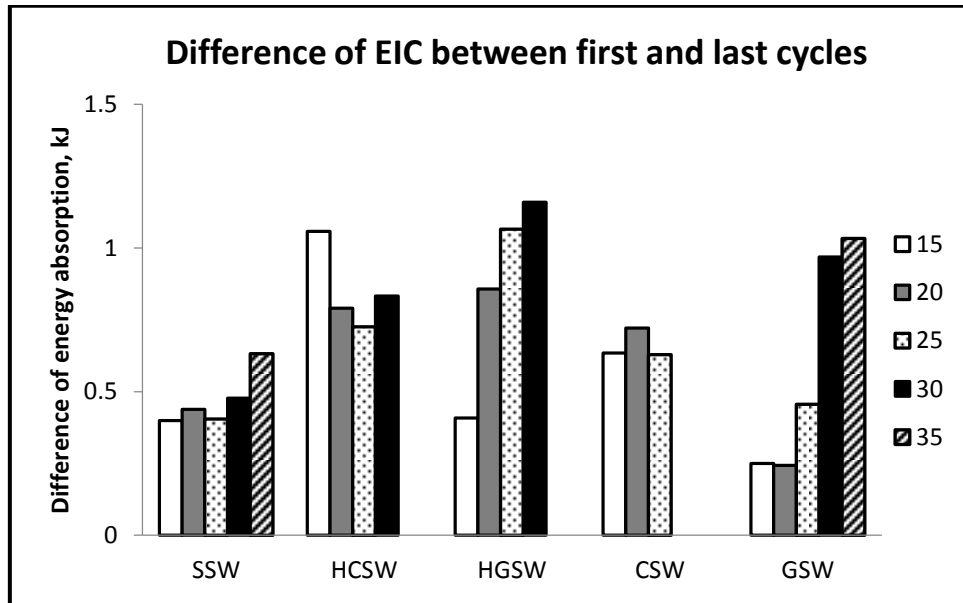


Figure 6.14. Differences for energy absorption between cycles at the same level of loading for all specimens.

For the SSW, HGSW and GSW specimens the increase in the load is the cause of the gradual increase in the EIC difference between the first and the last cycles at the specific level of loading. For the CSW and HCSW such tendency is not obvious probably due to the relative brittle failure of the CFRP layers at relatively early stages of loading.

### 6.6.2 Energy absorption at any specific level of displacement, ESD

The EA by shear wall specimens was calculated from the enclosed area within hysteresis loops. Figure 6.15 shows energy absorbed by specimens for the tested interval. As mentioned before in Chapter 4, according to ATC-24 protocol up to 15 mm three cycles were applied, at 15 mm displacement and above it, two cycles were applied. The ESD was calculated as sum of the areas of all cycles for each level of displacement.

The hybrid specimens HCSW and HGSW have the highest energy absorption in comparison with all the other specimens up to 28 mm displacement. These two specimens behave similarly up to 17 mm, then the difference between them slightly increases.

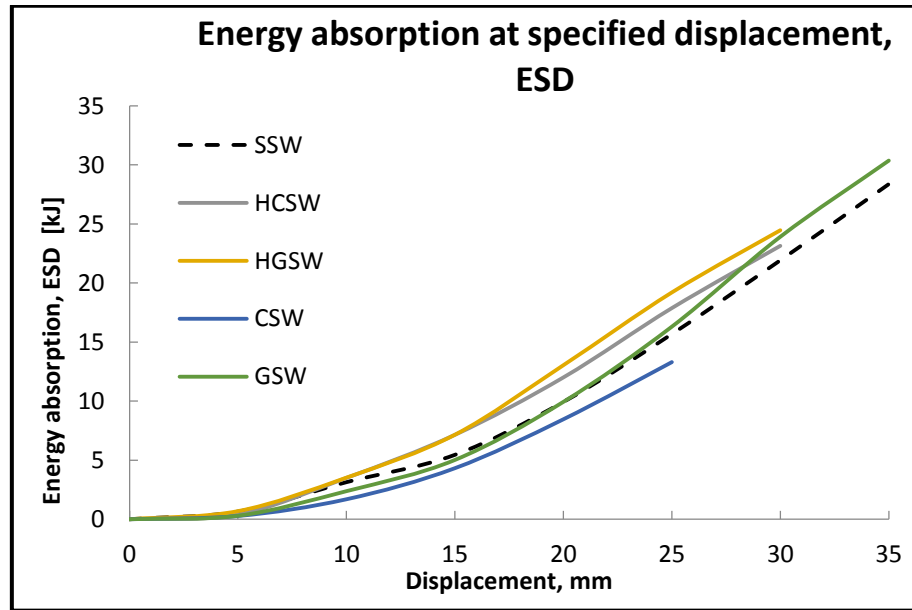


Figure 6.15. Variation of energy absorption at each level of loading for all specimens.

The energy absorption value of HGSW is higher than HCSW specimen by around 1 kJ at 20 mm and 1.3 kJ at 25 mm, respectively. Up to 10 mm displacement, hybrid specimens behaved similarly to the SSW specimen. After 10 mm displacement, the difference between hybrid specimens and SSW control specimen increases more significantly, at 15 mm displacement, this difference is around 1.7 kJ. Up to the maximum applied level of loading, the HGSW specimen behaves better than the HCSW one. This is due to the higher deformability of GFRP which delayed the beginning of the delamination process. This is an additional contributing factor to the stiffness, ultimate load and energy absorption capacity.

Similarly for pure FRP specimens, the sample with the GFRP infill plate has better behaviour and higher values of ESD than the specimen constructed with pure CFRP infill plate. The ESD of both pure FRP specimens were similar up 15 mm displacement, then the difference between the two specimens increased to 3.0 kJ at 25 mm. The values of energy absorption for the GSW specimen were close to the values of SSW control specimen up to 25 mm displacement. The differences between SSW specimen and GSW started to increase

from 25 mm displacement and were 2 kJ at 35 mm displacement. The ESD of the CSW specimen was lower in comparison to other specimen at all levels of loading. The ESD values of CSW were lower by approximately 1.3 kJ between 10 mm and 20 mm displacements and by 2.4 kJ at 25 mm displacement in comparison with the control SSW.

The ESD of hybrid group is higher than the pure FRP group until 28 mm displacement. At 28 mm displacement the ESD values of GSW specimen became higher than the HCSW specimen. At 30 mm displacement, the ESD values of HGSW specimen were similar to GSW specimen.

Figure 6.16 shows the differences in the ESD between different intervals of loading. For the control SSW increases in the differences were considerably less for adjacent intervals. After initial significant increase by 93% for interval 15 mm- 20 mm, the increases for other intervals were by 28%, by 8% and by 4% for intervals 20 mm-25 mm, 25 mm- 30 mm and 30 mm- 35 mm respectively in comparison to adjacent intervals.

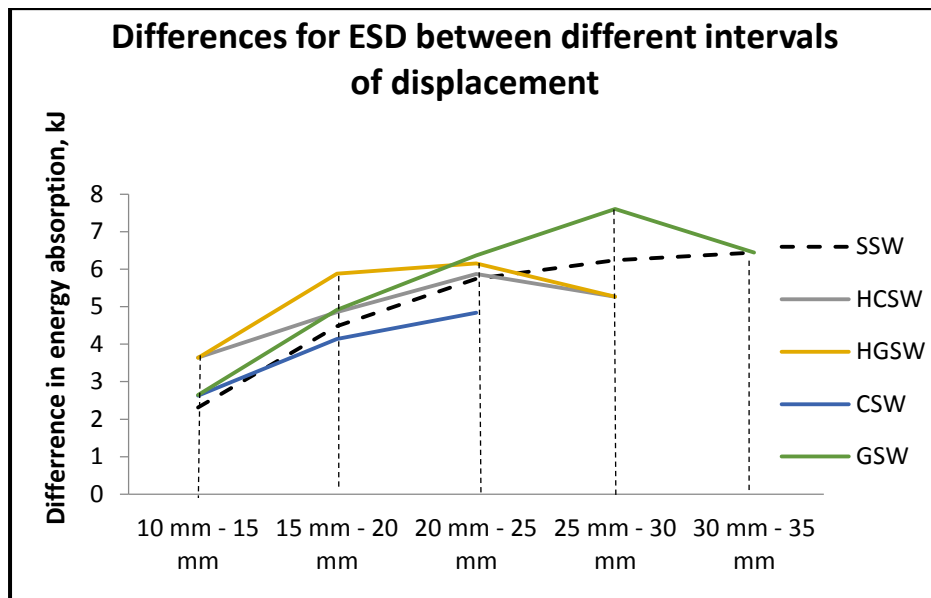


Figure 6.16. Differences in ESD at different intervals.

The hybrid specimens HCSW and HGSW had similar absolute differences values to each other at intervals 10 mm-15 mm and at interval 25 mm-30 mm. The ESD of HGSW was by 21% higher for region 15 mm- 20 mm and by 5% higher for region 20 mm- 25 mm in comparison with HCSW specimen.

For the CSW specimen, the initial difference in ESD was very similar to SSW and GSW specimens, then its values were lower in comparison with all other specimens. This test was terminated at 25 mm displacement due to the significant damages to the infill plate.

For the GSW specimen, the ESD has higher values to that of SSW specimen. Above 20 mm-25 mm region difference in ESD were higher than for other specimens. Highest absolute difference of ESD (7.6 kJ) was achieved at 25 mm-30 mm interval for GSW specimen. Then this value decreased to 6.4kJ, which was 15% in comparison with the adjacent interval.

### **6.6.3 Cumulative energy absorption (CEA)**

The cumulative energy absorption at specific level of loading was calculated by taking the sum of the ESD for all previous cycles of loading. The CEA for all specimens at 15 mm, 20 mm, 25 mm and 30 mm displacement is shown in Figure 6.17.

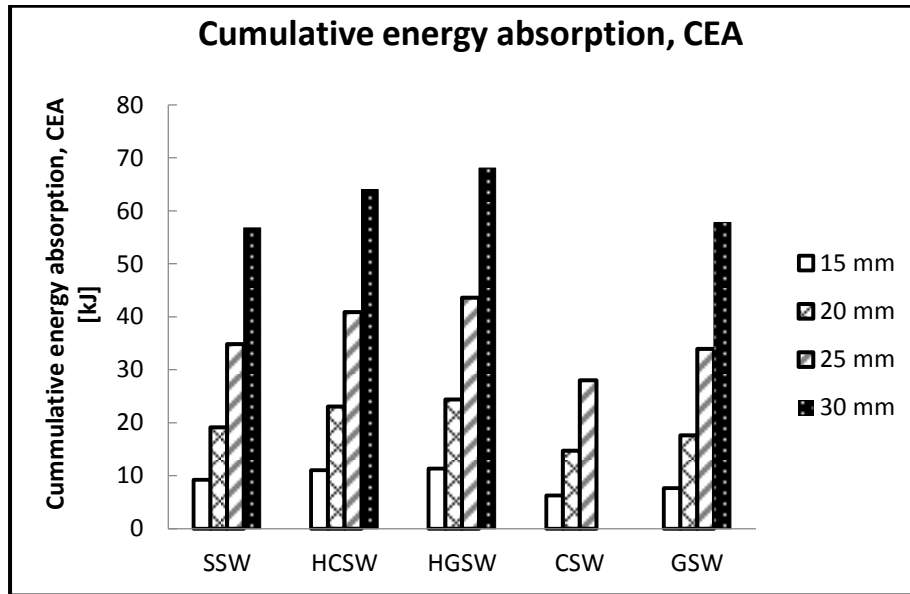


Figure 6.17. Comparison of cumulative energy absorption.

For HCSW and HGSW specimens the CEA is higher at all levels of loading in comparison with other specimens. The CEA values for HCSW and HGSW specimens are similar with a slightly better performance of HGSW of 0.3 kJ, 1.4 kJ, 2.7 kJ and 1.3 kJ at 15 mm, 20 mm, 25 mm and 30 mm, respectively. The GSW specimen has slightly lower CEA values than the SSW control specimen for the indicated three levels of loading. CSW specimen has a lower CEA in comparison with all the other specimens.

For hybrid specimens, the CEA increased as average approximately by 12.5 kJ at 20 mm, by 31 kJ at 25 mm and by 55 kJ at 30 mm in comparison to the CEA at 15 mm displacement. For the GSW specimen changes in CEA are similar to SSW control specimen. The increases in CEA for GSW specimen are around 9.9 kJ at 20 mm, 26 kJ at 25 mm and 50 kJ at 30 mm displacements in comparison to the CEA at 15 mm displacement. For CSW specimen CEA are smaller relative to other specimens, CEA of 6.3 kJ at 15 mm displacement, increased by 8.5 kJ at 20 mm and by 22 kJ at 25 mm displacement.

A comparison of the energy absorption at any specific level of displacement to the cumulative energy absorption at 25 mm displacement is demonstrated in Figure 6.18.

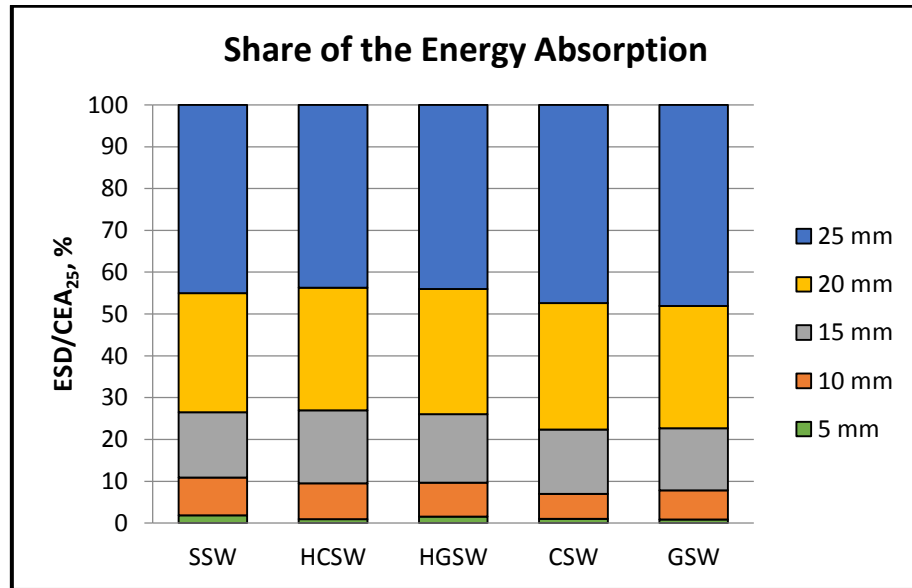


Figure 6.18. Share of the energy absorption at various stage of loading for all shear wall systems.

For the tested range of the displacements, the share of the percentage energy absorption increases at higher displacements for all specimens. For hybrid specimens, share is approximately 30% at 20 mm displacement and 45% at 25 mm displacement, while for pure FRP specimens it is approximately 30% at 20 mm displacement and 48% at 25 mm displacement. In pure FRP infill plate higher percentage of energy (blue areas) is absorbed at higher displacement loading relative to the hybrid and steel shear wall systems.

## 6.7 Summary of the experimental results

Figure 6.19 shows the average load values for all specimen and includes results for steel frame only without infill plate. Steel frame was tested by Ahmed Maleki (Maleki, 2014) in accordance to ATC-24 protocol. Frame reached its ultimate capacity of 159 kN at 30 mm displacement.

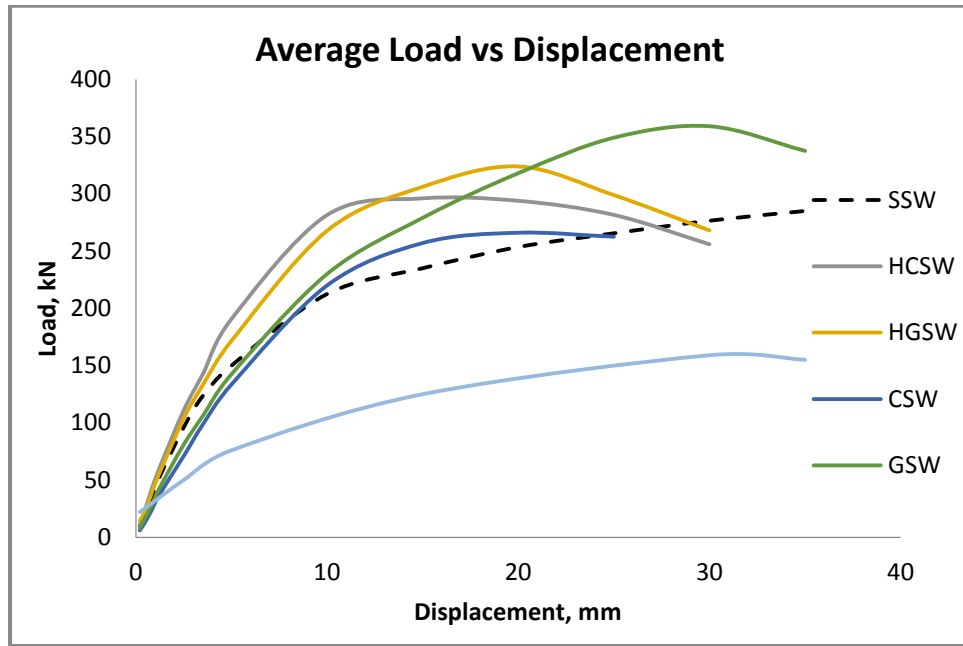


Figure 6.19. Steel frame contribution.

Comparison of the results demonstrated that infill plate in the shear wall design gives a significant increase in the load capacity. Control steel shear wall specimen has increase in load values of 73% at 30 mm displacement in comparison to steel frame only specimen. For specimens with hybrid plate up to 28 mm displacement, there is even higher load values increase due to the infill plate contribution.

In Table 6.1 various parameters for all five new shear wall systems together with the control SSW specimen are compared. HCSW has highest initial stiffness, whereas GSW specimen has ultimate load.

Table 6.1. Summary of the key important results for various shear wall systems.

Type of shear wall	Initial Stiffness, $K_0$ (kN/mm)	Ultimate Load, $F_{max}$ (kN)	Displacement at Ultimate Load, $\Delta$ at $F_{max}$ (mm)	Cumulative Energy Absorption, $CEA_{25mm}$ (kJ)
SSW (control)	37.3	285.0	35.0	34.8
HCSW	44.2	307.8	15.0	40.9
HGSW	38.2	330.0	20.0	43.6
CSW	28.5	266.0	25.0	28.0
GSW	31.8	359.0	30.0	33.9
Steel Frame only	NA	159.0	30.0	NA

### 6.8 Comparison between experimental and normalised results

For high-rise buildings, the weight of the structure is a crucial factor in the structural design due to the heavy vertical loading and increased mass at high levels. Therefore, a normalisation by weight was carried out and results after normalisation were found as normalised average load, normalised ultimate load, normalised ESD and specific CEA (SEA). Normalised values (Figure 6.20 a-d) were calculated based on the weight of the tested shear wall specimens.

Table 6.2. Weight of the specimen and their factors.

	Weight, kg	Normalisation factor
<b>SSW</b>	77.08	1.00
<b>HCSW</b>	78.53	1.02
<b>HGSW</b>	78.95	1.02
<b>CSW</b>	75.24	0.98
<b>GSW</b>	76.26	0.99

Table 6.2 shows the total weight of the shear wall systems (i.e. infill plate and the frame) for different specimens. Due to the light weight of the infill plate compared to the total weight of the shear wall system, the differences between experimental and normalised results are small. The normalised results of the HCSW and HGSW specimens will be 2% lower than experimental results, and CSW are 2% higher and GSW are 1% higher. The hybrid specimens have reduced values for their characteristics due to the fact that the steel plate in the infill plate design is the same as the one used for SSW specimen with addition of the FRP layers, their weight is slightly higher than SSW specimen. For specimens with pure FRP infill plates due to the significantly lower weight of FRP material relative to steel, the results for the average load, ultimate load and energy absorption increase.

After normalisation to the weight, the average load results, ultimate load and energy absorption of HCSW and HGSW continue to be higher than SSW specimen.

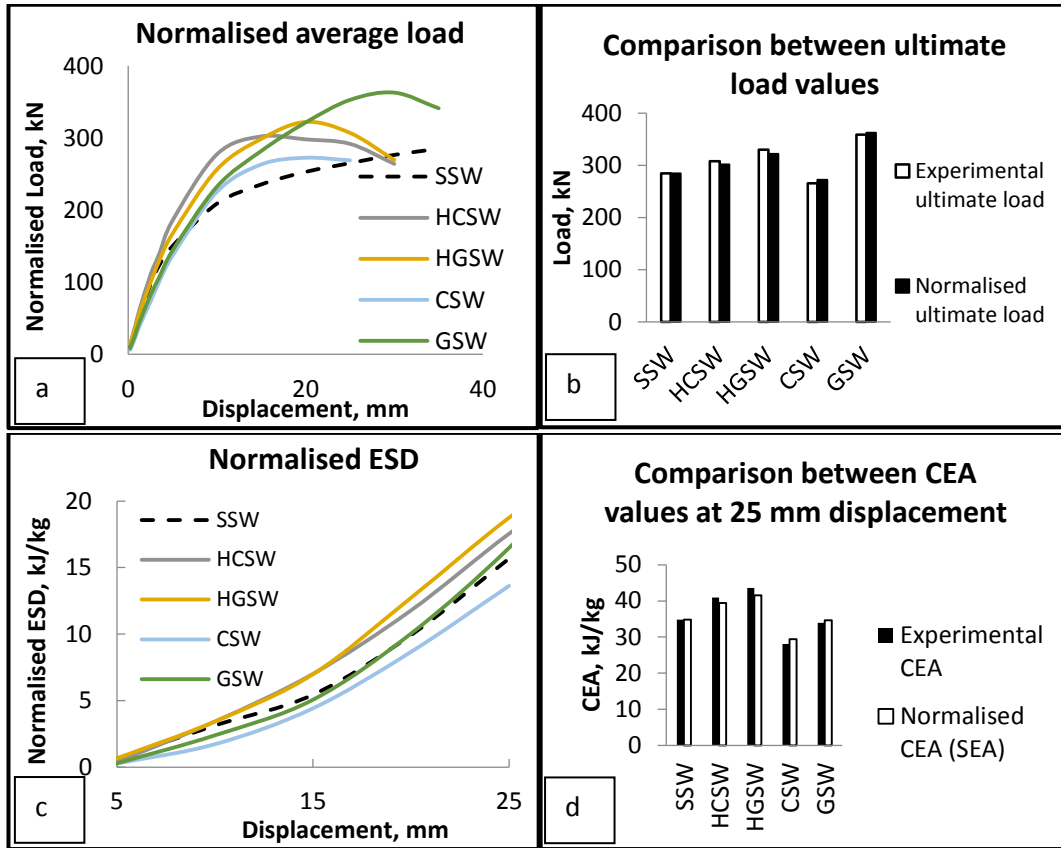


Figure 6.20. Normalised results for a) average load b) ultimate load c) ESD and d) CEA.

The GSW specimen has higher specific results in terms of average load and ultimate load, whereas energy absorption is very close to the SSW specimen. CSW specimen has achieved lower normalised ultimate load and energy absorption values in comparison with other specimens due to the higher brittleness and significant defects developed at early stages of loading.

## 6.9 Conclusions

Generally, several factors influencing initial stiffness, ultimate load capacity, and deformability and energy absorption of different shear wall systems were discussed in this Chapter. The important features affecting these parameters are steel frame of the shear

wall, type of infill plate and type of connection between frame and infill plate. In this Chapter varying the type of infill plate and the connection between fish plates and infill plates were presented.

From the experimental studies carried out the following conclusions can be made:

- The hybrid specimens HCSW and HGSW have higher loading capacities than the control SSW and CSW specimens for a testing range between 0.4 mm and 30 mm displacement.
- The highest ultimate load capacity is achieved by the GSW specimen due to better bonding at the connection and more deformable behaviour of the GFRP layer. Load values of GSW specimen exceeded the results of hybrid HCSW for displacements above 18 mm and those of hybrid HGSW above 21 mm displacement.
- The hybrid HGSW specimen achieved higher ultimate load results than the hybrid HCSW specimen. The reduced capacity of HCSW is probably due to the lower deformability of CFRP material causing earlier failure of the connections between infill plate and the frame and faster and widespread development of delamination of CFRP from steel core in the infill plate.
- The CSW specimen achieved the lowest ultimate load capacity due to a sudden and fast developing of intensive delamination and cracking within the CFRP fabric, leading to a relatively brittle failure of the infill plate.
- Up to 250 kN loading, the hybrid shear walls systems were less deformable than the control SSW specimen and pure FRP specimens (GSW and CSW). At 250 kN the displacements for HCSW and HGSW were 7.9 mm and 9.1 mm, respectively, whereas SSW, CSW and GSW specimens experience 19 mm and 13.5 and 11.8 mm displacements, respectively.

- Up to 30 mm displacement, the energy absorption at any specified level of displacement (ESD) of control specimen was lower than energy absorption of hybrid specimens and higher than energy absorption of the CSW specimen.
- For hybrid HCSW and HGSW specimens cumulative energy absorption (CEA) was higher at all levels of loading in comparison with the other specimens.
- First cycle of loading had higher EA in comparison to the following ones. For SSW, HGSW and GSW specimens, the differences between energy absorption from first and last cycles at the specific level of loading gradually increase with subsequent displacement level.
- Important factor for hybrid shear wall design is consideration of the connections between infill plates and fish plates and the resin volume fraction of the FRP prepreg to create a firm bond between steel plate and the FRP surfaces. Using an adhesive film before bonding FRP to steel infill plate and improving connections enhanced the performance of the hybrid shear wall system.
- After normalisation to the weight of shear wall system, main characteristics describing behaviour of all tested specimens such as average load, ultimate load capacity and energy absorption continue to have the same trends as before.

## Chapter 7: Strengthening of shear walls

This Chapter is going to discuss the strengthening method for steel shear walls and hybrid steel/FRP shear walls using CFRP laminates and GFRP fabric. The strengthening was developed in two different options- temporary strengthening, which is applied immediately after earthquake and permanent strengthening. Analysis of the results was done by comparing the behaviour and failure modes for new (later named as pristine specimens) and strengthened specimens after initial testing (later named retrofitted specimens).

First stage of development of strengthening system was a temporary repair of the steel plate shear wall specimen (SPSW). Damaged steel shear wall was strengthened with GFRP fabric and tested under quasi-static loading.

Second stage of loading was permanent strengthening of the damaged SSW, HCSW and HGSW, tested under quasi-static loading and analysed in Chapter 6. Strengthening of boundary elements of shear walls was done via application of FRP fabric and laminates, replacement of infill plates with new ones.

## 7.1 Introduction to the strengthening of shear walls

When buildings are subjected to earthquake loading, severe damage to shear walls can occur. It is important to use cost-effective techniques to recover initial strength, stiffness of the shear wall structure in order avoid demolition of the building or introduction of new additional elements. This Chapter will discuss **a)** the use of the composites to provide method for a temporary solution, before permanent strengthening solution can take place; and **b)** permanent strengthening of shear walls after earthquake damages or for increase of the capacity of undamaged walls, when structures require supporting higher loads for future use. It describes experimental studies investigating behaviour of steel and hybrid shear walls under quasi-static loading and their behaviour with strengthening techniques via GFRP and CFRP application.

## 7.2 Temporary strengthening to steel plate shear wall specimen (SPSW)

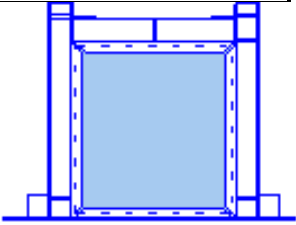
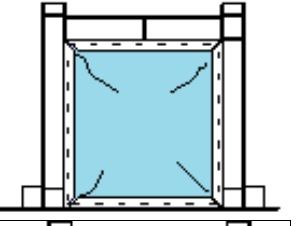
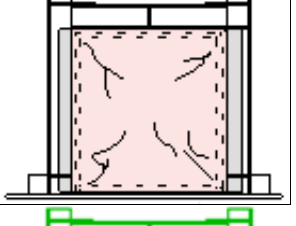
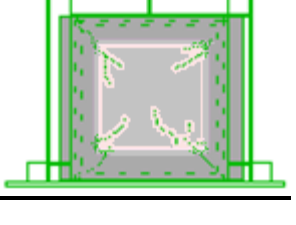
### 7.2.1 Scheme for strengthening of steel plate shear wall specimen SPSW

Temporary strengthening was done to the steel plate shear wall specimen (SPSW), made from the same type of steel frame as for other shear wall specimens and infill plate with a thickness of 0.675 mm. SPSW was initially tested by Maleki (2014). The same testing procedure was used to check the capacity before and after strengthening with one layer of GFRP and two layers of the FRP (around steel columns). The SPSW specimen was tested in the following stages (Table 7.1):

Strengthening of the SRSW-D specimen was done via strengthening with one layer of bi-directional woven glass fibre wrapping (manufactured by Weber) around columns and infill plate from both sides of the frame as shown in Figure 7.1. Further this specimen is

named SPSW-str1. Additional repair for the specimen was done by restoring weld between primary fish plate and the column of the shear wall.

Table 7.1. Scheme for testing of temporary strengthened specimens.

Stage of testing:	Abbreviation used for the specimen during testing:	Scheme of the specimen
Loading of an undamaged specimen as part of the A. Maleki's PhD project (2014)	SPSW	
Testing of damaged specimen	SPSW-D	
Strengthening (1) of the damaged specimen (SPSW-str1) with one layer of GFRP	SPSW-str1	
Strengthening (2) of the damaged specimen (SPSW-str2) with two layers of GFRP	SPSW-str2	

After testing the specimen SPSW-str1 to displacement reaching 15 mm, this specimen was strengthened with another layer of GFRP fabric (Figure 7.1).

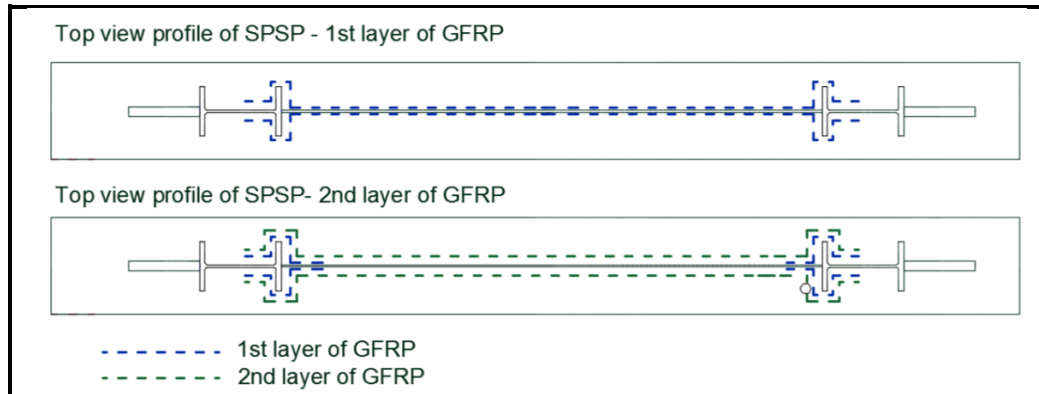


Figure 7.1. Scheme for 1st layer of GFRP wrapping around SRSW-str1 and 2nd layer of GFRP wrapping around SRSW-str2.

After removing the first layer of GFRP from infill plate due to extensive delamination during previous test, the steel infill plate was cleaned. Further this specimen was named as SPSW-str2. Additionally adhesive was injected in the areas where delaminated areas around fish plates and columns have been developed.

Applying of GFRP fabric was done by preliminary cleaning with white spirit and thoroughly degreasing the surface of the steel shear wall. It was cleaned to obtain a firm bond between bi-directional woven glass fibre wrapping (Weber) and steel surface. Then a basecoat of Weber adhesive, mixed by epoxy resin and epoxy hardener (2:1 by mass), was applied on the surface of the shear wall. Second layer of the adhesive was applied to ensure that all areas are coated. Specimen was left for curing for 48 hours before testing.

Discussion of results for the steel shear wall specimen

### **7.2.2 Discussion of results for temporary strengthening**

After testing of the steel shear wall specimen (SPSW) to the maximum displacement of the 25 mm, the following damages have been detected: further development of the plastic hinges, buckling of the infill plate and local damage of the weld between steel columns and primary fish plates.

To estimate the behaviour of already damaged specimen SPSW, secondary testing has been conducted on SRSW-D specimen till further development of the plastic hinges with amplitudes of 0.2 mm, 1 mm, 3 mm and 5 mm. After testing to small displacements, the following damages have been discovered: further buckling of the infill plate, significant tearing of the weld between fish plate and column (Figure 7.2 a) and appearance of hinges in columns.

The mode of the failure of the strengthening system is via delamination of GFRP fabric from steel infill plate and steel frame sections. For SPSW specimen (SPSW-str1)

specimen after testing to 15 mm displacement, significant progressive delamination between infill plate and GFRP wrapping developed with the increase of the amplitude (Figure 7.2 c). For SPSW-str2 specimen, delamination within infill plate between GFRP fabric and steel plate was less in comparison to SPSW-str1 specimen at the same level of loading (Figure 7.2 d). Further development of the plastic hinges at the steel column of the shear wall was observed.

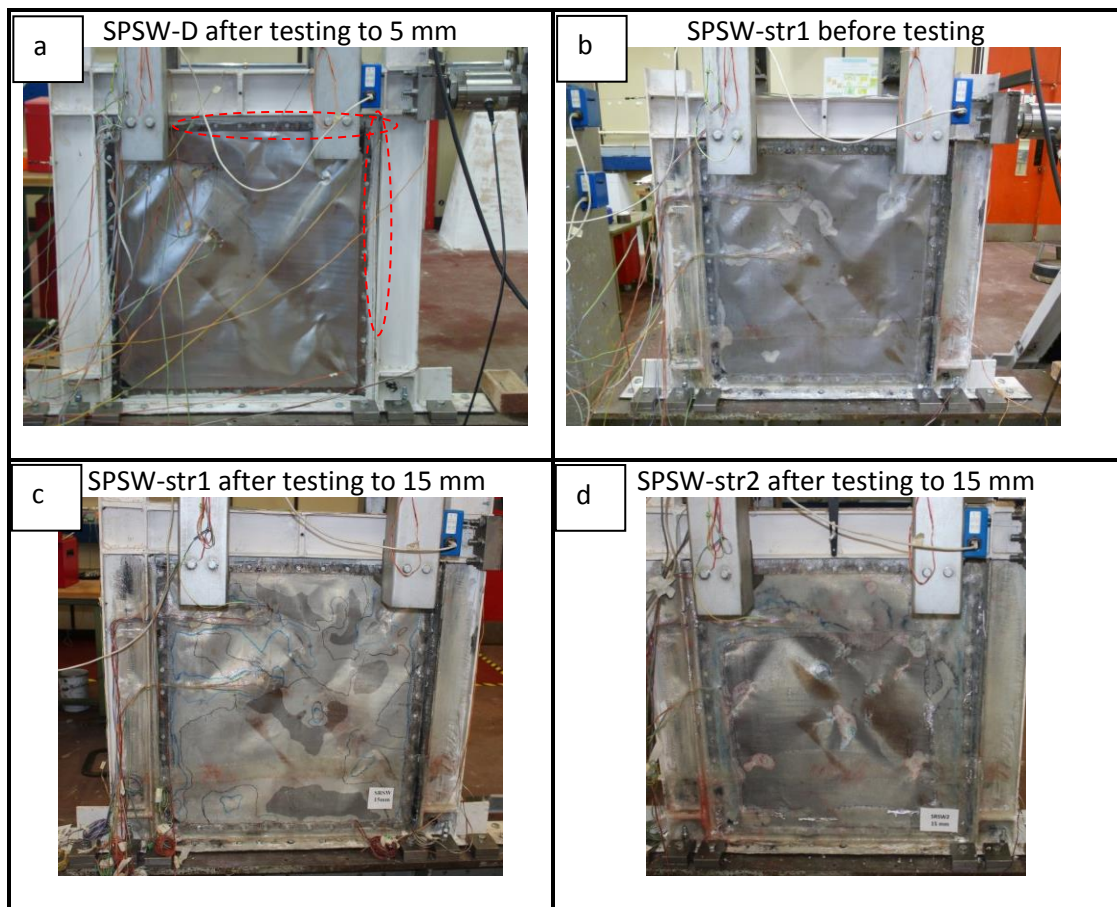


Figure 7.2. Steel shear wall specimen SPSW at different stages of loading.

Average load values were compared on the basis of the load vs displacement graphs for all specimens. An example of the hysteresis curve at 5 mm displacement for SPSW-D and SPSW-str1 is shown in Figure 7.3a and b. Three cycles of specified amplitude were performed. The hysteresis graph for damaged SSW-D specimen shows relatively similar behaviour for each of the three cycles. The loading and unloading branches are close to each other due to a high flexibility of the damaged sample. At the same level of the

displacement, strengthening of the specimen with GFRP wrapping for SPSW-str-1 resulted in an increase of energy absorption within the system and increase in load in comparison to SPSW-D.

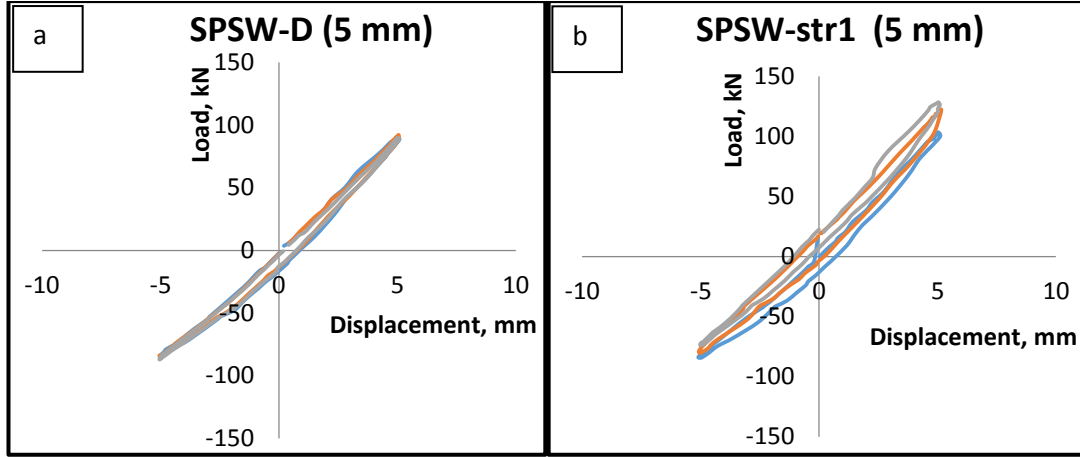


Figure 7.3. a) SRSW-D b) Strengthened shear wall specimen with 2 layers of GFRP wrapping after loading to 15 mm.

Comparison of the average load values at the same level of displacement for all specimens is demonstrated in Figure 7.4 and Figure 7.5. At small displacements of 1 mm and 3 mm, specimen after strengthening with GFRP fabric had slightly higher results than before strengthening (SPSW-D). At 5 mm displacement specimen after initial loading (SPSW-D) had average load results 40 kN lower, in comparison to initial test (SPSW).

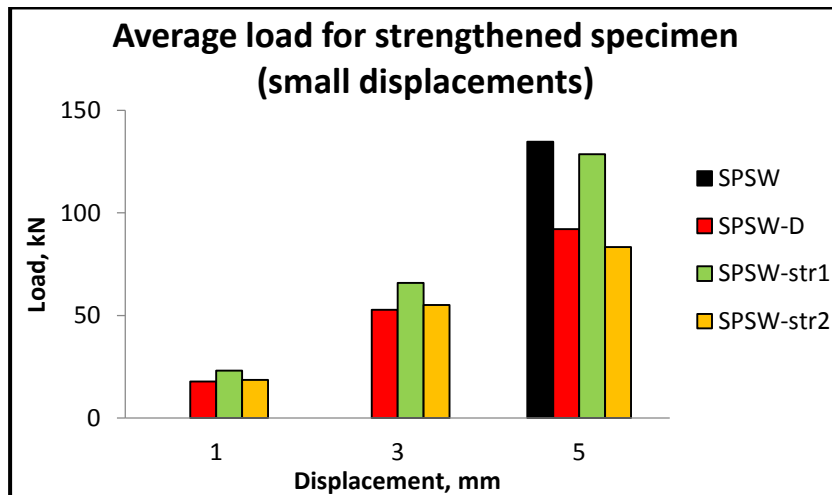


Figure 7.4. Average load for strengthened specimen at small displacements.

After strengthening with first layer of the GFRP (SPSW-str1), the average load capacity of the specimen improved and its values were similar to the initial test (SPSW) at 5 mm and 10 mm displacements and slightly higher at 15 mm displacement.

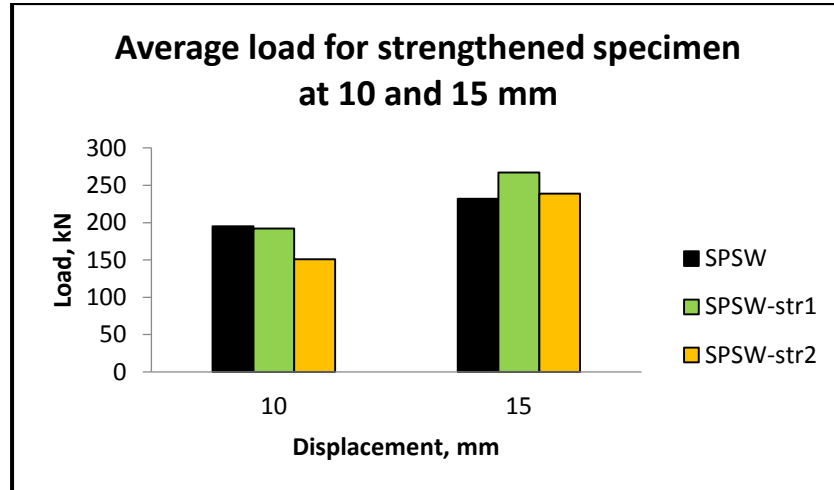


Figure 7.5. Average load comparison for SPSW, SPSW-str1, SPSW-str2 specimens at 10 and 15 mm displacement.

However, after testing the specimen with the 1<sup>st</sup> layer of GFRP (SPSW-str1) and further damages occurring to the specimen, its capacity was not restored after applying a second layer of GFRP (SPSW-str2). Load values of SPSW-str2 were lower at all levels of loading (Figure 7.4) in comparison to strengthening with SPSW-str1. At 15 mm load value of SPSW-str2 was similar to initial capacity of the specimen (SPSW).

Results demonstrated that the use of the GFRP wrapping has a potential as a strengthening material for damaged steel shear walls but applying of layer of GFRP on the damaged infill plate is not sufficient effective. In comparison to the damaged specimen, the application enhances to the small extent the energy absorption capacity of the specimen, as well as the loading capacity and stiffness of the system. However, due to the delamination between infill plate and GFRP wrapping, this scheme is more suitable as temporary solution for retrofitting structures before a permanent way of the refurbishing can take place.

### 7.3 Permanent strengthening of shear walls

#### 7.3.1 Scheme for permanent strengthening

Comparison of the permanent strengthening results was carried out for steel shear wall specimen and two hybrid specimens.

Newly developed specimens analysed in Chapters 5 and 6 are later described in text as pristine specimens. Those specimens after initial loading and damages were retrofitted and retested under the same type of quasi-static cyclic loading.

Specimens are identified as SSW-R, HCSW-R and HGSW-R. The structural repair of specimens was undertaken by replacing the damaged infill plates with new infill plates of the same type, and strengthening the vertical steel frame elements with CFRP laminates and GFRP fabric.

The specifications of all specimens are summarised in Table 7.2.

Table 7.2. Description of SSW and HSW specimens.

Name of the specimen	Labels	Stacking sequence of the infill plate	Total thicknesses of the infill plate, mm
Steel Shear Wall	SSW	Steel [S]	0.80
Retrofitted Steel Shear Wall	SSW-R	Steel [S]	1.40
Hybrid Steel/CFRP Shear Wall	HCSW	[+45/-45/A/S/A/-45/+45]	1.70
Retrofitted Hybrid Steel/CFRP Shear Wall	HCSW-R	[+45/-45/A/S/A/-45/+45]	1.70
Hybrid Steel/GFRP Shear Wall	HGSW	[+45/-45/A/S/A/-45/+45]	2.40
Retrofitted Hybrid Steel/GFRP Shear Wall	HGSW-R	[+45/-45/A/S/A/-45/+45]	2.40

Note: A- adhesive film (EF72)

The procedure for repairing the original specimens was as following:

- Removal of damaged infill plates
- Strengthening of the frame with CFRP laminates
- Wrapping of the frame with GFRP fabric
- Replacement of infill plate with a new one

Due to the lack of visual damage in the horizontal members of the frame, CFRP S&P CFK 150/2000 unidirectional laminates 1.2 mm thick (Weber, 2008a) were attached to the vertical boundary elements only, aiming to cover the area where plastic hinges were formed after previous loading in phase one. The plastic hinges were developed at the bottom and top sections of the vertical elements.

The repairs were undertaken by firstly removing the paint with a mechanical wire brush in areas where CFRP laminates and GFRP fabric were planned to be applied. This improved the bonding between the steel and the FRP composites. Then the frame was cleaned with white spirit to remove dust and oil. CFRP laminates were bonded to the frame (Figure 7.6) with a moisture-tolerant structural adhesive from “Weber”. The adhesive has two parts: bisphenol epoxy resin and polyamine hardener, which were mixed with a mass ratio of 2.4:1 according to the supplier’s instructions. The adhesive thickness was approximately 3 mm.

**Table 7.3. Properties of the FRP materials used for retrofitting of shear walls.**

Properties of CFRP laminates (Weber, 2008a)		Properties of GFRP fabric (Weber, 2008b)	
Density, g/cm <sup>3</sup>	1.7	Fibre density, kg/cm <sup>3</sup>	2.6
Fibre content $v_f$ , %	70	Area weight, g/cm <sup>2</sup>	350
Elastic modulus in fibre direction $E_{11}$ , GPa	165+	Modulus of elasticity $E_{cu}$ , GPa	65+
Tensile strength in fibre direction $f$ , MPa	2800+	Tensile strength $f_{cu}$ , MPa	2000+

The A-A section of the I-beam was strengthened with 300 mm (bottom part) and 200 mm (top part) long and 65 mm wide CFRP laminates. The B-B section of I-beam was strengthened with 25 mm wide CFRP laminates with the same lengths as for A-A section. Mechanical properties of FRP materials provided by manufacturer are tabulated in Table 7.3.

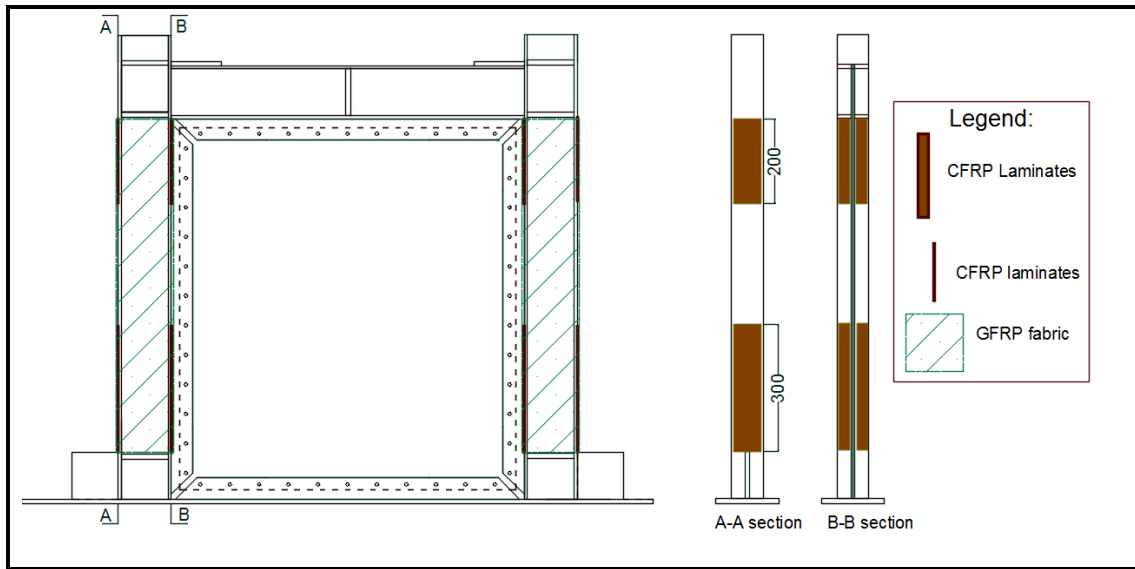


Figure 7.6. Retrofitting scheme: position of CFRP laminates on shear wall columns (A-A and B-B sections).

After curing of CFRP laminates and adhesive bond, Weber bi-directional woven GFRP wrapping was laid on the frame (Figure 7.7) using a mixture of epoxy resin and hardener (2:1 by mass ratio). GFRP fabric was applied in two stages: firstly GFRP fabric was applied along the web of the I-beam and along the A-A section of the I-beam as the first layer to allow for proper attachment of the fabric in the areas of internal corners of the section. Then GFRP was wrapped around the whole surface of the columns (Figure 7.6) as the second layer of GFRP for the areas where first layer is applied. Due to the shape of the I-beam, double wrapping allowed avoidance of “air pockets” in the corners of the section.

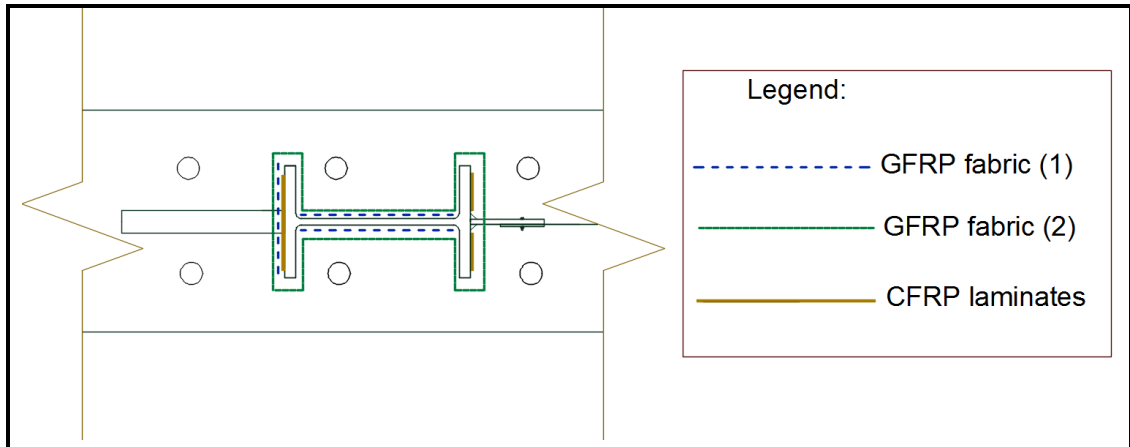


Figure 7.7. Positioning of CFRP laminates and GFRP fabric on the plan view of the frame.

The damaged 0.8 mm thick infill plate from the steel shear wall specimen was replaced with a steel infill plate of thickness of 1.4 mm. The choice of a higher thickness of steel infill plate in this case was due to strengthening considerations. Hybrid specimens were replaced with infill plates with the same steel plate and FRP design specifications as in the pristine specimens.

The behaviour of the pristine specimens was described in Chapter 5 and behaviour of retrofitted specimens is discussed below including the information about failure mechanisms occurring during the tests including delamination of the CFRP laminates and GFRP fabric from columns.

### 7.3.2 Permanent strengthening of SSW

In the retrofitted SSW-R specimen (Figure 7.8) visible diagonal tension field development started at a displacement of 3.5 mm in both directions of loading and produced wave-type deformations, which did not fully recover after the end of 3.5 mm loading cycle. Further development of the diagonal tension field was recorded with an increase of the applied displacement. At a displacement of 10 mm, buckling of the primary fish plate occurred where the diagonal tension field waves developed. At displacements above 15 mm, plastic hinges at the bottom of the columns were developed, which led to the development of delamination in GFRP fabric. Sliding between primary fish plates and

infill plates was initially recorded for the top and side boundary elements. At 25 mm displacement, development of debonding of the CFRP laminates attached to the top of the columns occurred. With the increase of the loading displacement to 30 mm, further development of the diagonal tension field led to pinching in the centre of the plate with the appearance of small holes. At 35 mm displacement of loading, further progression of the debonding for all CFRP laminates and delamination for GFRP fabric occurred in the lower section of the columns.

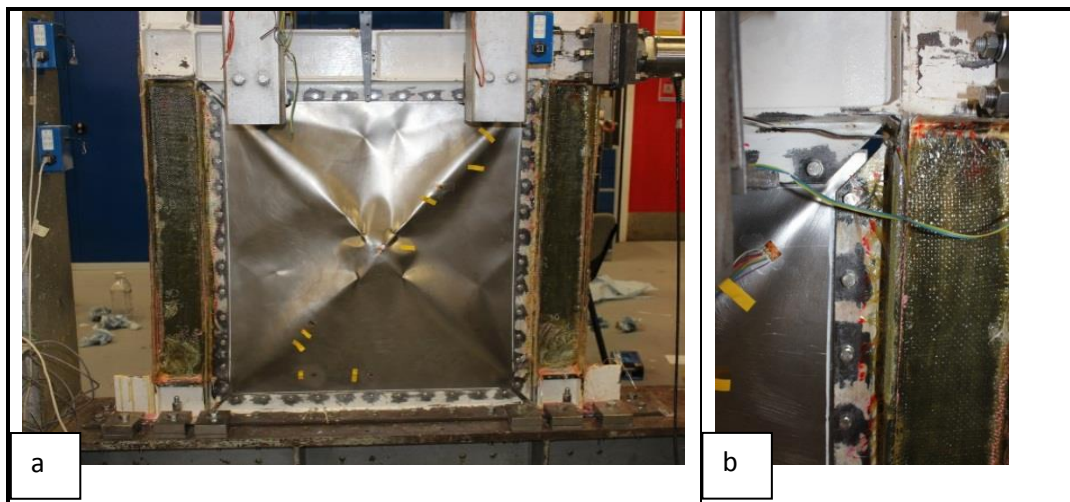


Figure 7.8 a) Pristine SSW and b) retrofitted SSW-R specimens after loaded to 35 mm displacement.

### 7.3.3 Permanent strengthening of HCSW

In retrofitted HCSW-R specimen (Figure 7.8), visible diagonal tension field development started at the displacement of 2.5 mm, the resulting lateral deformations did not fully recover after the end of 2.5 mm loading cycle. Further diagonal tension field waves both in size and number developed with increase of the loading displacement. Other visible changes to the frame and infill plate were noticed at 10 mm displacement, such as cracking in CFRP layers along diagonal tension field action recorded in both directions, which was increased at higher levels of the loading displacement. The integrity of the bond in the connection between fish plates and infill plate was compromised at 15 mm displacement and further cracking in the adhesive developed with increase of the displacements. At 20 mm displacement, cracks in the CFRP layers developed at the bottom

part of the infill plate. At 25 mm displacement plastic hinges developed at the bottom of the columns. Similar snapping of the infill plate occurred in the top corners near fish plates, as it occurred in pristine HCSW specimen. Further damage to the connection between infill plates and fish plates occurred at 30 mm displacement, when bolt holes elongations became visible. The test was terminated at 35 mm displacement.

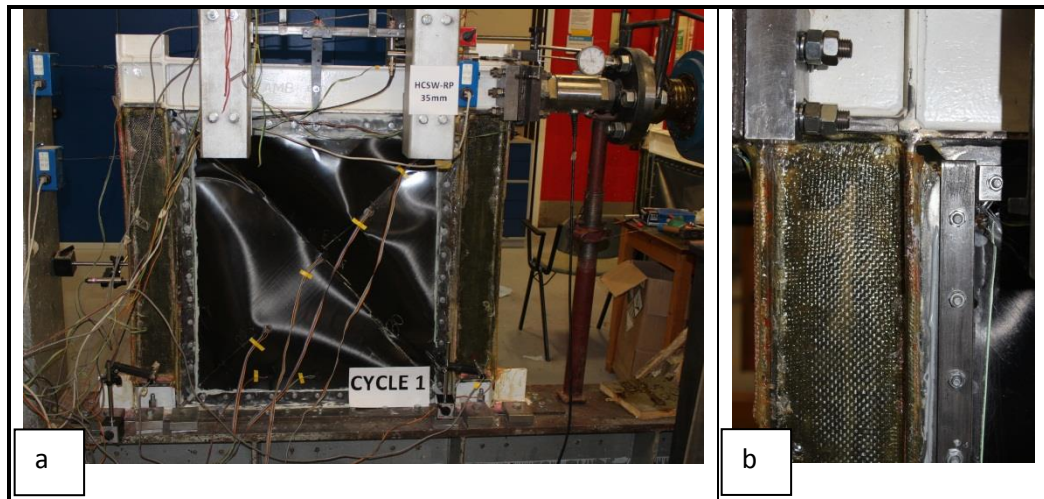


Figure 7.9. HCSW-R specimen tested to 35 mm.

#### 7.3.4 Permanent strengthening of HGSW

In the retrofitted HGSW-R specimen (Figure 7.10), diagonal tension field action became visible at 2.5 mm displacement and did not fully recover at the end of the loading cycle. The first sign of cracking in the adhesive layer between fish plates and infill plate was noticed at the displacement of 10 mm. Delamination of the GFRP layer from steel infill plate started at displacement loading of 15 mm at the top corners. Development of the plastic hinges at the bottom of the columns was noticed at 20 mm displacement, which led to the debonding of the GFRP fabric from the columns. Snapping of the infill plate in the top corners occurred at the same level of displacement of 30 mm as in the pristine HGSW specimen. At 30 mm displacement, plastic hinges were developed at top of the column; it also led to the debonding of the CFRP laminates around the top sections of the columns. Additionally a crack in the connection between beam and column appeared. As the crack further progressed, the test was terminated at the end of first cycle of 35 mm

displacement. GFRP delamination area from steel infill plate was smaller in comparison with pristine HGSW specimen.



Figure 7.10. HGSW-R specimen tested to 35 mm.

### 7.3.5 Analysis of the results on the basis of load-displacement curves

The load-displacement behaviours of pristine and retrofitted specimens are compared in Figures 7.11, 7.12 and 7.13 to investigate the opportunity for effective structural repair of steel and hybrid shear wall systems after they were subjected to seismic loading. Loads were calculated by taking the average from the extreme values of the cycles at the same displacement amplitude.

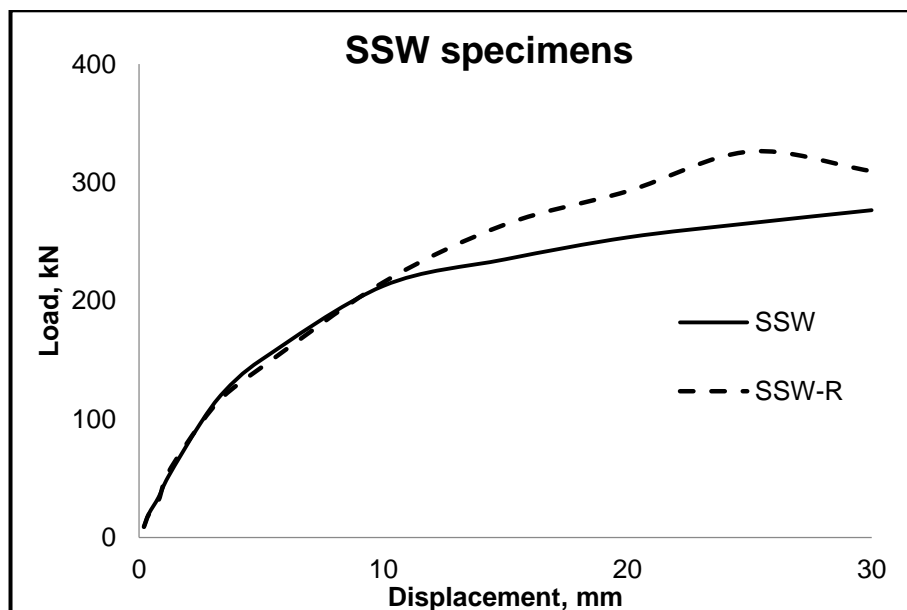


Figure 7.11. Load-displacement results for pristine SSW and retrofitted SSW-R specimens.

Up to 10 mm displacements, for SSW and SSW-R specimens (Figure 7.11) the load values for corresponding displacements are approximately the same. The highest difference of 22% was recorded at 25 mm displacement in load values in favour of retrofitted specimen. Maximum load for the whole range of displacements for SSW was 285 kN and for SSW-R was 336 kN.

For HCSW and HCSW-R specimens (Figure 7.12), load values are nearly the same up to 7 mm displacement. In retrofitted HCSW-R specimen a larger increase in load was recorded for displacements between 7 mm and 15 mm displacements compared with HCSW specimen. Above 15 mm displacement, load was dropping for both specimens, however load values for retrofitted specimens were more than 10% higher compared to HCSW specimen. HCSW-R specimen achieved higher ultimate load in comparison with pristine HCSW specimen, the difference in the ultimate load was recorded as 11% at 15 mm displacement.

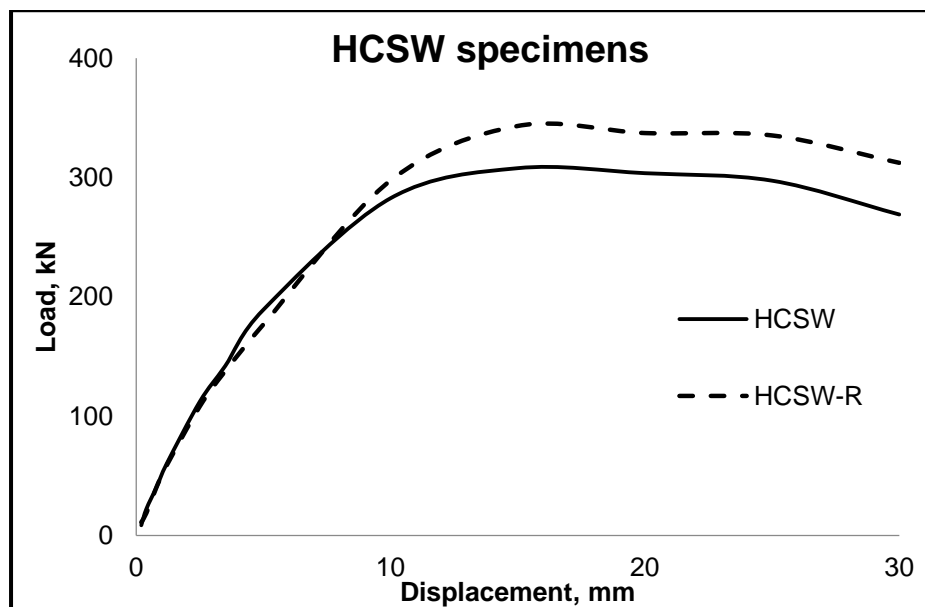


Figure 7.12. Load-displacement results for pristine HCSW and retrofitted HCSW-R specimens.

For HGSW and HGSW-R specimens (Figure 7.13) load values were approximately the same up to 5 mm displacement. At displacements between 5 mm and 15 mm, load was higher for retrofitted HGSW-R specimen in comparison with HGSW. The highest load

increase of 20% was recorded at 15 mm and at 30 mm displacements compared to pristine HGSW specimen. For HGSW-R specimen load was dropping above 15 mm displacement, whereas for HGSW-R it was dropping above 20 mm displacement. The difference in ultimate load between retrofitted HGSW-R and pristine HGSW specimens was 14%.

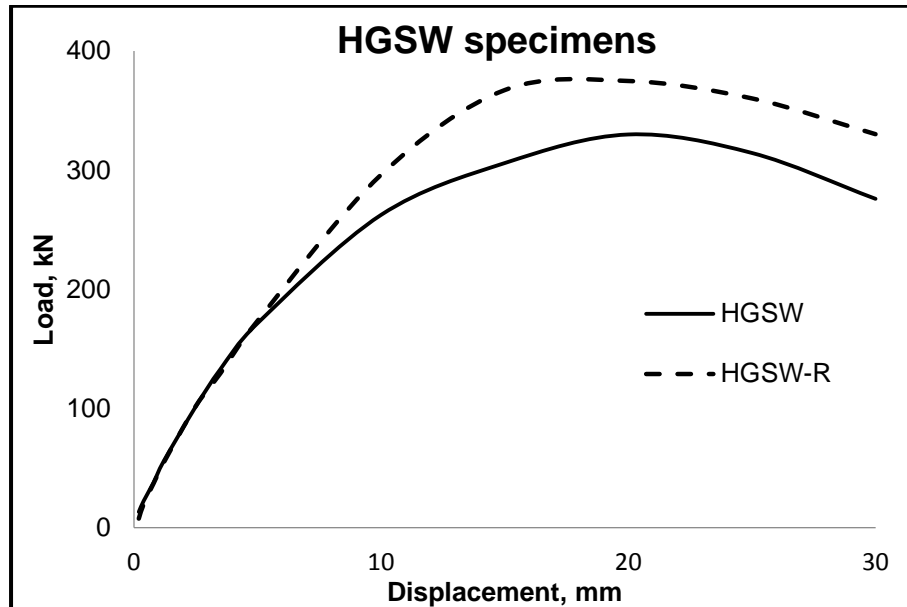


Figure 7.13. Load-displacement results for pristine HGSW and retrofitted HGSW-R specimens.

For all types of the specimens, those with structural repair discussed above gave better results in respect of stiffness, ultimate load values and energy absorption than the pristine specimens in the interval between 10 mm and 30 mm displacements.

Figure 7.14 compares load carrying capacity of pristine and retrofitted specimens starting at 5 mm displacement loading. From the behaviour of these two groups of specimens, it is noted that pristine and retrofitted hybrid carbon and hybrid glass have higher loading capacity than SSW specimens at every level of displacement loading. At 30 mm applied displacement due to significant delamination of FRP from infill plates in the direction of the tension field action, the behaviour of HSWs and SSW are nearly the same. As it was discussed in Chapter, the use of the hybrid infill plates improves ultimate load values significantly. The same pattern of higher load carrying capacity for HSW specimens compared to SSW specimen was noted for retrofitted specimens.

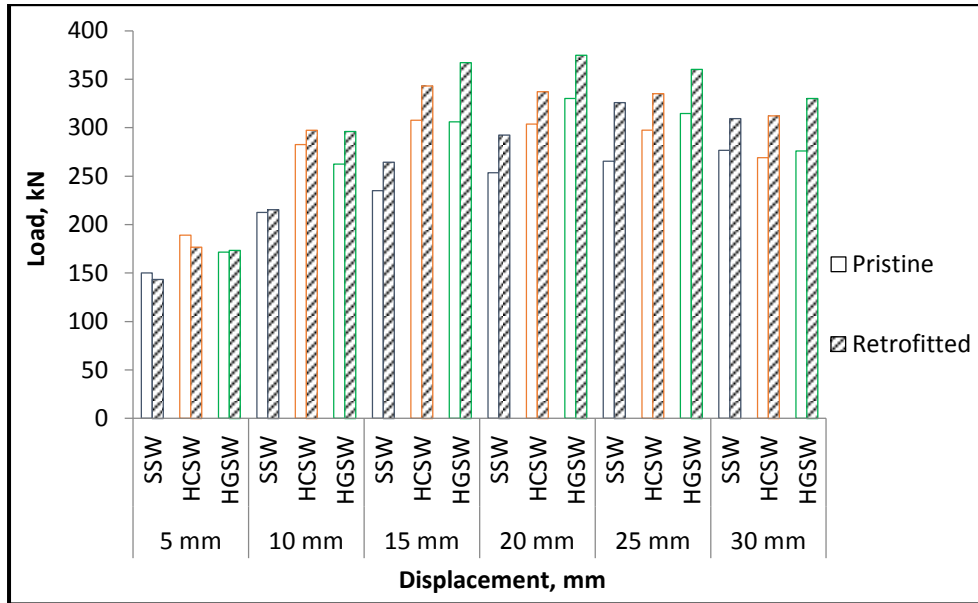


Figure 7.14. Comparison of the load-displacement results of different shear wall systems.

### 7.3.6 Energy absorption in different types of shear wall specimens

Figure 7.16 shows energy absorption at the specified level of displacement (ESD) for pristine and retrofitted specimens SSW, HCSW and HGSW at different stages of cyclic loading. An example of the hysteresis loop for hybrid carbon and hybrid glass specimens at 25 mm displacement is shown in Figure 7.15.

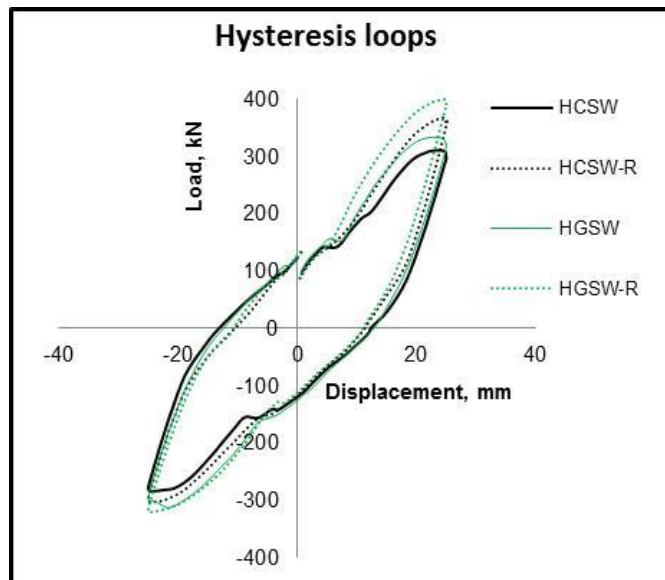


Figure 7.15. Hysteresis loops for hybrid specimens at 1<sup>st</sup> cycle of 25 mm displacement loading.

In the retrofitted SSW-R specimen ESD relative to the pristine specimens is higher between 10 mm and 30 mm displacement, difference in values reaching 1.4 kJ at 30 mm displacement mainly due to increased thickness of the infill plate.

For hybrid specimens, energy absorption in pristine and retrofitted ones were approximately the same. Retrofitted hybrid specimens had an increase in energy absorption at 30 mm displacement, retrofitted HCSW-R had 0.53 kJ increase and retrofitted HGSW-R had an increase of 0.98 kJ.

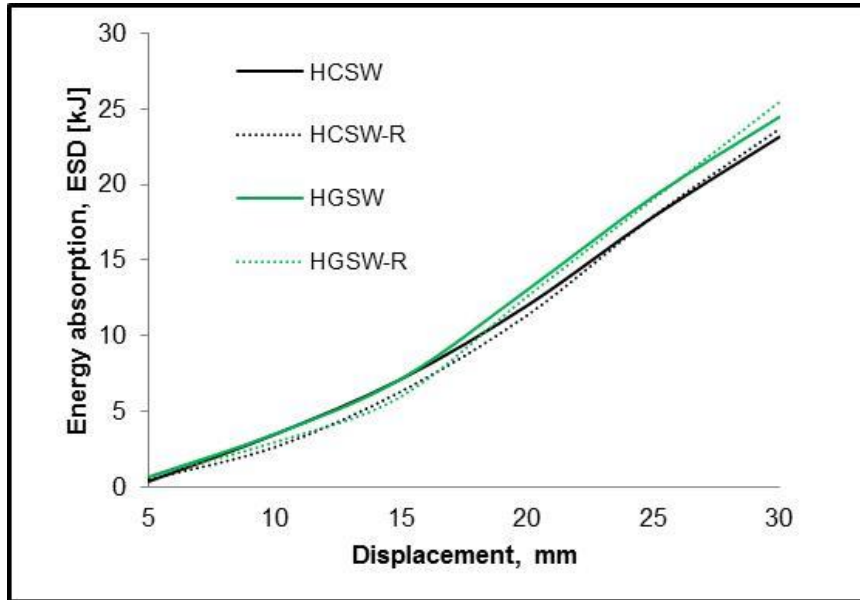


Figure 7.16. Energy absorption in hybrid specimens between 5 mm and 30 mm.

Energy absorption values (ESD) at different stages of loading are summarised in Figure 7.17. Energy absorption increases continuously from 5 mm to 30 mm displacement in all specimens.

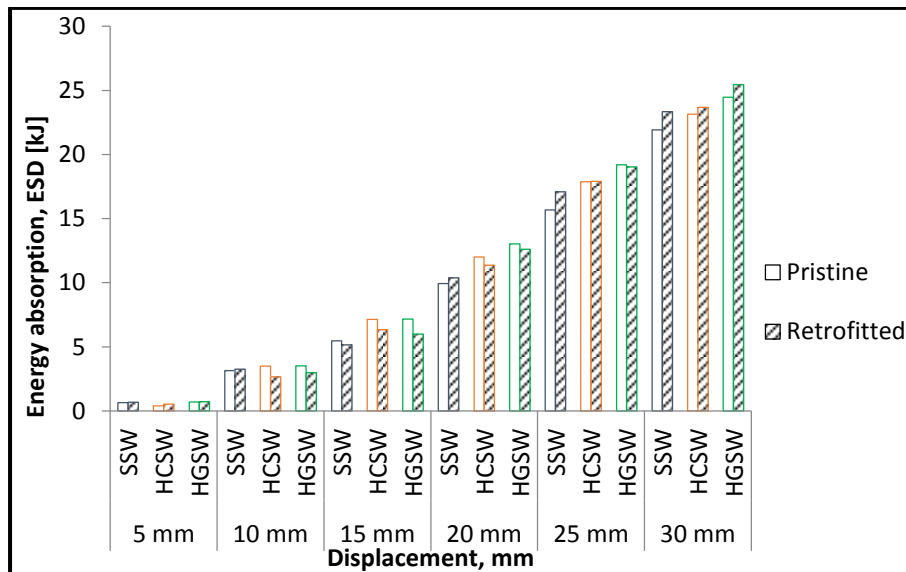


Figure 7.17. Comparison of energy absorption in different types of shear wall specimens.

In Chapter 6 it was shown that energy absorption in pristine hybrid specimens is higher than in steel specimens. The same tendency has been observed for retrofitted specimens between 15 mm and 30 mm displacements loading, and the highest result is achieved in retrofitted HGSW-R specimen.

#### **7.4 Conclusions to Chapter 7**

Based on the temporary strengthening, within this study it was demonstrated that the use of the GFRP wrapping has a potential as a temporary strengthening material for damaged steel shear walls. The application enhances the energy absorption capacity of the specimen, as well as the ultimate loading capacity and stiffness of the system. However, due to the delamination between infill plate and GFRP wrapping, this scheme is more suitable as temporary solution for retrofitting structures before a permanent way of the refurbishing can take place.

For permanent strengthening, in this work pristine steel and hybrid FRP shear walls were tested and after structural repair of the columns with CFRP laminates and GFRP fabric and replacement of the infill plate with a new one, retrofitted specimens were retested. From the test results the following conclusions can be made:

- As it was concluded in Chapter 6, hybrid steel/CFRP and steel/GFRP shear walls have higher ultimate load and higher load values in comparison with steel shear wall system within the applied levels of loading for both groups of tested specimens.
- Using the structural repair procedure outlined in the Chapter, resulted in higher load values and higher ultimate load in retrofitted samples above 10 mm displacement in comparison with pristine specimens.

- After retrofitting of the hybrid shear walls, the increases of load values are up to 16% higher for HCSW and up to 20% higher for HGSW. Corresponding increases of the ultimate load are 11% for HCSW and 14% for HGSW specimens.
- The energy absorption of retrofitted specimens is very close to energy absorption of the pristine specimens. The differences for cumulative energy absorption between them during the full spectrum of loading are less than 10%.
- Proposed methodology for the repairing of shear walls by bonding FRP materials to the frame and replacement of the infill plate is effective for all three configurations of specimens.

## **Chapter 8: Conclusions and recommendation for future work**

Conclusions based on the PhD project and recommendations for further studies are included in this Chapter.

### 8.1 Conclusions to the thesis

During this project, the behaviour of hybrid and pure FRP shear walls was critically analysed and compared with the behaviour of steel shear walls. Strengthening of the specimens was done as a second stage of the experimental work.

Generally, there are several parameters influencing initial stiffness, ultimate load capacity, deformability and energy absorption of different shear wall systems tested to the same type of loading. The important elements affecting these parameters are the steel frame of the shear wall, type of infill plate and type of connection between frame and infill plate.

For steel shear walls the damage happens through the plastic deformations of the infill plate, plastic hinges in boundary elements and deformations of the connections between infill plate and steel frame. For hybrid and pure FRP specimens as result of the use of FRP material the range of damage of the specimens is widened with fibre de-bonding, fibre fracture, delamination, fibre pull-out and matrix cracking.

*From the experimental studies carried out on small connection tests:*

- Applying adhesive in the connection increases the capacity of the specimens for all groups of tested specimens; the highest increase was achieved for GHa2 specimens (Figure 3.10).
- The average increase in ultimate load of 24% was achieved for steel specimens and pure CFRP and GFRP specimens. For hybrid CFRP specimens 30% increase and for hybrid GFRP 66% increase in ultimate load was recorded.

*From the experimental studies carried out on the newly developed specimens:*

- The hybrid specimens HCSW and HGSW have higher loading capacities than the control SSW and CSW specimens for a testing range between 0.4 mm and 30 mm displacement (Figure 6.2).
- The highest ultimate load capacity was achieved by the GSW specimen due to better bonding and more deformable behaviour of the GFRP layer (Figure 6.12). Load values of the GSW specimen exceeded the results of hybrid HCSW for displacements above 18 mm and those of hybrid HGSW above 21 mm displacement (Figure 6.11).
- Up to 29 mm displacement, hybrid HCSW and HGSW specimens have the highest values in the energy absorption at any specified level of displacement (ESD) (Figure 6.15) and the highest cumulative energy absorption (CEA) (Figure 6.17).
- For the GSW specimen up to 25 mm displacement, ESD and CEA were similar to the SSW specimen (Figures 6.15 and 6.17). At 30 mm displacement ESD of GSW was similar to the HCSW and HGSW specimen, whereas CEA of GSW was lower in comparison to hybrid specimens. For CSW specimen values for ESD and CEA were lowest in comparison to other specimens.
- The first cycle of loading had higher EA in comparison to the following ones (Figure 6.13). For SSW, HGSW and GSW specimens, the differences between energy absorption from first and last cycles at the specific level of loading gradually increase with subsequent displacement level (Figure 6.14).

*From the IRT results:*

- The application of MATLAB analytical for processing both active and passive thermography allows for obtaining better precision of the obtained results.
- The results from passive IRT are clearly defining the opportunity to assess the increased plastic deformations on the basis of generated temperature differences for

steel and hybrid structural elements and the connections between them during the process of testing.

- Analysis of the active IRT is beneficial for estimating delamination between FRP and steel plate. It could be further improved through analysis of the series of images as one sequence.

*For strengthened specimens:*

- Using the structural repair procedure outlined in the thesis resulted in higher load values and higher ultimate load in retrofitted samples above 10 mm displacement in comparison with pristine specimens (Figure 7.14). This could be considered as proof of the effectiveness of the strengthening methodology.
- The energy absorption of retrofitted specimens is very close to the energy absorption of pristine specimens (Figure 7.17). The differences for cumulative energy absorption between them during the full spectrum of loading are less than 10%.

## **8.2 Recommendations for future studies**

As investigated and highlighted in the dissertation, the connection between primary fish plates and infill plates plays an important role in the design of the shear walls. Therefore, it is important to conduct further tests and investigations in this direction.

Energy absorption is an important parameter in shear wall behaviour, further study can be conducted to investigate the increase of energy absorption through modification of connections and infill plates.

Further investigation in more uniform heating of the specimens or analysis series of the photos can provide more reliable results in estimating delamination.

Investigating the effect of different properties of adhesive in the delamination process could provide additional knowledge about improvements of the energy absorption and ultimate capacity.

Development of the numerical and finite element modelling of the system and components as further studies would allow the analysis of the influence and contribution of the different components of the shear wall system and would be beneficial for clarifying conclusions from experimental results.

Fire resistance of the hybrid structure is another important parameter to investigate in future studies as for hybrid structures, FRP can act as a protective layer from corrosion and as thermal insulation during heating.

## References

- Alinia, M. & Dastfan, M., 2007. Cyclic behaviour, deformability and rigidity of stiffened steel shear panels. *Journal of Constructional Steel Research*, Volume 63, pp. 554-563.
- American Institute of Steel Construction, 2005. *ANSI/AISC 341-05 and ANSI/AISC 341s1-05: Seismic Provisions for Structural Steel Buildings*. Chicago: AISC.
- Astaneh-Asl, A., 2000. Steel Plate Shear Walls. *Proceedings, U.S.-Japan Partnership for Advanced Steel Structures, U.S.-Japan Workshop on Seismic Fracture issues in Steel Structures*. San Francisco.
- Astaneh-Asl, A., 2001. *Seismic behaviour and design of steel shear walls*. Structural Steel Educational Council.
- ASTM, 2000. D3039/D3039M-08: Standard Test Method for Tensile Properties of Polymer Matrix Composite Materials. United States.
- ASTM, 2007a. D3518/D3518M-94: Standard Test Method for In-Plane Shear Response of Polymer Matrix Composite Materials by Tensile Test of a  $\pm 45^\circ$  Laminate). United States.
- ASTM, 2007b. D3518/D3518M-94: Standard Test Method for In-Plane Shear Response of Polymer Matrix Composite Materials by Tensile Test of a  $\pm 45^\circ$  Laminate. United States.
- ATC-24, 1992. *Guidelines for Seismic testing of components of steel structures*. California: Applied Technology Council.
- Bagavathiappan, S., Lahiri, B.B., Saravanan, T., Philip, J., Javakumar, T., 2013. Infrared thermography for condition monitoring-A review. *Infrared Physics and Technology*, 60, pp. 35-55.
- Balaras, C. & Argiriou, A., 2002. Infrared thermography for building diagnostics. *Energy and Building*, Volume 34, pp. 171-183.
- Barbero, E., 2011. *Introduction to composite materials design*. 2nd ed. New York: CRC.
- Binici, B., Ozcere, G. & Ozcelik, R., 2007. Analysis and design of FRP composites for seismic retrofit of infill walls in reinforced concrete frames. *Composites: Part B.*, 38(5-6), pp. 575-583.

- British Standards Institution, 2004. *BS EN 1998-1:2004+A1:2013. Eurocode 8: Design of structures for earthquake resistance. Part 1: General rules, seismic actions and rules for buildings*. London: BSI Group.
- British Standards Institution, 2005a. *BS EN 1998-3:2005. Eurocode 8: Design of structures for earthquake resistance. Part 3: Assessment and retrofitting of buildings*. London: BSI.
- British Standards Institution, 2005b. *BS EN 1993-1-8:2005. Eurocode 3: Design of steel structures. Design of joints*. London: BSI Group.
- British Standards Institution, 2005c. *BS 4-1:2005. Structural steel sections Specification for hot-rolled sections*. London: BSI Group.
- British Standards Institution, 2009. *BS EN 3506-1:2009. Mechanical properties of corrosion-resistant stainless steel fasteners. Part 1: Bolts, screws and studs*. London: BSI Group.
- Caccese, V. and Elgaaly, M., 1993. Experimental Study of Thin Steel-Plate Shear Walls Under Cyclic Load, *Journal of Structural Engineering*, ASCE, 119 (2), pp. 573-587.
- Canadian Standards Association, 2001. *CAN/CSA-S16-01: Limit States Design of Steel Structures*. CSA.
- Cheng, C., Cheng, T.-M. & Chiag, C.-H., 2008. Defect detection of concrete structures using both infrared thermography and elastic waves. *Automation in Construction*, Volume 18, pp. 87-92.
- Chiew, S., Yu, Y., Lee, C., 2011. Bond failure of steel beams strengthened with FRP laminates – Part 1: Model development. *Composites: Part B*, 42(5), pp. 1114-1121.
- DataTaker, 2011/2012. *User's Manual DT85/85G*. [Online]  
Available at: <http://www.datataker.com> [Accessed 3 March 2011].
- Donchev, T., Stepien, T., Wertheim, D. & Dimov, D., 2013. *Effectiveness of Infrared Thermography for Detecting Defects in the Attached CFRP Laminates*. Sozopol, Bulgaria, International conference NDT days.
- Driver, R., Kulak, G., Kennedy, D. & Elwi, A., 1998. Cyclic test of four-story steel plate shear wall. *Journal of Structural Engineering*, 124(2), pp. 112-130.

- Driver, R.G., Kulak, Elwi, A. E. and G. L., Kennedy, D.J.L., 1998. Cyclic Tests of Four-Story Steel Plate Shear Wall, *Journal of St. Engineering*, ASCE, 124 (2), pp. 112-120.
- Duthinh, D., 2000. *Connections of Fiber- Reinforced Polymer (FRP) Structural Members: A review of the State of the Art*. NISTIR6532.
- FEMA, 2006. *Techniques for the Seismic Rehabilitation of Existing Buildings*. FEMA 547.
- Fujitani, H., Yamanouchi, H., Okawa, I. Sawai, N., Uchida, N. and Matsutani, T., 1996. *Damage and performance of tall buildings in the 1995 Hyogoken Nanbu earthquake*. Proceedings of the 67th Regional Conference, Council on Tall Building and Urban Habitat, Chicago, pp. 103-125.
- Grande, E., Milani, G. & Sacco, E., 2008. Modelling and analysis of FRP-strengthened masonry panels. *Engineering Structures*, 30(7), pp. 1842-1860.
- Haghani, R., Al-Emrani, M., 2008. A new design model for adhesive joints used to bond FRP laminates to steel beam- Part A: Background and theory. *Constructional and Building Materials*, 30(7), pp. 1842-1860.
- Haghani, R., Al-Emrani, M., 2012. A new design model for adhesive joints used to bond FRP laminates to steel beam- Part B: Experimental Verification. *Construction and Building Materials*, Volume 34, pp. 686-694.
- Halliwel, S. & Reynolds, T., 2004. *Effective use of fibre reinforced polymer materials in construction*. BRE centre for composites in construction.
- Hatami, F., Ghamari, A. & Rahai, A., 2012. Investigating the properties of steel shear walls reinforced with Carbon Fiber Polymers (CFRP). *Journal of Construction Steel Research*, Volume 70, pp. 36-42.
- Kubota, R., Numata, D. Anyouji, M., Shimamoto, A., Takayama, K., 2008. High--Velocity Impact Characteristic of CFRP Composite. *Advanced Non-destructive Evaluation*, p. 276.
- Kulak, G.L., 1985. *Behaviour of steel plate shear walls*. Proceedings of AISC International Engineering Symposium on Structural Steel, American Institute of Steel Construction, Chicago.

- Levar, J. & Hamilton, H., 2003. Nondestructive evaluation of carbon fiber-reinforced polymer-concrete bond using infrared thermography. *ACI Materials Journal*, 100(1), pp. 63-72.
- Lombard, J., Lau, D., Humar, J. & Foo, S., 2000. *Sesimic Strengthening and Repair of Reinforced Concrete Shear Walls*. Auckland, New Zeland, 12 WCEE 2000: 12th World Conference on Earthquake Engineering.
- Maierhofer, C., Arndt, R. & Rollig, M., 2007. Influence of concrete properties on the detection of voids with impulse-thermography. *Infrared Physics and Technology*, 49, pp. 213-217.
- Maierhosef, C., Brink, A., Rolling, M. & Wiggengerhauser, 2005. Quantitative impulse-thermography as non-destructive testing method in civil engineering-Experimental results and numerical simulations. *Construction and Building Materials*, 19 (10), pp. 731-737.
- Maleki, A., 2014. *Improving Seismic Behaviour of Steel Plate Shear Walls with and without cut-outs*, London: Kingston University London: Thesis.
- Maleki, A., Donchev, T., Hadavinia, H. & Limbachiya, M., 2011. *Numerical modelling and experimental investigation of GFRP-steel sandwich shear walls*. Timisoara, Romania, ICTWS 2011 The 6th International Conference on Thin Walled Structures.
- Maleki, A., Donchev, T., Hadavinia, H. & Limbachiya, M., 2012. *Improving the seismic resistance of structure using FRP/steel shear walls*. Rome, Italy, Proceedings 6th International Conference CICE 2012.
- Marcari, G., Manfredi, G., Prota, A. & Pecce, M., 2007. In-plane shear performance of masonry panels strengthened with FRP. *Composites: Part B*, Volume 38, pp. 887-901.
- Meola, C. & Carlomagno, G., 2010. Impact damage in GFRP: New insights with infrared thermography. *Composites Part A: Applied Science and Manufacturing*, 41(12), pp. 1839-1847.
- Meola, C., 2012. Origin and Theory of Infrared Thermography. *Infrared Thermography Recent Advances and Future Trends*. Benham Science Publisher, pp. 3-28.

- Nateghi-Alahi, F. & Khazaei-Poul, M., 2012. Experimental study of steel plate shear walls with the infill plates strengthened by GFRP laminates. *Journal of Construction Steel Research (Elsevier)*, Volume 78, pp. 159-172.
- Oehlers, D., Seracino, R., 2004. *Design of FRP and Steel Plated RC Structures. Retrofitting Beams and Slabs for Strength, Stiffness and Ductility*. Elsevier.
- Petkune, N., Donchev, T., Hadavinia, H., Limbachiya, M., Wertheim, D. (2014) *Investigation of the behaviour of hybrid steel and FRP shear walls*. The 7th international Conference on Fibre Reinforced Polymer (FRP) Composites in Civil Engineering (CICE 2014), August 2014. Vancouver, British Columbia, Canada.
- Petkune, N., Donchev, T., Hadavinia, H., Wertheim, D., Limbachiya, M. (2015) *Strengthening of steel and hybrid shear walls*. The 12<sup>th</sup> International Symposium on Fibre-Reinforced Polymers for Reinforced Concrete Structures & The 5<sup>th</sup> Asia-Pacific Conference on Fibre-Reinforced Polymers in Structures. FRPRCS-12/APFIS-2015. December 2015. Nanjing, China.
- Petkune, N., Donchev, T., Hadavinia, H., Wertheim, D., Limbachiya, M., (2016) Performance of pristine and retrofitted hybrid steel/fibre reinforced polymer composite shear walls. *Journal of Construction & Building Materials*, 117, pp. 198-208.
- Petkune, N., Donchev, T., Petkova, D., Hadavinia, H., Limbachiya, M., Hussein, Y. (2012) *Opportunities for strengthening of damaged steel shear walls*. CECOM: Conference on Civil Engineering Infrastructure Cased on Polymer Composites. November 2012. Krakow, Poland.
- Rahai, A. & Alipour, M., 2011. Behavior and Characteristics of Innovative Composite Plate Shear Walls. *Procedia Engineering*, Volume 14, pp. 3205-3212.
- Rezaii, M., 1999, Seismic behaviour of steel plate shear walls by shake table testing", Ph.D. Dissertation, University of British Columbia, Vancouver, Canada.
- Rezaii, M., Ventura, C. E. and Prion, H.G.L., 2000. *Numerical investigation of thin unstiffened steel plate shear walls*. Proceedings of 12th World Conference on Earthquake Engineering.
- Rizkalla, S., Dawood, M. & Schnerch, D., 2008. Development of a carbon fiber reinforced polymer system for strengthening steel structures. *Composites Part A*, 36, pp. 388-397.
- Roberts, T., 1995. Seismic resistance of steel plate shear walls. *Engineering Structures*, 17(5), pp. 344-351.

Sabelli, R., Bruneau, M. & Driver, R., 2008. *Steel Plate Shear Walls in the Upcoming 2010 AISC Seismic Provisions and 2009 Canadian Standard S16*, ASCE: Structures 2008: Crossing Borders.

Sabouri-Ghomi, S., and Roberts, T.M., 1992. Nonlinear dynamic analysis of steel plate shear walls including shear and bending deformations, *Engineering Structures*, 14 (5), pp. 309-317.

Seilie, I., Hooper, J., 2005. Steel plate shear walls: Practical design and construction. *Modern Steel Construction AISC*, 45(4), pp. 37-43.

Teng, J., Yu, T. & Fernando, D., 2012. Strengthening of steel structures with fiber-reinforced polymer composites. *Journal of Construction Steel Research*, Volume 78, pp. 131-143.

Thorburn, L.J., Kulak, G.L., and Montgomery, C.J., 1983. *Analysis of Steel Plate Shear Walls*. Structural Engineering Report No. 107, Department of Civil Engineering, University of Alberta, Edmonton, Alberta, Canada.

Timler, P.A. and Kulak, G.L., 1983, *Experimental Study of Steel Plate Shear Walls*. Structural Engineering Report No. 114, Department of Civil Engineering, University of Alberta, Edmonton, Alberta, Canada.

Vishay, 2014a. *Linear Displacement Sensor's Specifications*. [Online]  
Available at: <http://www.vishaypg.com/docs/11350/hs.pdf> [Accessed 12 January 2014].

Vishay, 2014b. *Cable Displacement Sensor's Specifications*. [Online]  
Available at: <http://www.vishaypg.com/docs/11004/cds.pdf> [Accessed 12 January 2014].

Vishay, 2014c. *Strain Gauge Specifications*. [Online]  
Available at: <http://www.vishaypg.com/micro-measurements/stress-analysis-strain-gages/knowledge-base-list/> [Accessed 12 January 2014].

Wang, Y., Hsu, K., 2009. Design recommendations for the strengthening of reinforced concrete beams with externally bonded composite plates. *Composites Part B*, 88(2), pp. 323-332.

Weber, 2008a. *Weber Tec Force Carbon Plate*. [Online]  
Available at:

[http://www.netweber.co.uk/uploads/tx\\_weberproductpage/10.010\\_weber.tec\\_force\\_carbon\\_plate.pdf](http://www.netweber.co.uk/uploads/tx_weberproductpage/10.010_weber.tec_force_carbon_plate.pdf) [Accessed July 2015].

Weber, 2008b. *Weber Tec Force Glass Sheet*. [Online]

Available at:

[http://www.netweber.co.uk/uploads/tx\\_weberproductpage/10.030\\_weber.tec\\_force\\_glass\\_sheet.pdf](http://www.netweber.co.uk/uploads/tx_weberproductpage/10.030_weber.tec_force_glass_sheet.pdf) [Accessed July 2015].

## Appendices

Appendix A: Additional graphs and figures for chapters

Appendix B: Drawings

Appendix C: Publications

**Appendix A:****Appendix for CHAPTER 3: CFRP tensile testing.**

CHa specimen

**Theoretical calculation  $F/\Delta L$** 

$$\frac{F}{\Delta l} = \frac{EA}{L}$$

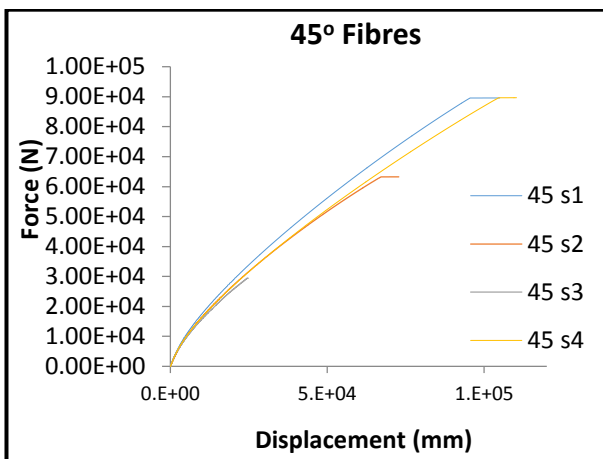
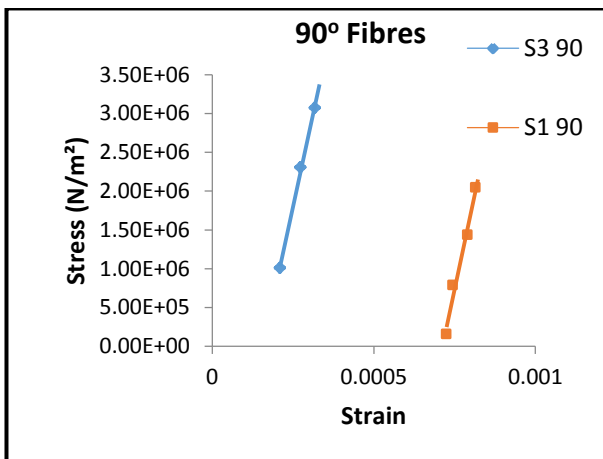
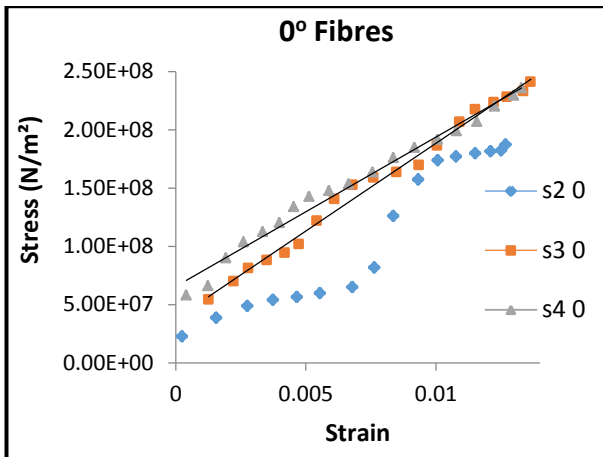
Where

Elongation	$\Delta l =$	1 mm
Length of specimen	$L =$	110 mm
Width of specimen	$b =$	70 mm
Thickness of steel plate	$d_{st} =$	0.68 mm
Thickness of CFRP layers	$d_{cfrp} =$	0.78 mm
Thickness of epoxy layers	$d_{epoxy} =$	0.06 mm
Thickness of specimen	$d =$	1.52 mm
Area of specimen	$A = d * b =$	106.4 mm <sup>2</sup>
Young Modulus of steel	$E_{st} =$	210 GPa
Young Modulus of CFRP	$E_{cfrp} =$	140 GPa
Young Modulus of GFRP	$E_{grfp} =$	40 GPa
Young Modulus of epoxy	$E_{epoxy} =$	3.5 GPa
Combined Young Modulus	$E = (E_{st}d_{st} + 0.4E_{cfrp}d_{cfrp} + E_{epoxy}d_{epoxy})/d$	
	$E =$	123 GPa

Therefore **theoretical**  $F/\Delta L =$  119 kN/mm

**Experimental**  $F/\Delta L =$  94.1 kN/mm

Appendix for CHAPTER 4: CFRP tensile testing.



## Appendix for CHAPTER 4: Datataker programme with description of parameters and commands.

DeX programme is divided in several steps below, comments of the programme are shown in blue. All commands were given in uppercase. Yellow colour indicates varying parameters.

### 1. Beginning of the programme operation

```
BEGIN"JOB1"
CATTN
```

### 2. Scaling, Calibrations

Spans (s) and polynomial declarations (y) show calibrations for CDS, LVDT and strain gauges.

Span is defined as

Sn= a, b, c, d "units"

n= polynomial/span number

a, d= physical coordinates of 2 points on the calibration line

c, d= signal coordinates

Polynomial declaration is defined as

yn= k0, k1, k2, k3, k4, k5 "units"

'Spans and polynomial declarations

S1=0,262,-42.35368,9098.7224"mm"

Cable displacement sensor (CDS)

Y2=0,0.963855"uStrain"

Linear Strain Gauge

Y3=0,0.94786"uStrain"

Rosette Strain Gauge

S4=0,262,-43.85,8841.1"mm"

CDS

S5=0,262,-14.54,9312.6"mm"

CDS

S6=0,26,6703,-25.5"mm"

Linear variable displacement traducer (LVDT)

S7=0,26,6720,9.9"mm"

LVDT

S8=0,26,6720,-111.4"mm"

LVDT

S9=0,26,6753,-77.3"mm"

LVDT

S10=0,26,7002,68"mm"

LVDT

S11=0,0,0,0"mm"

LVDT

Y12=0,50.05,0.376,-.001,-.002"kN"

Load cell

### 3. Definition of the displacement, degree and cycle application, where CV is channel variable

'Thermistor declarations

'Switches declarations

'Parameter declarations

'Global declarations

RS1S

Statistical sub-schedule: read every second

'schedule definition

'Constants

13CV("AC1Amplitude(mm)")=0.2 'mm

Amplitude- changed throughout the test

800CV("AC1revAmplitude(mm)")=0.2 'mm

Rev. Amplitude- changed throughout the test

12CV("numOfCycles")=1

Number of cycles- changed throughout the test

650CV=5

Hz Frequency of the motor (inverter) - changed throughout the test

413CV("Degree Stage1 limit")=10

'Limit of Stage1 of Quarter cycle, degree

414CV("Degree Stage2 limit")=30

'Limit of Stage2 of Quarter cycle, degree

700CV("Degree Stage3 limit")=60

'Limit of Stage3 of Quarter cycle, degree

701CV("Degree Stage4 limit")=80

'Limit of Stage1 of Quarter cycle, degree

'Stage 5 ends at 90 and 270 degrees

417CV("DegreeInc1")=5

'Quarter cycle increment 1, degree

418CV("DegreeInc2")=10

'Quarter cycle increment 2, degree

419CV("DegreeInc3")=10

'Quarter cycle increment 3, degree

702CV("DegreeInc4")=10

'Quarter cycle increment 4, degree

703CV("DegreeInc5")=5

'Quarter cycle increment 5, degree

#### 4. Take zeros for CDS, LDS, Load Cell (inverter not moving)

024: 'zero CDS,LDS,LoadCell  
 ' Variables used 5,15-21CV  
 1BGI(4W,S1,"AC1z",=5CV) CDS  
 2BGI(4W,S4,"AC2z",=15CV) CDS  
 3BGI(4W,S5,"AC3z",=16CV) CDS  
 16BGI(4W,S6,"AT16z",=17CV) LVDT  
 1419BGI(4W,S7,"BT119z",=18CV) LVDT  
 1420BGI(4W,S8,"BT120z",=19CV) LVDT  
 1519BGI(4W,S9,"CT219z",=20CV) LVDT  
 1520BGI(4W,S10,"CT220z",=21CV) LVDT  
 4HV(Y12,"AL4z",W,=300CV,GL30V) Load Cell  
 6CV=5CV-13CV 'maximum deflection CDS Zero - amplitude  
 7CV=5CV+13CV 'minimum deflection CDS Zero + amplitude  
 8CV=5CV+0.1 'Cycle Complete deflection CDS Zero +0.1 (near to mean but a bit backward)  
 9CV=5CV  
 14CV=12CV-0.5 'nos of cycle -0.5  
 710CV=12CV+0.5 'nos of cycle +0.5

#### 5. Commands for screw jack, motor

600CV=1 '1=CDS\_A1, 2=LDS\_C20 Controlled Control by CDS or LVDT  
 10CV=1 'load cycle stage 1= forward, 2= reverse,  
 '3= back to mean  
 11CV=0 'Current loading cycle 0=first cycle  
 1CV=3 '3= stop motor, 2=reverse, 0= forward  
 411CV=0 'starting increment of cycle  
 412CV=0 'starting angle of cycle  
 405CV=0 'Initial delay time before stopping motor

#### 6. Channel variables for zero strain gauges, where

AR- rosette strain gauges  
 BU- uni- directional strain gauges  
 CR- rosette strain gauges

'zero STRAIN GAUGES Variables 24-68CV  
 5BGI(3W,Y3,"AR5z",=24CV) 6BGI(3W,Y3,"AR6z",=25CV)  
 7BGI(3W,Y3,"AR7z",=26CV) 8BGI(3W,Y3,"AR8z",=27CV)  
 9BGI(3W,Y3,"AR9z",=28CV) 10BGI(3W,Y3,"AR10z",=29CV)  
 11BGI(3W,Y3,"AR11z",=30CV) 12BGI(3W,Y3,"AR12z",=31CV)  
 13BGI(3W,Y3,"AR13z",=32CV) 1401BGI(3W,Y2,"BU101z",=33CV)  
 1402BGI(3W,Y2,"BU102z",=34CV) 1403BGI(3W,Y2,"BU103z",=35CV)  
 1404BGI(3W,Y2,"BU104z",=36CV) 1405BGI(3W,Y2,"BU105z",=37CV)  
 1406BGI(3W,Y2,"BU106z",=38CV) 1407BGI(3W,Y2,"BU107z",=39CV)  
 1408BGI(3W,Y2,"BU108z",=40CV) 1409BGI(3W,Y2,"BU109z",=41CV)  
 1410BGI(3W,Y2,"BU110z",=42CV) 111BGI(3W,Y2,"BU111z",=43CV)  
 1412BGI(3W,Y2,"BU112z",=44CV) 113BGI(3W,Y2,"BU113z",=45CV)  
 1414BGI(3W,Y2,"BU114z",=46CV) 1415BGI(3W,Y2,"BU115z",=47CV)  
 1416BGI(3W,Y2,"BU116z",=48CV) 1417BGI(3W,Y2,"BU117z",=49CV)  
 1418BGI(3W,Y2,"BU118z",=50CV) 1501BGI(3W,Y3,"CR201z",=51CV)  
 1502BGI(3W,Y3,"CR202z",=52CV) 1503BGI(3W,Y3,"CR203z",=53CV)  
 1504BGI(3W,Y3,"CR204z",=54CV) 1505BGI(3W,Y3,"CR205z",=55CV)  
 1506BGI(3W,Y3,"CR206z",=56CV) 1507BGI(3W,Y3,"CR207z",=57CV)  
 1508BGI(3W,Y3,"CR208z",=58CV) 1509BGI(3W,Y3,"CR209z",=59CV)  
 1510BGI(3W,Y3,"CR210z",=60CV) 1511BGI(3W,Y3,"CR211z",=61CV)  
 1512BGI(3W,Y3,"CR212z",=62CV) 1513BGI(3W,Y3,"CR213z",=63CV)  
 1514BGI(3W,Y3,"CR214z",=64CV) 1515BGI(3W,Y3,"CR215z",=65CV)  
 1516BGI(3W,Y3,"CR216z",=66CV) 1517BGI(3W,Y3,"CR217z",=67CV)  
 1518BGI(3W,Y3,"CR218z",=68CV)

#### 7. Definition for inveter and motor

RA"CtrMotor"("B:",ALARMS:OV:100KB,DATA:OV:10MB) LOGONA GA  
 'schedule definition

Where:

RA report schedule ID

"Ctr Motor"

schedule name

"B:"  
ALARMS:OV:100KB,DATA:OV:10MB

Logged data stored on the internal flash disc  
Schedule name and size. Data will be overwritten if disc full

HB  
Commands for inverter are given through digital nibble state

1DNO=1CV

Digital channel, DNO- output as nibble= 1CV. When 1CV=3 stop; 1CV=2 reverse; 1CV=0 forward)

DELAY=405CV  
1DNO=3  
DELAY=1000+405CV  
1BGI(4W,S1,"CDS1")  
GB

Digital channel

## 8. Channel variables for displacement sensors

RB"LogData"("B:",ALARMS:OV:100KB,DATA:OV:50MB) LOGONB GB

'schedule definition

' Displacement Sensors Variables 4,22,23,159-163CV

1BGI(4W,S1,"AC1live",W,=4CV)  
2BGI(4W,S4,"AC2live",W,=22CV)  
3BGI(4W,S5,"AC3live",W,=23CV)  
16BGI(4W,S6,"AT16live",W,=159CV)  
1419BGI(4W,S7,"BT119live",W,=160CV)  
1420BGI(4W,S8,"BT120live",W,=161CV)  
1519BGI(4W,S9,"CT219live",W,=162CV)  
1520BGI(4W,S10,"CT210live",W,=163CV)

' Displacement Sensors Normalized readings Variables 164-171CV

164CV("AC1")=5CV-4CV 'CDS1  
165CV("AC2")=15CV-22CV 'CDS2  
166CV("AC3")=16CV-23CV 'CDS3  
167CV("AT16")=17CV-159CV 'LDS1  
168CV("BT119")=18CV-160CV 'LDS2  
169CV("BT120")=19CV-161CV 'LDS3  
170CV("CT219")=20CV-162CV 'LDS4  
171CV("CT220")=21CV-163CV 'LDS5

## 9. Conditions for the inverter to operate: stop, move forward and backwards.

2CV(W)=9CV-4CV  
410CV(W)=ABS(164CV/13CV)  
415CV(W)=SIN(D2R(413CV)) 416CV(W)=SIN(D2R(414CV))  
IF(410CV><0,415CV){411CV=417CV}  
IF(410CV><415CV,416CV){411CV=418CV}  
IF(410CV>416CV){411CV=419CV}  
412CV(W)=412CV+411CV  
IF(412CV>360){412CV=412CV-360}  
403CV(W)=ABS(ABS(SIN(D2R(412CV))))\*13CV-ABS(164CV))  
IF(403CV<0.762){405CV=6.48\*SQRT(403CV/2)\*1000}  
IF(403CV>0.762){405CV=(4+(403CV-0.762)/0.19)\*1000}  
ALARM(10CV><0.5,1.5)AND  
ALARM(4CV>6CV)"FORWARD"{1CV=0}  
ALARM(10CV><0.5,1.5)AND  
ALARM(4CV<6CV)"REVERSE"{10CV=2}  
ALARM(10CV><1.5,2.5)AND  
ALARM(4CV<7CV)"REVERSE Started"{1CV=2}  
ALARM(10CV><1.5,2.5)AND  
ALARM(4CV>7CV)"Last Forward"{10CV=3}  
ALARM(10CV><2.5,3.5)AND  
ALARM(4CV>7CV)"FORWARD to mean"{1CV=0}  
ALARM(10CV><2.5,3.5)AND  
ALARM(4CV<8CV)"Cycle COMPLETE"{10CV=1 11CV=11CV+1 1CV=3}  
ALARM(11CV><14CV,15CV)"STOPPED"{10CV=0 1CV=3 H}  
9CV(W)=4CV

## 10. Direct and final readings for displacement sensors

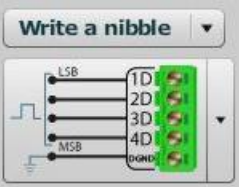
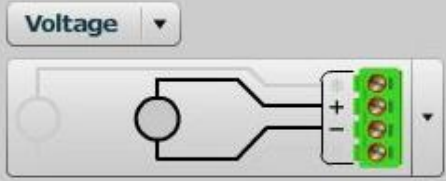
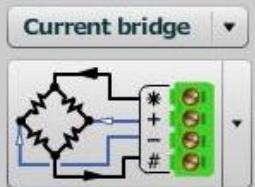
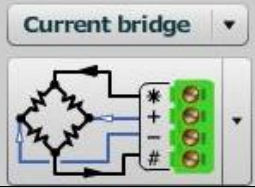
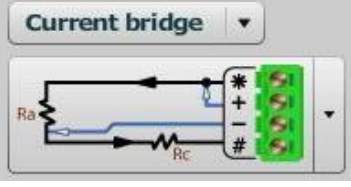
'Log STRAIN GAUGES & LoadCell  
4HV(Y12,"AL4",W,=301CV,GL30V) 302CV("AL4")=301CV-300CV  
' direct reading Variables 69-113CV

```
' final corrected Variables 114-158CV
58GI(3W,Y3,W,=69CV) 114CV("AR5")=69CV-24CV 68GI(3W,Y3,W,=70CV) 115CV("AR6")=70CV-25CV
78GI(3W,Y3,W,=71CV) 116CV("AR7")=71CV-26CV 88GI(3W,Y3,W,=72CV) 117CV("AR8")=72CV-27CV
98GI(3W,Y3,W,=73CV) 118CV("AR9")=73CV-28CV 108GI(3W,Y3,W,=74CV) 119CV("AR10")=74CV-29CV
118GI(3W,Y3,W,=75CV) 120CV("AR11")=75CV-30CV 128GI(3W,Y3,W,=76CV) 121CV("AR12")=76CV-31CV
138GI(3W,Y3,W,=77CV) 122CV("AR13")=77CV-32CV 14018GI(3W,Y2,W,=78CV) 123CV("BU101")=78CV-33CV
14028GI(3W,Y2,W,=79CV) 124CV("BU102")=79CV-34CV 14038GI(3W,Y2,W,=80CV) 125CV("BU103")=80CV-35CV
14048GI(3W,Y2,W,=81CV) 126CV("BU104")=81CV-36CV 14058GI(3W,Y2,W,=82CV) 127CV("BU105")=82CV-37CV
14068GI(3W,Y2,W,=83CV) 128CV("BU106")=83CV-38CV 14078GI(3W,Y2,W,=84CV) 129CV("BU107")=84CV-39CV
14088GI(3W,Y2,W,=85CV) 130CV("BU108")=85CV-40CV 14098GI(3W,Y2,W,=86CV) 131CV("BU109")=86CV-41CV
14108GI(3W,Y2,W,=87CV) 132CV("BU110")=87CV-42CV 14118GI(3W,Y2,W,=88CV) 133CV("BU111")=88CV-43CV
14128GI(3W,Y2,W,=89CV) 134CV("BU112")=89CV-44CV 14138GI(3W,Y2,W,=90CV) 135CV("BU113")=90CV-45CV
14148GI(3W,Y2,W,=91CV) 136CV("BU114")=91CV-46CV 14158GI(3W,Y2,W,=92CV) 137CV("BU115")=92CV-47CV
14168GI(3W,Y2,W,=93CV) 138CV("BU116")=93CV-48CV 14178GI(3W,Y2,W,=94CV) 139CV("BU117")=94CV-49CV
14188GI(3W,Y2,W,=95CV) 140CV("BU118")=95CV-50CV 15018GI(3W,Y3,W,=96CV) 141CV("CR201")=96CV-51CV
15028GI(3W,Y3,W,=97CV) 142CV("CR202")=97CV-52CV 15038GI(3W,Y3,W,=98CV) 143CV("CR203")=98CV-53CV
15048GI(3W,Y3,W,=99CV) 144CV("CR204")=99CV-54CV 15058GI(3W,Y3,W,=100CV) 145CV("CR205")=100CV-55CV
15068GI(3W,Y3,W,=101CV) 146CV("CR206")=101CV-56CV 15078GI(3W,Y3,W,=102CV) 147CV("CR207")=102CV-57CV
15088GI(3W,Y3,W,=103CV) 148CV("CR208")=103CV-58CV 15098GI(3W,Y3,W,=104CV) 149CV("CR209")=104CV-59CV
15108GI(3W,Y3,W,=105CV) 150CV("CR210")=105CV-60CV 15118GI(3W,Y3,W,=106CV) 151CV("CR211")=106CV-61CV
15128GI(3W,Y3,W,=107CV) 152CV("CR212")=107CV-62CV 15138GI(3W,Y3,W,=108CV) 153CV("CR213")=108CV-63CV
15148GI(3W,Y3,W,=109CV) 154CV("CR214")=109CV-64CV 15158GI(3W,Y3,W,=110CV) 155CV("CR215")=110CV-65CV
15168GI(3W,Y3,W,=111CV) 156CV("CR216")=111CV-66CV 15178GI(3W,Y3,W,=112CV) 157CV("CR217")=112CV-67CV
15188GI(3W,Y3,W,=113CV) 158CV("CR218")=113CV-68CV
```

### ***11. Recording of the new zeros (for next cycle loading)***

```
'schedule definition
RC"Zeros"("B:",ALARMS:OV:100KB,DATA:OV:1MB)1M LOGONC GC
'zero CDS,LDS,LoadCell=300CV
' Variables used 5,15-21CV
5CV
15..21CV
300CV
'zero STRAIN GAUGES Variables 24-68CV
24..68CV
END
'end of program file
```

Appendix for CHAPTER 4: Wiring configurations of equipment connected to datataker.

Type of equipment connected	Channel Type	Wiring Scheme: Channel type and wiring	Details	Additional parameters specified
Inverter	DNO- digital nibble output		4-wire configuration Digital terminal 1	Digital input and output specified as 1DNO
Loadcell	HV- high voltage		2-wire connection	<ul style="list-style-type: none"> <li>scaling factor</li> <li>polynomial</li> </ul>
Cable Displacement Sensor (CDS)	BGI- bridge current		4-wires configuration	<ul style="list-style-type: none"> <li>scaling factor</li> <li>span resistance (500Ω)</li> </ul>
Linear Displacement Sensor (LDS)	BGI- bridge current		4-wires configuration	<ul style="list-style-type: none"> <li>scaling factor-span</li> <li>resistance 320Ω</li> </ul>
Strain Gauge	BGI- bridge current		3-wire connection Bridge excitation	<ul style="list-style-type: none"> <li>scaling factor- span</li> <li>resistance 120/350Ω</li> <li>2.5mA precision current source, used as a default</li> </ul>

**Appendix for CHAPTER 6: Initial stiffness.**

Correlation factor between experimental results and results for analytical approximations is approximately 0.99 and standard deviation error for each level of the displacement was found less than 10%. To calculate the initial stiffness of different shear wall systems were obtained by finding the slope of linear fitted line to the initial linear behaviour of the SW systems.

**Linear functions developed for initial stiffness.**

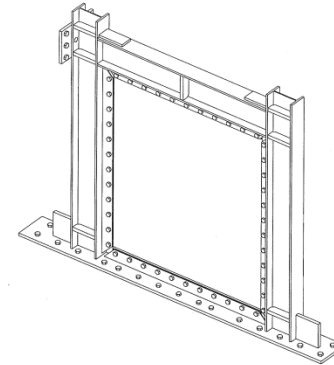
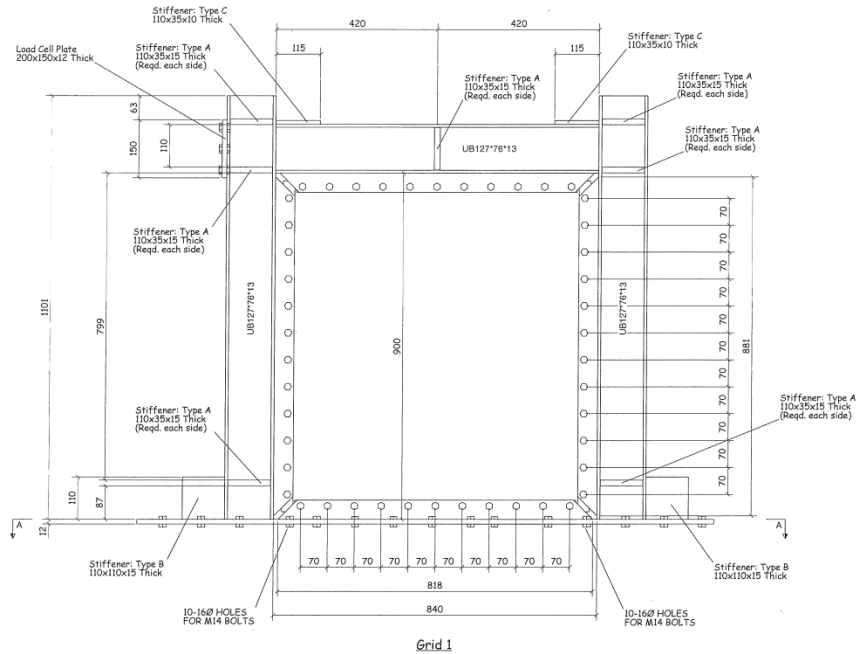
<b>Specimen:</b>	<b>Linear functions for specimen:</b>	<b>Correlation between experimental results and results from analytical approximations:</b>
SSW	$F(d) = 37.287d + 4.0676$	0.998
HCSW*	$F(d) = 29.239d + 10.617$	0.996
HCSW	$F(d) = 44.185d + 3.6286$	0.997
HGSW	$F(d) = 38.152d + 7.2548$	0.999
CSW	$F(d) = 28.501d + 0.4294$	0.999
GSW	$F(d) = 31.798d + 2.1073$	0.999

**Note: F is load in kN, d is displacement in mm.**

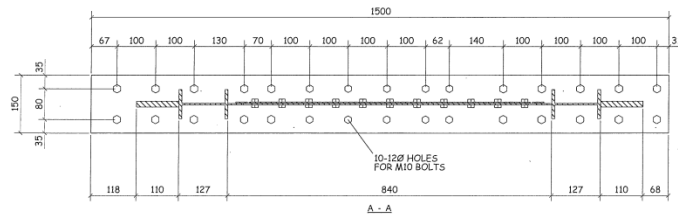
---

**Appendix B: Drawings**

# APPENDICES



3d



REV. MARK	REVISION DESCRIPTION	REVISION DATE
KINGSTON UNIVERSITY FASSETT ROAD		
DRAWING TITLE		ELEVATION
CONTRACT		STEEL FRAMES
CHECKED BY		ISSUE DATE
CONTRACT NO		SCALE 1:5 1:2.5
DRAWING NO		REVISION No.

**Appendix C: Publications**

C1: Petkune, N., Donchev, T., Hadavinia, H., Wertheim, D., Limbachiya, M., (2016) Performance of pristine and retrofitted hybrid steel / fibre reinforced polymer composite shear walls. *Journal of Construction & Building Materials*, 117, pp. 198-208.

C2: Petkune, N., Donchev, T., Hadavinia, H., Wertheim, D., Limbachiya, M. (2016) *Behaviour of steel framed shear walls with FRP infill plates*. CICE2016. December 2016. Hong Kong, China.

C3: Petkune, N., Donchev, T., Hadavinia, H., Wertheim, D., Limbachiya, M. (2015) Strengthening of steel and hybrid shear walls. The 12<sup>th</sup> International Symposium on Fibre-Reinforced Polymers for Reinforced Concrete Structures & The 5<sup>th</sup> Asia-Pacific Conference on Fibre-Reinforced Polymers in Structures. FRPRCS-12/APFIS-2015. December 2015. Nanjing, China.

C4: Petkune, N., Donchev, T., Wertheim, D., Hadavinia, H., Limbachiya, M. (2015) The use of the IRT to assess Steel and FRP hybrid elements. SMAR 2015: Third Conference on Smart Monitoring Assessment and Rehabilitation of Civil Structures. September 2015. Antalya, Turkey.

C5: Petkune, N., Donchev, T., Hadavinia, H., Limbachiya, M., Wertheim, D. (2014) *Investigation of the behaviour of hybrid steel and FRP shear walls*. The 7th international Conference on Fibre Reinforced Polymer (FRP) Composites in Civil Engineering (CICE 2014), August 2014. Vancouver, British Columbia, Canada.

---

C6: Petkune, N., Donchev, T., Hadavinia, H., Limbachiya, M., (2014) *Investigation in connections between steel, composite and hybrid structural elements*. MCM-2014: Mechanics of composite materials. June 2014, Riga, Latvia.

C7: Petkune, N., Donchev, T., Wertheim, D., Limbachiya, M., Hadavinia, H. (2013) *Application of infrared thermography for assessment of condition of structural element*. SMAR 2013: Second Conference on Smart Monitoring Assessment and Rehabilitation of Civil Structures. September 2013. Istanbul, Turkey.

C8: Petkune, N., Donchev, T., Petkova, D., Hadavinia, H., Limbachiya, M., Hussein, Y. (2012) *Opportunities for strengthening of damaged steel shear walls*. CECOM: Conference on Civil Engineering Infrastructure Cased on Polymer Composites. November 2012. Krakow, Poland.